N O T I C E

THIS DOCUMENT HAS BEEN REPRODUCED FROM MICROFICHE. ALTHOUGH IT IS RECOGNIZED THAT CERTAIN PORTIONS ARE ILLEGIBLE, IT IS BEING RELEASED IN THE INTEREST OF MAKING AVAILABLE AS MUCH INFORMATION AS POSSIBLE

JUL 1980
RECEIVED
NASA STI FACILITY
ACCESS DEPT.

COLLEGE OF ENGINEERING

VIRGINIA POLYTECHNIC INSTITUTE AND STATE UNIVERSITY

BLACKSBURG, VIRGINIA

(NASA-CR-163294) THERMAL CYCLING GRAPHITE-POLYIMIDE (Virginia Polytechnic Inst. and State Univ.) 134 p HC A07/MF A01 CSCL 11D
N80-26397
Unclas
G3/24 24245

VPI-E-79-15 April 1979

THERMAL CYCLING OF GRAPHITE-POLYIMIDE

Michael W. Hyer[1]

Jane A. Hagaman[2]

(1) Assistant Professor, Dept. of Engineering Science and Mechanics, Virginia Polytechnic Institute and State University, Blacksburg, Virginia 24061

(2) Research Assistant, Dept. of Mechanical Engineering and Mechanics, Old Dominion University, Norrolk, Virginia 23508

BIBLIOGRAPHIC DATA SHEET	1. Report No. VPI-E-79-15	2.	3. Recipient's Accession No.
4. Title and Subtitle Thermal Cycling of Graphite-Polyimide			5. Report Date April 1979 6.
7. Author(s) Michael W. Hyer, Jane A. Hagaman (Old Dominion Univ.)			8. Performing Organization Rept. No.
9. Performing Organization Name and Address Virginia Polytechnic Institute and State University Engineering Science and Mechanics Department Blacksburg, VA 24061			10. Project/Task/Work Unit No. 802-068-1 11. Contract/Grant No. NSG-1167 ODU/NASA
12. Sponsoring Organization Name and Address Old Dominion University Research Foundation P.O. Box 6369 Norfolk, VA 23508			13. Type of Report & Period Covered 14.

15. Supplementary Notes

16. Abstracts

The report describes a study designed to determine the effects of repetitive thermal cycling on the temperature-thermal deformation relation of graphite-polyimide. The bending and axial strains, measured with strain gages, of unsymmetric $[0^\circ_2/90^\circ_2]$ and $[0^\circ_4/90^\circ_4]$ laminates were used as an indication of thermal deformation. The strains were measured as a function of temperature and two temperature ranges were used, room temperature to 180°C and room temperature to 315°C. Five cycles were run in each temperature range and the cycling was done in quasi-static fashion. The response of a flat $[0^\circ_8]$ laminate was measured as were the effects of repetitive cycling on the strain gages themselves. A piecewise linear theory, based on classical lamination theory and using the variation of mechanical and thermal expansion properties with temperature, was compared with the experimental results.

17. Key Words and Document Analysis. 17a. Descriptors

Composites
Graphite-Polyimide
Unsymmetric Laminates
Thermal Cycling
High Temperature Strain Gaging
Coefficient of Thermal Expansion
Thermally Induced Strains
Temperature Effects
Nonlinear Laminate Theory

17b. Identifiers/Open-Ended Terms

17c. COSATI Field/Group

18. Availability Statement	19. Security Class (This Report)	21. No. of Pages
Unlimited	UNCLASSIFIED	123
	20. Security Class (This Page) UNCLASSIFIED	22. Price

Table of Contents

	Page
Introduction	1
Scope of the Study	2
Specimen Description	4
Experimental Set-up	6
Experimental Results	8
Room Temperature to 180°C Cycle Results	8
Response of Gages on Titanium Silicate	8
Flat $[0^\circ_8]$ Laminate	9
Curved $[0^\circ_4/90^\circ_4]$ Laminate	11
Curved $[0^\circ_2/90^\circ_2]$ Laminate	14
Room Temperature to 315°C Cycle Results	16
Response of Gages on Titanium Silicate	17
Flat $[0^\circ_8]$ Laminate	18
Curved $[0^\circ_4/90^\circ_4]$ Laminate	19
Curved $[0^\circ_2/90^\circ_2]$ Laminate	20
Combined Results	20
Response of Gages on Titanium Silicate	21
Flat $[0^\circ_8]$ Laminate	21
Curved $[0^\circ_4/90^\circ_4]$ Laminate	21
Curved $[0^\circ_2/90^\circ_2]$ Laminate	22
Discussion of Results	22
Concluding Remarks	26
References	27

List of Tables

No.	Title	Page
1.	Room Temperature Out-of-Plane Displacements of Curved Specimens	28
2.	Apparent Strain vs. Temperature for Gages on Titanium Silicate, RT-180°C	29
3.	Thermal Expansion of Flat $[0^\circ_8]$ Laminate in Matrix Direction, RT-180°C	30
4.	Thermal Expansion of Flat $[0^\circ_8]$ Laminate in Fiber Direction, RT-180°C	31
5.	Thermal Bending Strain vs. Temperature for Curved $[0^\circ_4/90^\circ_4]$ Laminate, RT-180°C	32
6.	Thermal Axial Strain vs. Temperature for Curved $[0^\circ_4/90^\circ_4]$ Laminate, RT-180°C	32
7.	Thermal Bending Strain vs. Temperature for Curved $[0^\circ_2/90^\circ_2]$ Laminate, RT-180°C	33
8.	Thermal Axial Strain vs. Temperature for Curved $[0^\circ_2/90^\circ_2]$ Laminate, RT-180°C	33
9.	Apparent Strain vs. Temperature for Gages on Titanium Silicate, RT-315°C	34
10.	Thermal Expansion of Flat $[0^\circ_8]$ Laminate in Matrix Direction, RT-315°C	34
11.	Thermal Bending Strain vs. Temperature for Curved $[0^\circ_4/90^\circ_4]$ Laminate, RT-315°C	35
12.	Thermal Axial Strain vs. Temperature for Curved $[0^\circ_4/90^\circ_4]$ Laminate, RT-315°C	35
13.	Thermal Bending Strain vs. Temperature for Curved $[0^\circ_2/90^\circ_2]$ Laminate, RT-315°C	36
14.	Thermal Axial Strain vs. Temperature for Curved $[0^\circ_2/90^\circ_2]$ Laminate, RT-315°C	36

List of Figures

No.	Title	Page
1.	Curved Specimens	37
2.	Initial Out-of-Plane Displacements for 4-layer (top) and 8-layer (bottom) Curved Specimens	38
3.	Tripod Used for Supporting Specimens	39
4.	Apparent Strain vs. Temperature, RT-180°C, Cycle 1	40
5.	Apparent Strain vs. Temperature, RT-180°C, Cycle 2	41
6.	Apparent Strain vs. Temperature, RT-180°C, Cycle 3	42
7.	Apparent Strain vs. Temperature, RT-180°C, Cycle 4	43
8.	Apparent Strain vs. Temperature, RT-180°C, Cycle 5	44
9.	Apparent Strain vs. Temperature, RT-180°C, Cycle 6	45
10.	Apparent Strain vs. Temperature, RT-180°C, Cycle 7	46
11.	Apparent Strain vs. Temperature, RT-180°C, Cycle 8	47
12.	Apparent Strain vs. Temperature, RT-180°C, Cycle 9	48
13.	Apparent Strain vs. Temperature, RT-180°C, Cycle 10	49
14.	Apparent Strain vs. Temperature, RT-180°C, Cycle 11	50
15.	Apparent Strain vs. Temperature, RT-180°C, Cycle 12	51
16.	Apparent Strain vs. Temperature, RT-180°C, Cycle 13	52
17.	Apparent Strain vs. Temperature, RT-180°C, Cycle 14	53
18.	Apparent Strain vs. Temperature, RT-180°C, Cycle 15	54
19.	Apparent Strain vs. Temperature, RT-180°C, Least-Squares Fit, All 15 Cycles	55
20.	Thermal Expansion of $[0^\circ_8]$ Laminate in Matrix Direction, RT-180°C, Cycle 1	56
21.	Thermal Expansion of $[0^\circ_8]$ Laminate in Matrix Direction, RT-180°C, Cycle 2	57
22.	Thermal Expansion of $[0^\circ_8]$ Laminate in Matrix Direction, RT-180°C, Cycle 3	58
23.	Thermal Expansion of $[0^\circ_8]$ Laminate in Matrix Direction, RT-180°C, Cycle 4	59

24. Thermal Expansion of $[0_8^\circ]$ Laminate in Matrix Direction, RT-180°C, Cycle 5 60

25. Thermal Expansion of $[0_8^\circ]$ Laminate in Matrix Direction, RT-180°C, Least-Squares Fit, All 5 Cycles 61

26. Thermal Expansion of $[0_8^\circ]$ Laminate in Fiber Direction, RT-180°C, Cycle 1 62

27. Thermal Expansion of $[0_8^\circ]$ Laminate in Fiber Direction, RT-180°C, Cycle 2 63

28. Thermal Expansion of $[0_8^\circ]$ Laminate in Fiber Direction, RT-180°C, Cycle 3 64

29. Thermal Expansion of $[0_8^\circ]$ Laminate in Fiber Direction, RT-180°C, Cycle 4 65

30. Thermal Expansion of $[0_8^\circ]$ Laminate in Fiber Direction, RT-180°C, Cycle 5 66

31. Thermal Expansion of $[0_8^\circ]$ Laminate in Fiber Direction, RT-180°C, Least-Squares Fit, All 5 Cycles 67

32. Thermal Bending Strain, $[0_4^\circ/90_4^\circ]$ Laminate, RT-180°C, Cycle 1 68

33. Thermal Bending Strain, $[0_4^\circ/90_4^\circ]$ Laminate, RT-180°C, Cycle 2 69

34. Thermal Bending Strain, $[0_4^\circ/90_4^\circ]$ Laminate, RT-180°C, Cycle 3 70

35. Thermal Bending Strain, $[0_4^\circ/90_4^\circ]$ Laminate, RT-180°C, Cycle 4 71

36. Thermal Bending Strain, $[0_4^\circ/90_4^\circ]$ Laminate, RT-180°C, Cycle 5 72

37. Thermal Axial Strain, $[0_4^\circ/90_4^\circ]$ Laminate, RT-180°C, Cycle 1 73

38. Thermal Axial Strain, $[0_4^\circ/90_4^\circ]$ Laminate, RT-180°C, Cycle 2 74

39. Thermal Axial Strain, $[0_4^\circ/90_4^\circ]$ Laminate, RT-180°C, Cycle 3 75

40. Thermal Axial Strain, $[0_4^\circ/90_4^\circ]$ Laminate, RT-180°C, Cycle 4 76

41. Thermal Axial Strain, $[0_4^\circ/90_4^\circ]$ Laminate, RT-180°C, Cycle 5 77

42. Least-Squares Thermal Bending Strains and Theoretical Prediction, $[0^\circ_4/90^\circ_4]$ Laminate, RT-180°C 78

43. Least-Squares Thermal Axial Strains and Theoretical Prediction, $[0^\circ_4/90^\circ_4]$ Laminate, RT-180°C 79

44. Thermal Bending Strain, $[0^\circ_2/90^\circ_2]$ Laminate, RT-180°C, Cycle 1 80

45. Thermal Bending Strain, $[0^\circ_2/90^\circ_2]$ Laminate, RT-180°C, Cycle 2 81

46. Thermal Bending Strain, $[0^\circ_2/90^\circ_2]$ Laminate, RT-180°C, Cycle 3 82

47. Thermal Bending Strain, $[0^\circ_2/90^\circ_2]$ Laminate, RT-180°C, Cycle 4 83

48. Thermal Bending Strain, $[0^\circ_2/90^\circ_2]$ Laminate, RT-180°C, Cycle 5 84

49. Thermal Axial Strain, $[0^\circ_2/90^\circ_2]$ Laminate, RT-180°C, Cycle 1 85

50. Thermal Axial Strain, $[0^\circ_2/90^\circ_2]$ Laminate, RT-180°c, Cycle 2 86

51. Thermal Axial Strain, $[0^\circ_2/90^\circ_2]$ Laminate, RT-180°C, Cycle 3 87

52. Thermal Axial Strain, $[0^\circ_2/90^\circ_2]$ Laminate, RT-180°C, Cycle 4 88

53. Thermal Axial Strain, $[0^\circ_2/90^\circ_2]$ Laminate, RT-180°C, Cycle 5 89

54. Least-Squares Thermal Bending Strains and Theoretical Prediction, $[0^\circ_2/90^\circ_2]$ Laminate, RT-180°C 90

55. Least-Squares Thermal Axial Strains and Theoretical Prediction, $[0^\circ_2/90^\circ_2]$ Laminate, RT-180°C 91

56. Apparent Strain vs. Temperature, RT-315°C, Cycle 1 92

57. Apparent Strain vs. Temperature, RT-315°C, Cycle 2 93

58. Apparent Strain vs. Temperature, RT-315°C, Cycle 3 94

59. Apparent Strain vs. Temperature, RT-315°C, Cycle 4 95

60. Apparent Strain vs. Temperature, RT-315°C, Cycle 5 96

61. Apparent Strain vs. Temperature, RT-315°C, Least-Squares Fit, All 5 Cycles 97

62. Thermal Expansion of $[0^\circ_8]$ Laminate in Matrix Direction, RT-315°C, Cycle 1 98

63. Thermal Expansion of $[0_8^\circ]$ Laminate in Matrix Direction, RT-315°C, Cycle 2 99

64. Thermal Expansion of $[0_8^\circ]$ Laminate in Matrix Direction, RT-315°C, Cycle 3 100

65. Thermal Expansion of $[0_8^\circ]$ Laminate in Matrix Direction, RT-315°C, Cycle 4 101

66. Thermal Expansion of $[0_8^\circ]$ Laminate in Matrix Direction, RT-315°C, Cycle 5 102

67. Thermal Expansion of $[0_8^\circ]$ Laminate in Matrix Direction, RT-315°C, Least Squares Fit, All 5 Cycles 103

68. Thermal Bending Strain, $[0_4^\circ/90_4^\circ]$ Laminate, RT-315°C, Cycle 1 104

69. Thermal Bending Strain, $[0_4^\circ/90_4^\circ]$ Laminate, RT-315°C, Cycle 2 105

70. Thermal Axial Strain, $[0_4^\circ/90_4^\circ]$ Laminate, RT-315°C, Cycle 1 106

71. Thermal Axial Strain, $[0_4^\circ/90_4^\circ]$ Laminate, RT-315°C, Cycle 2 107

72. Least-Squares Thermal Bending Strains and Theoretical Prediction, $[0_4^\circ/90_4^\circ]$ Laminate, RT-315°C 108

73. Least-Squares Thermal Axial Strains and Theoretical Prediction, $[0_4^\circ/90_4^\circ]$ Laminate, RT-315°C 109

74. Thermal Bending Strain, $[0_2^\circ/90_2^\circ]$ Laminate, RT-315°C, Cycle 1 110

75. Thermal Bending Strain, $[0_2^\circ/90_2^\circ]$ Laminate, RT-315°C, Cycle 2 111

76. Thermal Bending Strain, $[0_2^\circ/90_2^\circ]$ Laminate, RT-315°C, Cycle 3 112

77. Thermal Axial Strain, $[0_2^\circ/90_2^\circ]$ Laminate, RT-315°C, Cycle 1 113

78. Thermal Axial Strain, $[0_2^\circ/90_2^\circ]$ Laminate, RT-315°C, Cycle 2 114

79. Thermal Axial Strain, $[0_2^\circ/90_2^\circ]$ Laminate, RT-315°C, Cycle 3 115

80. Least-Squares Thermal Bending Strains and Theoretical Prediction, $[0_2^\circ/90_2^\circ]$ Laminate, RT-315°C 116

81. Least-Squares Thermal Axial Strains and Theoretical Prediction, $[0_2^\circ/90_2^\circ]$ Laminate, RT-315°C 117

82. Least-Squares Apparent Strain vs. Temperature, RT-180°C and RT-315°C 118

83. Comparison of Least-Squares Matrix Direction Strains, $[0_8^\circ]$ Laminate, RT-180°C and RT-315°C 119

84. Comparison of Least-Squares Bending Strains, $[0_4^\circ/90_4^\circ]$ Laminate, RT-180°C and RT-315°C 120

85. Comparison of Least-Squares Axial Strains, $[0_4^\circ/90_4^\circ]$ Laminate, RT-180°C and RT-315°C 121

86. Comparison of Least-Squares Bending Strains, $[0_2^\circ/90_2^\circ]$ Laminate, RT-180°C and RT-315°C 122

87. Comparison of Least-Squares Axial Strains, $[0_2^\circ/90_2^\circ]$ Laminate, RT-180°C and RT-315°C 123

ABSTRACT

The report describes a study designed to determine the effects of repetitive thermal cycling on the temperature-thermal deformation relation of graphite-polyimide. The bending and axial strains, measured with strain gages, of unsymmetric $[0^\circ_2/90^\circ_2]$ and $[0^\circ_4/90^\circ_4]$ laminates were used as an indication of thermal deformation. The strains were measured as a function of temperature and two temperature ranges were used, room temperature to 180°C and room temperature to 315°C. Five cycles were run in each temperature range and the cycling was done in quasi-static fashion. The response of a flat $[0^\circ_8]$ laminate was measured as were the effects of repetitive cycling on the strain gages themselves. A piecewise linear theory, based on classical lamination theory and using the variation of mechanical and thermal expansion properties with temperature, was compared with the experimental results. Because of difficulties with the strain gaging at the higher temperatures, the results for the room temperature to 315°C cycling were not as conclusive as the results for the room temperature to 180°C tests. From the low temperature range cycling data it can be concluded (1), there was a hysteresis-like effect in the temperature-thermal deformation relation for one cycle, (2), there was no detectable difference in the temperature-thermal deformation relation from one cycle to the next and finally, (3), the predictions for the response of the thicker laminate agreed with experimental observation. The correlation between theoretical predictions and experimental results for the thinner laminate was poor.

Introduction

Since graphite fiber reinforced materials have resulted in structural efficiencies far greater than efficiencies achieved with conventional homogeneous materials, there has been an effort to develop these materials for use at elevated temperatures. For nonmetal-matrix composites, this has required the development of resins which retain their strength at elevated temperatures. Substantial progress has been made in this effort with polyimide resins. Compared to the earlier first-generation epoxy-matrix composites, there has been a remarkable increase in strength retention at elevated temperatures for composites which use polyimide resins.

As with any structure intended for high temperature operation, generally speaking, the structure will not operate at elevated temperatures continuously. It is more likely the operating temperature will fluctuate with time. The temperature may start at some low value, increase to some maximum value, hold at that temperature for a period of time and then perhaps return to the low temperature again. In short, the structure will be subjected to some sort of thermal cycle. For example, during one flight, the aftbody flap on the shuttle orbiter experiences temperatures ranging from -157°C to + 315°C. Graphite-polyimide honeycomb panels are being considered as a replacement for the current aluminum design of the flap. Thus the question of thermal cycling is pertinent in this situation. In addition, since each orbiter is expected to be used for 125 missions, the question of repeated thermal cycling becomes important. In other applications, fiber reinforced materials may be used for large orbiting space structures (ref. 1) and in that case, the structure could see cyclic heating and cooling as the

orbit carries the structure repeatedly from the cold of the earth's shadow to the heat of the direct sun. In aircraft, there are numerous potential applications in which a structural component would experience repetitive heating and cooling, as for example, in an engine. With the automotive industry investigating the use of fiber-reinforced composite materials for reducing fuel consumption, the question of repeated heating and cooling certainly will be an issue.

It seems worthwhile, therefore, to study the behavior of fiber-reinforced composite materials, and the structures fabricated from them, when they are subjected to repetitive heating and cooling. There are many facets of the problem to be considered, both material and structural. However, this report summarizes the results of a study which had as a primary goal the determination of the effects of thermal cycling on the temperature-thermal deformation characteristics of flat and curved graphite-polyimide laminates..

Scope of the Study

As is well known, fiber reinforced materials have thermal expansion properties dependent on the direction of the fibers. For a lamina, the coefficient of thermal expansion (CTE) in the matrix direction is approximately $30 \times 10^{-6}/°C$ while in the fiber direction, the CTE can be slightly negative, zero or slightly positive, depending on the volume fraction of fibers. Because of these properties, substantial internal stresses are generated in a laminate when it is cooled from its curing temperature. From this view point, the difference in CTE in the fiber and matrix directions is undesirable. However, this difference can be used to advantage to design materials with a specific CTE (ref. 2). As the temperature of a fiber reinforced material is changed, the internal

stresses change. If the temperature change is drastic enough, internal failures, in the form of microcracking, occur and the mechanical and thermal expansion properties of the laminate will change. Thus, as a laminate is repeatedly heated and cooled, its properties may change continuously from one cycle to the next. In addition, since thermal cycling, in a precisely controlled fashion, is an integral part of the fabrication process for epoxy-matrix materials, further thermal cycling could act as additional post-curing and alter the mechanical behavior of the material. As a structure is repeatedly heated and cooled, the question arises as to whether the changes in material properties are reflected in changes in the load-deformation behavior from one cycle to the next. More importantly the question arises as to whether these changes be detected by methods commonly used to measure structural response. The study reported on here addressed these issues and in particular examined the changes in the deformation characteristics from cycle to cycle in the absence of mechanical loads. Thus the study considered only thermally-induced deformations. Since internal stresses affect the deformation, the results can be used indirectly to study changes in internal stresses from one cycle to the next.

To assess the effects of thermal cycling, unsymmetric laminates were fabricated and the change in curvature as a function of temperature was used as a measure of thermal deformation. This configuration was chosen since it is particularly sensitive to both elastic and thermal expansion properties. In addition, several unidirectional laminates were fabricated to determine the mechanical and thermal expansion properties of a single lamina. The specimens were placed in an oven at room temperature (RT), heated to an elevated temperature and then cooled to RT. The temperature and deformation were recorded as a function of

time during the heating and cooling. The basic questions to be answered were: (1) Was the thermal deformation at a given temperature dependent on the number of thermal cycles? (2) Was the thermal deformation at a given temperature dependent on whether the specimen was being heated or cooled? and, (3) Using properties of a single lamina, could simple lamination theory be used to predict the thermal deformation of the unsymmetric lay-ups? This report briefly describes the specimens, the experimental set-up and procedure, but is intended primarily to present the experimental data and the comparison with theory. The experimental data is presented in both raw data and least-squares polynomial reduced form. The coefficients of the least-squares polynomial are presented so other investigators may more conveniently compare their theories or experimental results with the results observed in this study. The raw data presentations and the statistical curve fitting for the report were done with the aid of the computer program described in ref. 3.

Specimen Description

The specimens used in the experiment were sized to fit into existing oven facilities and were roughly 150 mm long, 25 mm wide (6 inches x 1 inch) and a variable number of layers in thickness. The specimens were fabricated from HTS/PMR-15 in the following lay-ups: $[0^\circ_8]$, $[90^\circ_8]$, $[(+45^\circ/-45^\circ)_2]_s$, $[0^\circ_2/90^\circ_2]$, $[0^\circ_4/90^\circ_4]$ and $[0^\circ_6/90^\circ_6]$. The first three laminates were used to determine the material properties of a single lamina and the last three resulted in curved specimens. Unfortunately the last specimen was inadvertently broken before any tests were conducted with it but it is interesting to note that such a thick unsymmetric laminate was fabricated. Actually the specimens were cut from large laminates which were C-scanned to determine an area of high quality.

Figure 1 shows the curved specimens and Fig. 2 shows the RT out-of-plane displacements for the 4-layer and 8-layer curved specimens. These displacements were measured with a linear differential variable transformer (LDVT). The LDVT was oriented perpendicular to the specimen and the specimens were moved lengthwise with the transformer core following the contour of the curved specimen. The data shown is the average of several measurements on both sides of the specimens. Least-squares cubics passed through the data indicate the curvature was not constant along the length. The radii of curvature, calculated at the center of each specimen, were: 440 mm (17.3 in) for the 4-layer specimen and 470 mm (18.5 in) for the 8-layer specimen. The RT radius of curvature of the thinner specimen was much larger than expected. Lamination theory predicts the thinner laminate should have had a radius of curvature half that of the thicker laminate. This was not the case and this discrepancy was indicative of the behavior of the 4-layer specimen throughout the testing. The least-squares cubic expressions for the RT out-of-plane displacements, as a function of distance measured from mid-span of the specimens, are given in Table 1. The average thickness of the 8-layer specimen was 1.46 mm (0.0575 in.) while the 4-layer specimen averaged 0.870 mm (0.0323 in.) in thickness.

Tensile tests on the $[0_8^\circ]$, $[90_8^\circ]$ and $[(+45^\circ/-45^\circ)_2]_s$ laminates indicated the RT mechanical properties to be:

E_{11} = 137.4 MPa (19.93 x 10^6 psi)

ν_{12} = .3703

E_{22} = 9.044 MPa (1.312 x 10^6 psi)

G_{12} = 4.281 MPa (.6208 x 10^6 psi)

Experimental Set-Up

Two temperature ranges were used to thermally cycle the specimens. The first range was from RT to 180°C (356°F) and the second range was from RT to 315°C (600°F). Two temperature ranges were used to determine what effect the maximum temperature of the cycle had on the repeated cycling. The lower temperature cycling was done using a natural convection oven while the higher temperature range cycles were conducted in a fan-forced convection oven. The original scheme was to measure the change in the out-of-plane displacements of the specimens with LDVT's. The LDVT's were mounted outside the oven and were fitted with core extensions, the extensions passing through specially drilled holes in the oven door window. In order to have the core extensions remain in constant contact with the specimens, a light spring was required. The force from the spring, small as it was, was enough to cause deformations in the thinner laminate. Thus the LDVT's were abandoned in favor of strain gages. Four back-to-back pairs, spaced at equal intervals along the length, were used on the 8-layer specimen while two back-to-back pairs were used on the 4-layer specimen. On the flat $[0^\circ_8]$ specimen, one back-to-back pair was used in the fiber direction and one back-to-back pair was used in the matrix direction. With this arrangement on the flat specimen, the longitudinal and transverse thermal strain of an unloaded lamina could be measured. The gages used were Micro-Measurements type WK-125UW-350 and they were bonded to the specimens with a Baldwin-Lima-Hamilton polyimide adhesive. The bonding technique required an elevated temperature cure with the maximum cure temperature at least as high as the temperature of the thermal cycle. Thus, before cycling, the test specimens had been exposed to one thermal cycle.

To account for the apparent strain of the gages due to thermal effects on the gage material, two identical gages were mounted on a piece of titanium silicate and placed in the oven alongside the particular graphite-polyimide specimens being tested. Titanium silicate is a near-zero CTE material which is very stable in the temperature ranges used in the experiment. Since the thermal expansion of the titanium silicate was known, the effect of temperature on the gage output could be determined. The output of the gages on the graphite-polyimide specimens was adjusted using the output of the gages on the titanium silicate and the true strain response of the graphite-polyimide test specimens could then be determined as a function of temperature.

For the RT to 180°C tests, the specimens were positioned in the oven by mounting them on a vertical post. The post was a 9.525 mm (.375 in.) diameter steel dowel and the specimens were attached by a single number 10 bolt going through a hole in the center of the specimen and the steel post. The specimen was supported from the steel rod by using fiber-type washers between the post and the specimen. The vertical post was in turn mounted on a tripod base. Figure 3 illustrates the stand. With this arrangement the specimens were located in the central portion of the oven, a region with very low temperature gradients. For the higher temperature range tests, the specimens were supported by knife edges at each end, using gravity to hold the specimens against the knife edges. The specimens were in the central portion of the oven and were completely free of axial restraint. The temperatures of the specimen and the titanium silicate were measured with thermocouples held against the specimens with polyimide tape. Owing to the quasi-static, and often times static, nature of the cycling process, there was never a question

of a nonequilibrium temperature state. The maximum heating/cooling rate was 42°C/hr (107°F/hr) for the RT-180°C tests and 65°C per hour (150°F/hr.) for the RT-315°C tests. All data was recorded by hand. At a given temperature, before the strain and temperature were recorded, the temperature was allowed to stabilize except for the usual dithering of the digital readouts. The strain gages were each wired into a 4-arm bridge using four identical gages and were excited with 6 volts d.c. by a Fluke Model 382A Voltage/Current Calibrator. The bridge voltages were measured with a Data Precision Model 3500 Digital Microvoltmeter and the thermocouples were monitored by a Fluke Model 2100A Digital Thermocouple.

Experimental Results

There was a considerable amount of data generated from the experimentation and for purposes of presentation, the results are presented in several subsections.

Room Temperature to 180°C Cycle Results

Response of Gages on Titanium Silicate

Perhaps the most important consideration was the effect of repeated heating and cooling on the strain gages themselves. These effects were assessed by examining the output of the gages on the titanium silicate.

The $[0^\circ_8]$, the $[0^\circ_2/90^\circ_2]$ and the $[0^\circ_4/90^\circ_4]$ laminates were each cycled seperately for five cycles in the lower temperature range. The same piece of titanium silicate, and the gages on it, was used for all 15 cycles. Figures 4 through 18 show the apparent strain, based on the output of the gages on the titanium silicate, for the 15 cycles. The data shown is the average of the two gages and the heating and cooling response is noted in the figures. Each cycle is plotted on a seperate

figure to avoid clutter and to indicate the minimal amount of scatter observed during a particular cycle. For most of the cycles, the apparent strains during heating were of slightly less magnitude than the apparent strains observed during cooling. For testing in the higher temperature range, the opposite trend occurred. Drift tests on the instrumentation revealed no particular drift problems and so the differences in the heating and cooling cycles are attributed to a small amount of hysteresis in the gage and/or the adhesive. The strain data was well represented by the third-order least-squares polynomials shown on the figures. Figure 19 shows all the polynomials on a common coordinate system. Cycles 1-5 refer to the cycling of the 8-layer $[0^\circ_4/90^\circ_4]$ curved laminate, cycles 6-10 refer to the cycling of the $[0^\circ_8]$ flat laminate and cycles 11-15 refer to the cycling of the 4-layer $[0^\circ_2/90^\circ_2]$ curved laminate. It was felt the gages might slowly change character from cycle to cycle, showing ever increasing or ever decreasing strain at a given temperature. This was not observed as evidenced by the mixed order of the cycling curves on Fig. 19. The scatter of the least-squares strains among the 15 cycles at 180°C was less than 4% of the average strain value at that temperature. The gages appeared quite stable and reliable in the RT to 180°C temperature range. Table 2 indicates the coefficients of the least-squares cubics for each of the 15 cycles.

Flat $[0^\circ_8]$ Laminate

Figures 20-24 show the raw data for the 5 cycles of thermal expansion in the matrix direction for the $[0^\circ_8]$ laminate. Again, to avoid clutter and to indicate the character of the heating and cooling portion of each thermal cycle, the raw data for each cycle is presented on a

separate figure. The data presented is an average of the two back-to-back gages in the matrix direction. Immediately noticeable was the hysteresis-like effect in the temperature-strain relations, a trend which was observed consistently in much of the data from the polyimide specimens. This hysteresis was much greater than that observed in the strain gages on the titanium silicate and thus was attributed to the graphite-polymide. The amount of hysteresis varied from cycle to cycle and it is not clear why there was such variation. However, from the data, the thermal strain in the matrix direction was always greater when heating the specimen than when cooling it. Shown in the figures are least-squares parabolas fitted to the data. Since the hysteresis was not consistent from cycle to cycle and since the theory used as a basis for comparison did not account for hysteresis, the least-squares curve computed was the average of the heating and cooling data and thus naturally laid half-way between the two portions of the thermal cycle. Several polynomials fit the data but a parabola seemed to be simple, fit the data well and allowed for slight nonlinearities. Unless otherwise noted, all the following least-squares relations are parabolic. Table 3 presents the coefficients of the parabolas for the five cycles while Fig. 25 shows the least-squares parabolas displayed on a common coordinate system. Because of the consistency, from cycle to cycle, in the response of the gages mounted on titanium silicate, any change in the matrix-direction strains from cycle to cycle would have been due to the graphite-polyimide. However, the order of the 5 parabolas was mixed and there did not appear to be any trend. The spread of the least-squares data at 180°C was 3.3% of the average value at that temperature.

Figures 26-30 show the raw data for the thermal expansion in the fiber direction. As expected, the thermal strains were quite small and because of the influence of experimental error, the least-squares scheme was important for interpretation of this data. Hysteresis was also present in the fiber direction. Figure 31 shows the least-squares parabolas for the five cycles of fiber-direction expansion. To put the results in context, the figure shows the least-squares thermal expansion strains (axial strains) and the least-squares thermally induced bending strains (theoretically zero), for the fiber direction, plotted on the same coordinate. It is apparent the thermal expansion of the fiber direction was being measured to a degree. It could be suggested that at each temperature the bending strain data should have been taken as the zero reference for the axial strain. If the fiber distribution and the curing process were completely uniform, the bending strain would have been zero. However, there was nothing to suggest the above-indicated bending strains were not actual and so they were not used as a zero reference for the axial strains. Although there was no trend to the data from cycle to cycle, the spread was about 40% of the average value and thus the data was not as reliable as the matrix direction strain data. Table 4 presents the coefficients of the least-squares parabolas for the fiber-direction thermal expansion data.

Curved $[0^\circ_4/90^\circ_4]$ Laminate

Ultimately the goal of most analyses involving composite materials is to use information from a micro- or mini-scale to predict the behavior on a macro-scale. For the case at hand, it was of interest to use the properties of a single lamina to predict the response of the curved

laminates. In particular, the goal was to predict the change in shape of the curved laminate when it was heated and cooled. Because the properties of a lamina change with temperature, any analysis becomes more involved than analysis of the response, say, at a fixed temperature. The mechanical and thermal expansion properties are influenced by temperature and so the prediction problem is in some sense path-dependent. Thus the shape of the structure at, say, 180°C can only be determined by starting the analysis at RT and then allowing the properties to vary in some fashion as the analysis follows the temperature increase from RT. This requires a continuum of values for the mechanical properties over the temperature range of interest. This information is generally not available so the properties are generally assumed to vary in some manner between known values at specific temperatures. In what follows, in addition to presenting experimental results from testing the curved specimens, the predicted responses of the curved laminates are presented. The predictions are based on a piecewise linear theory which was nothing more than classical lamination theory used in a tangent modulus approach. The thermal expansion properties of a single lamina as a function of temperature was taken from the results of a previous section. Information on the variation of mechanical properties with temperature is quite limited and using the results that were available, it was assumed E_{11} did not vary with temperature and E_{22} was reduced to 85% of its RT value at 180°C. The character of the reduction with temperature was determined by fairing a curve through RT, 180°C, 232°C, 260°C and 315°C data which was available. The fall-off in strength with temperature was allowed to occur in 10 equal increments from RT to 180°C. Since the elastic constants were based on no thermal cycling (actually one cycle

to roughly 100°C since the strain gages had to be installed to determine the elastic properties), the theoretical predictions should really only be compared with the first thermal cycle.

Figures 32-36 show the thermally induced bending strains vs. temperature for the first five thermal cycles and Figs. 37-41 show the thermally induced axial strain vs. temperature for those same cycles. The data shown is from one pair of the four back-to-back pairs distributed along the length of the specimen. The data from the other three gage pairs was practically identical. The uniformity of the data along the length of the specimen was a possible indication there were no large delaminations in the specimen. This was an important consideration because the 0°/90° lay-up produces severe interlaminar stresses between the 0° and 90° layers. Figure 42 shows all five experimental least-squares bending strain-temperature relationships and the theroetically predicted relation. Figure 43 shows similar results for the axial strain. The experimental bending strain vs. temperature relation had some initial curvature but after a temperature of 125°C, the curves tended to straighten out, the predicted relation being practically a straight line. The experimental axial strain vs. temperature relation had a constant curvature as did the theoretical prediction. Except for a slight downward shift, the nonlinear axial strain prediction followed the experimental data remarkably well. At 180°C, the spread of the least-squares bending strain values were 8.2% of their average value at that temperature while the axial strains had a 6% spread. Neither strain measure appears to have had a trend from cycle-to-cycle. Table 5 presents the coefficients for the least-squares bending strain-temperature relationships while Table 6 presents similar information for the axial strain data.

Curved $[0_2^\circ/90_2^\circ]$ Laminate

Because of the uniformity of the bending and axial strains along the length of the 8-layer curved specimen, only two back-to-back gage pairs were used on the 4-layer specimen. They were placed at 1/3 the specimen length from each end. Figures 44-48 show the experimental thermally induced bending strain vs. temperature for the five cycles while Figs. 49-53 show the experimental axial strain vs. temperature. Cycles 4 and 5 seemed quite different in that there appeared to be a large parmanent deformation of the specimen as it cooled to RT. Both strain gage pairs mounted at the two locations along the specimen indicated this behavior. When comparing the strain gage outputs of the first three cycles with the output of the fourth cycle, it can be seen the deviation began on the 4th heating cycle at a temperature of 135-140°C. In that temperature range, the slope of the strain-temperature relation suddenly decreased. The heating portion of the curve up to that point closely followed the three previous cycles and, except for a vertical shift, the cooling portion of the curve had the same general shape as the three previous cycles. The phenomenon was puzzling because when cycled later, at higher temperatures, the phenomenon disappeared and then reappeared again. When all testing was complete on the 8-layer and 4-layer specimens, the specimens were cut, their cross-sections polished and examined under a microscope. There were four cross-sectional cuts, at different points along the length of the specimens, and there were no major differences in microstructure between the 4-layer and the 8-layer specimens. There was some cracking, in the thickness direction, through the matrix of both specimens. However, it was felt major delaminations would be observed in the 4-layer specimen and this would account for the unexpected behavior of that specimen. This, however, was not

the case. There is a possibility the problem was a result of a snap-through in the shape of the laminate. Thin (2-4 layers), unsymmetric laminates are quite flexible and, even though they may be cut into long narrow strips, due to the dissymmetry of the lay-up, they actually have a double curvature or saddle shape. When handling the specimens used in this and other experiments, it became apparent thin unsymmetric laminates seem to have two RT equilibrium shapes. One shape is curved and the other shape is flatter. Either shape is possible for the laminate and to change from one shape to the other requires a simple snap-through action. It is theorized the higher the temperature, the closer the two geometric states. At the curing temperature, the two states converge into a single, flat, stress-free configuration. It is felt the apparent change in slope of the experimental temperature-strain relation could have been due to the laminate suddenly tending toward the other equilibrium position. Unfortunately the strain gage data was not reduced until after the specimen had been removed from the oven and there was not a close examination of the specimen upon removal to perhaps observe whether this snap-through had indeed occurred.

This situation was further complicated when the least-squares strain-temperature relations for the five cycles were compared with the theoretical predictions. For the $[0^\circ_n/90^\circ_n]$ laminates, lamination theory indicates the thermally induced curvature varies inversely with the laminate thickness while the axial strain is independent of thickness. The bending strains at the outer fibers are one-half the product of laminate thickness and curvature. As a result, the thermally induced bending strains are also independent of the laminate thickness. Thus the theoretical predictions for the 4-layer and 8-layer curved laminates were identical. Figures 54 and 55 show the least-squares strain-temperature

relations for the first five cycles and the theoretical predictions. The five cycles were consistent and different than the theory. The deviation among cycles was due to the phenomenon observed in cycles four and five, the first three cycles being quite close to each other. Obviously, some mechanism not accounted for in the theory was present. Qualitative observation of the axial strains indicated the slope of the experimental strain-temperature relation eventually paralleled the theoretical slope but differences in the initial slope caused substantial differences between the magnitudes of the observed and predicted strains. At 180°C, the spread of the least-squares bending strain value was 24% of their average value at that temperature while the axial strains had a 28% spread. There was no particular order to the cycling data in either case. Tables 7 and 8 summarize the least-squares coefficients for the two strain measures.

Room Temperature to 315°C Cycle Results

For testing in the higher temperature range, a slightly different procedure was used. The main differences were that all three specimens were tested at once, to shorten the required oven time, and, as mentioned earlier, the specimens were simply supported on each end with gravity holding the specimens against the supports. In addition, the heating rates were slightly faster than for the low temperature range. The titanium silicate was again positioned near the specimens. For these higher temperature tests, difficulties were encountered with the strain gaging. The results were erratic readings and generally unreliable data. These problems occurred most frequently with the graphite-polyimide specimens although there were some problems with the gaging on the titanium silicate. Because of these problems, the data for RT-315°C was

not as abundant nor was it felt to be as reliable. For each specimen there was only one back-to-back pair of gages monitored and not all of these worked continually. It might be pointed out the troubles were felt to be associated with the 315°C temperature extreme. Cycling to 260°C or even 290°C would probably not have been as difficult as the final increment to 315°C.

Three cycles from RT to 315°C were conducted on all three specimens. By the third cycle, there was no output from several of the gages and examination of the data on the second and third cycle indicated rather erratic results. At this point the strain gages on the graphite-polyimide specimens as well as those on the titanium silicate were closely examined. Several of the electrical connections on the gages were loose and the backings on several of the gages were cracked. The faulty gages were replaced and loose connections repaired and the testing continued. As a result of these three cycles, the first cycle for which reliable data was obtained was actually the fourth RT-315°C cycle. In addition, if the cycles used to cure the strain gage adhesives are included, there were six cycles of the lower range and four cycles at the higher range before reliable data at the higher temperature was taken. However, the five data-gathering cycles will be referred to as cycles 1-5.

Response of Gages on Titanium Silicate

Again, to judge the output of the gages on the graphite-polyimide specimens, it was important to assess the effects of repeated heating and cooling on the gages themselves. Figures 56-60 show the apparent strain, due to thermal effects, for the five RT-315° cycles. The results show the gage output was not as consistent for the higher-temperature

range as it was for the lower temperature range. In addition, as mentioned earlier, the hysteretic effects were opposite those for the low temperature cycles. The apparent strain for heating was always greater in magnitude that the apparent strain for cooling. Figure 61 shows the least-squares cubics fitted through the data for the five cycles while Table 9 shows the coefficients of the cubic equations. These gages, although the same type, were not the same ones as used for the low temperature cycles. Figure 61 indicates there was more scatter for the five cycles at RT-315°C than for the 15 cycles at RT-180°C. The scatter in the least-squares curves at 315°C was 8.4% of the average value at that temperature. There was evidence, though not strong, of some trend from cycle to cycle. The apparent strain at a given temperature seemed to decrease over the cycles.

Flat $[0^\circ_8]$ Laminate

Figures 62-66 show the raw data for the five cycles of the matrix-direction thermal strain. The somewhat scattered behavior of the data on the first cycle was similar to the behavior of the data on the previous three cycles when the faulty gages and electrical connections were discovered. However, close inspection produced no evidence of faulty strain gages and so testing proceeded. The remaining four cycles did not appear as scattered. Figure 67 shows the five least-squares matrix direction thermal strains. The scatter of the data at 315°C was 7.4% of the average value at that temperature. No trends were evident but the scatter was twice the scatter for the lower temperature cycling. However, since the scatter was under 10%, the data was felt to be reliable. Table 10 lists the coefficients associated with each cycle.

For the gages mounted in the fiber direction, the output was quite erratic. In view of the fact the strains were expected to be small, it

was felt the erratic data would lead to meaningless results for fiber-direction thermal strains. Thus, recording of the output from these gages was terminated.

Curved $[0_4^\circ/90_4^\circ]$ Laminate

As with the lower temperature range testing of the curved laminates, the experimental results for the higher temperature range testing were compared with a piecewise-linear theory. For thermal expansion properties of a single lamina, the matrix-direction thermal expansion from the just-described RT-315°C flat laminate tests was used and the polynomial for the RT-180°C fiber-direction tests was extended to provide fiber-direction information to 315°C. The value of E_{11} was again assumed constant but E_{22} was assumed to decrease by 25% at 232°C, 35% at 260°C and 50% by 315°C. The decrease from RT-180°C was the same as used previously while the decrease from 180°C to 315°C was assumed to take place in 11 temperature increments.

Figures 68 and 69 show the thermally induced bending strains vs. temperature for the first two of the five high temperature cycles. As mentioned previously, only one back-to-back gage pair was used for the high temperature tests and during the third cycle, one of the two gages failed to operate. It became apparent the extreme temperatures made it difficult to obtain reliable information from the strain gages. Figures 70 and 71 show the thermally induced axial strain from these first two cycles. Figure 72 shows the least-squares relations for the two cycles in addition to the theoretical predictions. Figure 73 shows similar results for the axial strains. The correlation between theory and experiment was not as close as for the lower temperature cycling. Even with just

two cycles, the spread between the first and second cycles was significant. For the bending strains, the spread at the maximum temperature was 23% of the average value while for the axial strains, at 150°C, the spread was 12% of the average. Tables 11 and 12 indicate the coefficients of the polynomials for the least-squares experimental bending and axial strain vs. temperature relations.

Curved $[0_2^\circ/90_2^\circ]$ Laminate

While in the fourth cycle of the higher temperature testing, one of the back-to-back gages on the thinner curved laminate open-circuited and as a result, only three cycles of data were obtained for that laminate. Figures 74-76 show the three cycles of bending strain data while Figs. 77-79 show the three cycles of axial strain data for the thinner curved laminate. Apparent in the first cycle was the large permanent set as the specimen cooled. However, in the second and third cycles this situation did not appear. The interior of the oven was illuminated and the thin curved laminate was observed closely to detect any snap-through. None was observed and so the behavior of the thinner laminate was still a puzzle. Figure 80 summarizes the least-squares curves passed through the bending strain data and also shows the theoretical predictions. The correlation was poor although at higher temperatures the experimental data and the theory paralleled each other. The same was true of the axial strain measurements and predictions as shown in Fig. 81. At 315°C the bending strain data had a spread of 15% of its average value while the axial strain spread was 31%. Tables 13 and 14 present the coefficients for the experimental bending strains and axial strains, respectively.

Combined Results

Of particular interest was the comparison between the results of the

high and low temperature range cycling. To compare the results, the high and low range experimental data for the bending and axial strain response of the various specimens were plotted on the same coordinate system.

Response of the Gages on Titanium Silicate

Since there were different gages on the titanium silicate, due to regaging, for the high temperature range cycles and the low temperature range cycles, a different apparent strain response was expected. However, as a matter of interest, the two sets of apparent strain response are plotted on a common coordinate in Fig. 82.

Flat $[0^\circ_8]$ Laminate

Figure 83 shows the thermal strain in the matrix direction for both the high and low temperature cycles. There appeared to be a difference in the overall slope for the two temperature ranges. Using a graphical approximation on the data, there appeared to be roughly a 10% difference in the overall slopes between the two temperature ranges. One explanation for the difference is as follows: the least-squares curves are an average of the heating and cooling strains at a given temperature. Hysteresis accounts for the differences between the two strains. During heating, the strains for the two temperature ranges were the same but, because of the higher temperature, the hysteresis loops were larger for the high temperature cycles. The cooling strains were thus lower, due to increased loop size, and the average was biased downward more for the higher temperature data than for the lower temperature data.

Curved $[0^\circ_4/90^\circ_4]$ Laminate

Figure 84 shows the least-squares bending strains for both tempera-

ture range cycles. It is interesting the two scattered high temperature cycles straddled the well-behaved low temperature cycles. Figure 85 displays the axial strains for the two temperature ranges. Again, the high temperature cycles bracketed the low temperature data. It should be mentioned the theory used for the high temperature cycles reflected the 10% difference between high and low temperature cycling overall slopes for the matrix direction thermal strain-temperature relation. Thus the high and low temperature theories, not shown together, were slightly different.

Curved $[0^\circ_2/90^\circ_2]$ Laminate

Figure 86 shows the bending strains for the high and low temperature cycles. The two sets of data followed the same general trends better than the bending strains of the 8-layer specimen. The axial strain comparison is shown in Fig. 87 and it appears the axial strains for the high temperature cycles were smaller than for the low temperature cycles. Although the correlation with the theory was poor for the thin specimen for both the high and low temperature cycling, experimental data from that specimen for the two temperature ranges were consistent.

Discussion of the Results

It seems appropriate to discuss the results in terms of the low temperature tests, the high temperature tests and then make some comments on the combined results.

Because of the stability and reliability of the strain gages during the RT-180°C cycling, the data from that series of tests is felt to be

quite accurate. The gages mounted on the titanium silicate indicated repeatibility and each gage on the titanium silicate showed similiar behavior. The thermal deformation-temperature relations are felt to accurately represent the behavior of graphite-polyimide laminates under the conditions of no mechanical load and repeated thermal load. It is apparent at a given temperature, the strain or deformation is a function of whether the laminate is being heated or cooled. The titanium silicate strain gage responses showed much less hysteresis than the gages mounted on the graphite-polyimide, indicating graphite-polymide exhibits hysteresis when heated and cooled.

For the flat specimen in the matrix direction, the scatter of the strains at the maximum temperature was comparable with the scatter in the measurements on the titanium silicate. Thus a meaningful temperature-dependent CTE for the matrix direction can be determined by differentiating the least-squares polynomial. In the fiber direction, the thermal strain measurements were not as reliable but certainly indicate the order of magnitude of the strains. From the data it was surprising to find the CTE in the fiber direction varied so much with temperature. In the matrix-direction, a constant CTE would be an excellent first-approximation.

The 8-layer curved specimen behaved much as the theory predicted and the temperature-strain relation could well be approximated by a straight line. However, the nonlinearity that was present was predictable. The scatter of data was the same order as the scatter on the titanium silicate and thus is felt to be reliable.

The behavior of the 4-layer specimen was not as predictable nor was the behavior from cycle to cycle as consistent as for the thicker

curved laminate. There was no obvious difference in the experimental set-up or the microstructure of the laminate compared to the 8-layer specimen. Perhaps four layers are not enough for classical lamination theory to be valid since for this case, half the layers are boundary layers and the other two layers are adjacent and have radically different properties in a given direction. The so-called laminate strain may not have had enough layers to develop. An extension of lamination theory was developed which allowed different transverse shear strains in each layer. The axial and bending strain of the outer layers (where the strain gages are mounted) depended on the first spatial derivative of the shear deformation. Except for possibly the ends of the beams, the shear deformations were constant along the length. Thus the shear contributed nothing to the bending and axial strain measures. Because of the experimental results obtained, it seems more work needs to be done, theoretically and experimentally, with thin laminates.

Generally speaking, the data from the high temperature cycling was not as reliable as the data from the low temperature cycling. Thus firm conclusions cannot be drawn. However, again there was evidence the strain depended on whether the specimen was being heated or cooled. The scatter of the data from the titanium silicate was larger than for the low temperature tests but was still under 10%. This is significant because it indicates some degree of repeatibility and stability of the gages themselves at the high temperatures.

For the flat specimen, in the matrix direction, the scatter of the data was also less than 10%. This results in useful CTE information in the matrix directions at high temperatures. Meaningful data in the fiber direction can only be obtained with a higher resolution technique such as

interferometry.

The 8-layer curved laminate behaved more erratically during the high temperature cycling than during the low temperature cycling. It is interesting to note the theoretical results indicated a slight reversal of curvature for the bending strain-temperature relation. This was due to an interaction between a softening E_{22} and the changing CTE's as the temperature increased. There was considerable spread in the data from the two cycles although the axial strains were more consistent than the bending strains. Based on the troubles with the gages mounted on the graphite-polyimide, as opposed to those mounted on the titanium silicate, the data should be viewed with caution.

During the high temperature tests, the 4-layer curved laminate behaved in much the same manner as in the low temperature tests. Some unaccounted-for mechanism caused wide deviations from theoretical predictions. In addition, strain gage problems probably contributed to much of the data scatter from run to run.

One of the issues to be addressed in the study was the effects of maximum temperature. The effects could be assessed by comparing data from the two cycling temperatures. Unfortunately the issue of reliability of the measurements for a majority of the high temperature cycles limits the conclusions which can be drawn regarding the effect of maximum temperature. The flat specimen behaved similarly for both temperature ranges. The 8-layer specimen exhibited considerable scatter although the high temperature results bracketed the low temperature results. For the thinner specimens, the higher temperature data showed a slightly different overall temperature-strain relation manifested by what could be considered differences in overall slopes to the relation. From all this, however, there is no reliable evidence to support any hypothesis.

Concluding Remarks

Overall, it is felt the experimental results from the low temperature tests were sound. It can be said that in the temperature range 20°-180°C, (1) for a given temperature, the thermal deformation depended on whether the specimen was being heated or cooled, (2) there was no evidence to indicate, using strain gages, thermal cycling affected the temperature-thermal deformation relation from one cycle to the next and, (3) for the thicker curved specimen, lamination theory predicted the response. Why the 4-layer specimen behaved the way it did is another issue. The results from the majority of the high temperature tests are open to question, at least from a quantitative aspect. The use of strain gages on composites at these temperatures is questionable. At the temperature extremes used, the gage adhesive may soften, there may be localized softening of the matrix near the gage and the resistivity of the electrical connections may change. In addition, large strain levels can be experienced with composites and this coupled with high temperatures may put a severe burden on the gage bond. It is felt much work needs to be done on strain gages as they are applied to composites, in particular, high temperature composites. In lieu of this, optical methods of measuring deformations should be explored as should the notion of using microcomputers to control the thermal cycling and acquire the data. In this way, high quality, long duration testing can be conducted conveniently.

References

1. Woods, A. A., Jr. and Karal, M., Considerations on the Use of Graphite-Reinforced Plastics for Space-Erectable Antennas, 7th Communications Satellite Systems Conference, AIAA, April 24-27, 1978, paper no. 78-591.

2. Nelson, Paul T. and Krim, Michael H., A Thermally Inert Cylindrical Truss Concept, Third Conference on Fibrous Composites in Flight Vehicle Design, NASA TM X-3377, April 1976, pp. 275-304.

3. Lightfoot, M. C. and Hyer, M. W., GILSA: General Interactive Least-Squares Analysis, Old Dominion University Research Foundation Report, June 1978.

4. Jones, R. M., Mechanics of Composite Materials, McGraw-Hill Publishers, New York, 1975.

Table 1

Room Temperature Out-of-Plane Displacements of Curved Specimens

$$W_0 = C_0 + C_1X + C_2X^2 + C_3X^3$$

4-Layer Specimen

C_0	C_1	C_2	C_3	
.359E-01	.766E-03	.114E-03	-.576E-06	$-76 \leq X \leq +76$
				W, X in mm
.219E-02	.756E-03	.289E-01	-.370E-03	$-3 \leq X \leq +3$
				W, X in in.

8-Layer Specimen

C_0	C_1	C_2	C_3	
.964E-02	-.425E-02	.105E-02	-.780E-07	$-76 \leq X \leq +76$
				W, X in mm
.380E-03	-.425E-02	.268E-01	-.503E-04	$-3 \leq X \leq +3$
				W, X in in.

Table 2

Apparent Strain vs Temperature for Gages on Titanium Silicate, RT-180°C

$$\varepsilon_{apparent} = C_0 + C_1T + C_2T^2 + C_3T^3$$

Cycle No.	C_0	C_1	C_2	C_3
1	192.9	-6.733	-.03869	.5361E-04
2	215.01	-7.669	-.02992	.2653E-04
3	227.4	-9.013	-.01551	-.1652E-04
4	255.3	-8.778	-.01878	-.8345E-04
5	196.1	-6.682	-.03768	.4296E-04
6	293.1	-8.621	-.01807	-.1492E-04
7	211.3	-7.460	-.03189	.3222E-04
8	192.7	-7.189	-.03569	.4588E-04
9	217.0	-7.633	-.02993	.2619E-04
10	178.4	-7.506	-.03084	.2500E-04
11	206.2	-7.118	-.03396	.3267E-04
12	197.3	-7.605	-.02982	.2150E-04
13	201.6	-7.571	-.02935	.1710E-04
14	161.5	-6.514	-.0407	.5329E-04
15	141.9	-5.935	-.04178	.4764E-04

Table 3

Thermal Expansion of Flat $[0_8^\circ]$ Laminate in Matrix Direction, RT-180°C

$$\varepsilon_{thermal} = C_0 + C_1T + C_2T^2$$

Cycle No.	C_0	C_1	C_2
1	-944.7	28.23	.01151
2	-725.3	23.95	.02876
3	-793.1	25.43	.02276
4	-653.0	23.11	.03064
5	-1108.0	27.30	.01737

Table 4

Thermal Expansion of Flat $[0_8^\circ]$ Laminate in Fiber Direction, RT-180°C

$$\varepsilon_{thermal} = C_0 + C_1T + C_2T^2$$

Cycle No.	C_0	C_1	C_2
1	25.81	-.8440	.005345
2	15.75	-.3275	.002562
3	18.84	-.4174	.003067
4	19.59	-.4368	.003067
5	14.45	-.5323	.003526

Table 5

Thermal Bending Strain vs Temperature for Curved $[0^\circ_4/90^\circ_4]$ Laminate, RT-180°C

$$\varepsilon_{\substack{\text{thermal}\\ \text{bending}}} = C_0 + C_1T + C_2T^2$$

Cycle No.	C_0	C_1	C_2
1	-342.16	9.868	.005811
2	-344.27	10.62	.002370
3	-368.4	11.54	-.001953
4	-284.85	9.496	.007645
5	-304.7	9.129	.009722

Table 6

Thermal Axial Strain vs Temperature for Curved $[0^\circ_4/90^\circ_4]$ Laminate, RT-180°C

$$\varepsilon_{\substack{\text{thermal}\\ \text{axial}}} = C_0 + C_1T + C_2T^2$$

Cycle No.	C_0	C_1	C_2
1	-239.0	6.933	.005122
2	-248.5	7.590	.002512
3	-257.0	8.074	.0002748
4	-176.6	6.192	.009351
5	-218.3	6.379	.008506

Table 7

Thermal Bending Strain vs Temperature for Curved $[0_2^\circ/90_2^\circ]$ Laminate, RT-180°C

$$\varepsilon_{\substack{\text{thermal}\\ \text{bending}}} = C_0 + C_1T + C_2T^2$$

Cycle No.	C_0	C_1	C_2
1	-63.28	1.0960	.01164
2	-34.64	0.5975	.01388
3	-45.67	0.6842	.01380
4	-153.00	1.8670	.00690
5	-168.90	1.7110	.01160

Table 8

Thermal Axial Strain vs Temperature for Curved $[0_2^\circ/90_2^\circ]$ Laminate, RT-180°C

$$\varepsilon_{\substack{\text{thermal}\\ \text{axial}}} = C_0 + C_1T + C_2T^2$$

Cycle No.	C_0	C_1	C_2
1	-121.7	2.300	.01290
2	-68.48	2.044	.01456
3	-76.96	1.878	.01544
4	-244.1	3.189	.007302
5	-213.8	2.237	.01334

Table 9

Apparent Strain vs Temperature for
Gages on Titanium Silicate,
RT-315°C

$$\varepsilon_{apparent} = C_0 + C_1T + C_2T^2 + C_3T^2$$

Cycle No.	C_0	C_1	C_2	C_3
1	209.7	-5.864	-.03714	.4585E-04
2	221.1	-6.970	-.02855	.2915E-04
3	217.9	-8.365	-.01281	.8956E-07
4	262.2	-9.80[illegible]	-.00254	-.1633E-04
5	271.8	-10.26	.00266	-.2893E-04

Table 10

Thermal Expansion of Flat $[0_8^\circ]$ Laminate in Matrix Direction,
RT-315°C

$$\varepsilon_{thermal} = C_0 + C_1T + C_2T^2$$

Cycle No.	C_0	C_1	C_2
1	-622.9	19.63	.02506
2	-702.0	22.62	.02167
3	-678.3	22.22	.02024
4	-605.7	20.88	.02005
5	-558.3	20.12	.02376

Table 11

Thermal Bending Strain vs Temperature for Curved $[0^\circ_4/90^\circ_4]$ Laminate, RT-315°C

$$\varepsilon_{\substack{\text{thermal}\\ \text{bending}}} = C_0 + C_1T + C_2T^2$$

Cycle No.	C_0	C_1	C_2
1	-289.8	8.310	.008849
2	-258.3	8.740	.01574

Table 12

Thermal Axial Strain vs Temperature for Curved $[0^\circ_4/90^\circ_4]$ Laminate, RT-315°C

$$\varepsilon_{\substack{\text{thermal}\\ \text{axial}}} = C_0 + C_1T + C_2T^2$$

Cycle No.	C_0	C_1	C_2
1	-240.1	6.198	.006753
2	-309.2	9.2627	-.002175

Table 13

Thermal Bending Strain vs Temperature for Curved $[0_2^\circ/90_2^\circ]$ Laminate

RT-315°C

$$\varepsilon_{\substack{\text{thermal}\\ \text{bending}}} = C_0 + C_1T + C_2T^2$$

Cycle No.	C_0	C_1	C_2
1	-.7424	-1.554	.02192
2	-10.107	.3103	.01739
3	27.2	-.5090	.1765

Table 14

Thermal Axial Strain vs Temperature for Curved $[0_2^\circ/90_2^\circ]$ Laminate

RT-315°C

$$\varepsilon_{\substack{\text{thermal}\\ \text{axial}}} = C_0 + C_1T + C_2T^2$$

Cycle No.	C_0	C_1	C_2
1	-50.15	.3906	.01208
2	-73.9	2.254	.00800
3	-8.607	.8088	.008064

Fig. 1 Curved Specimens

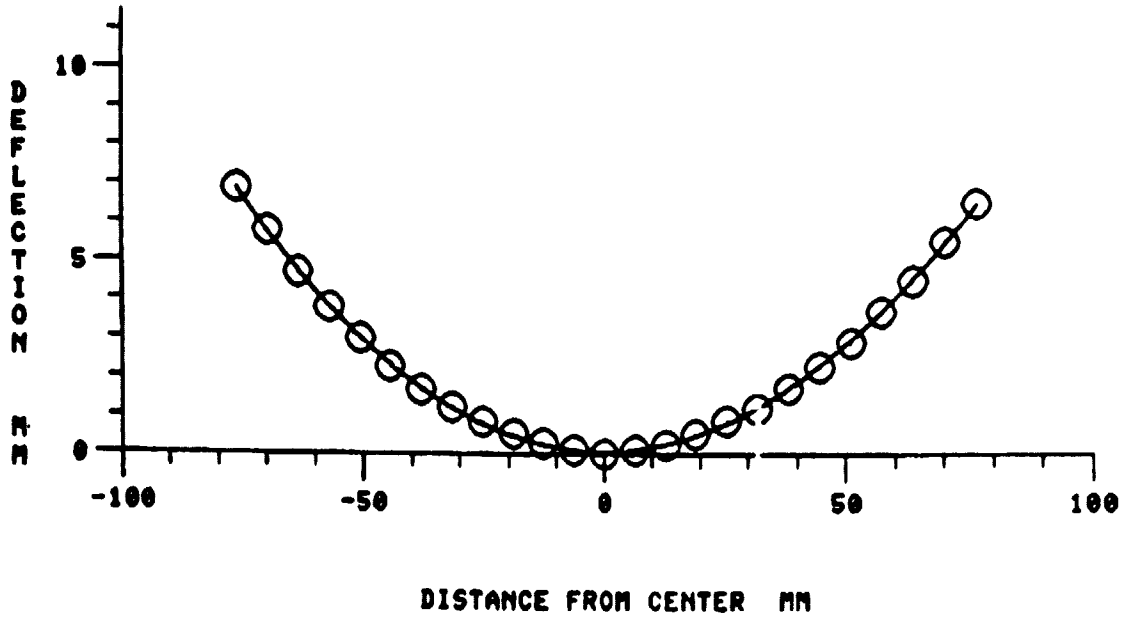

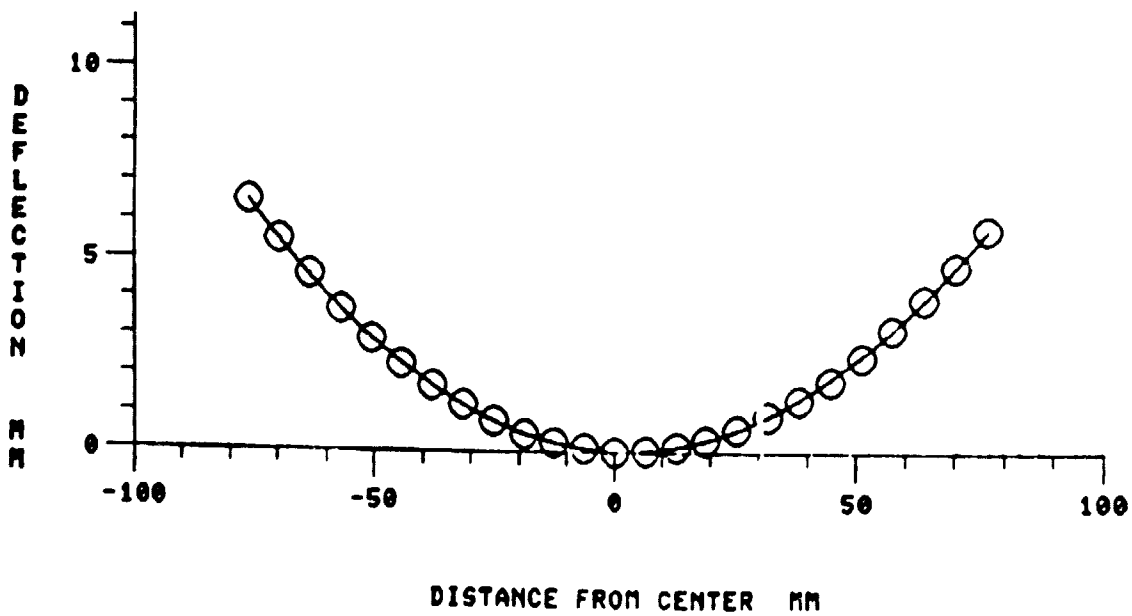

Fig. 2 Initial Out-of-Plane Displacements for 4-layer (top) and 8-layer (bottom) Curved Specimens

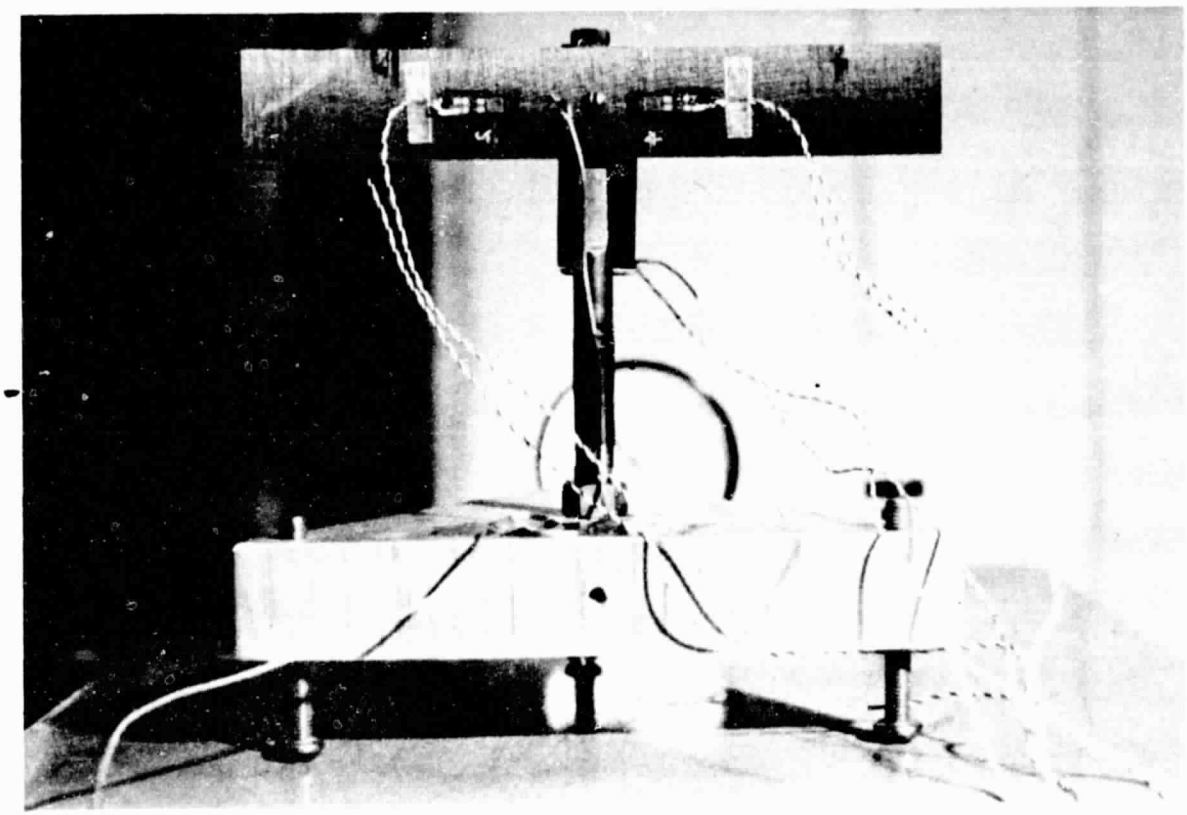

Fig. 3 Tripod Used for Supporting Specimens

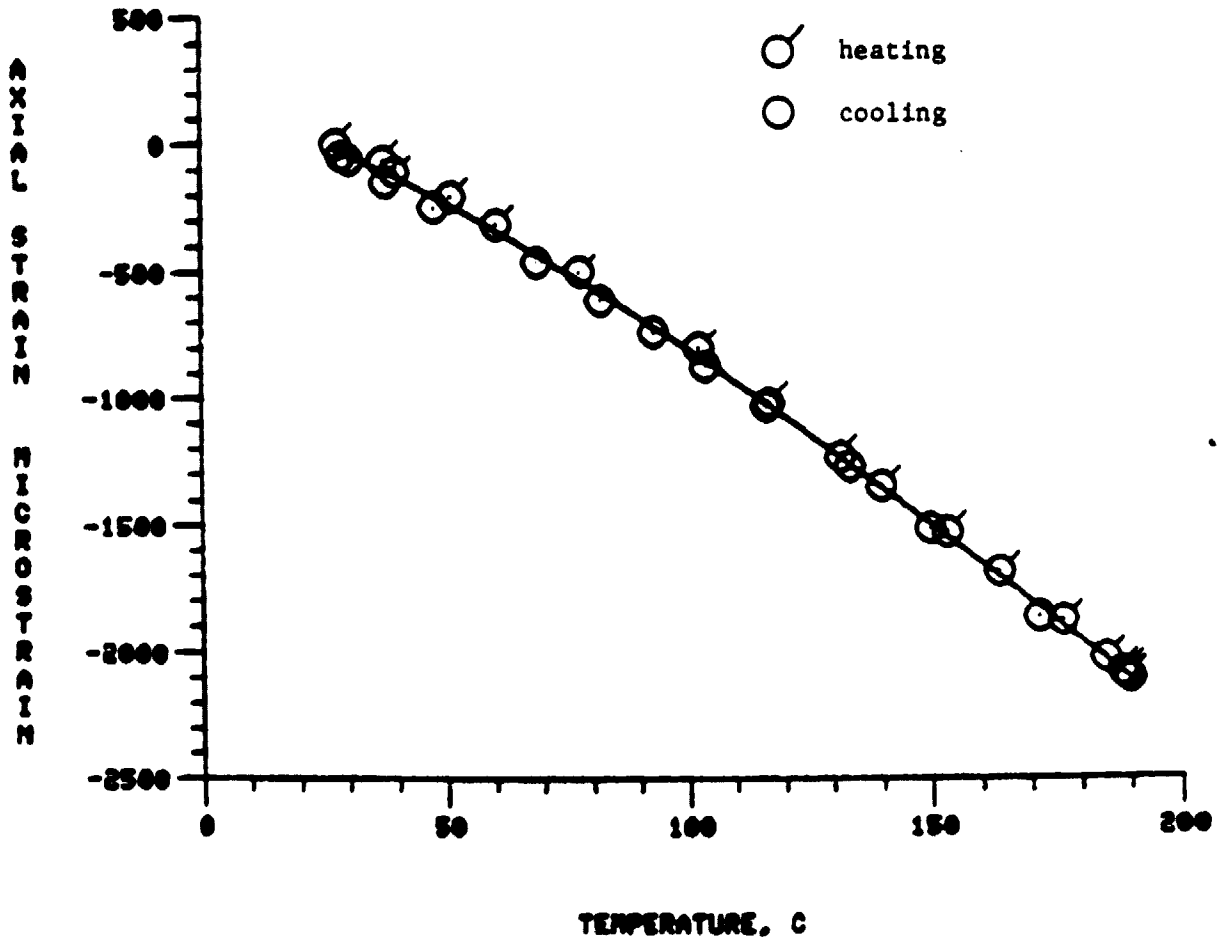

Fig. 4 Apparent Strain vs. Temperature, RT-180°C, Cycle 1

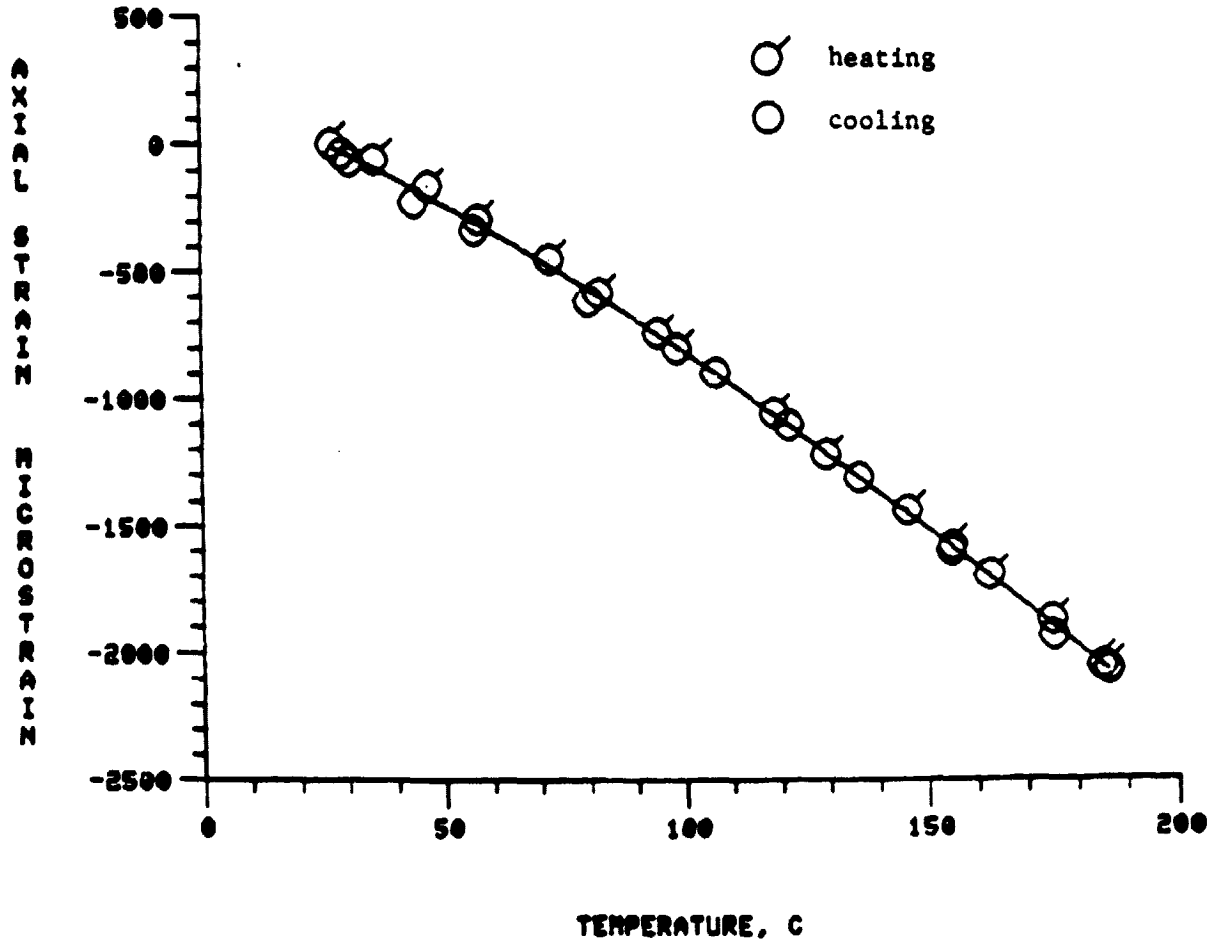

Fig. 5 Apparent Strain vs. Temperature, RT-180°C, Cycle 2

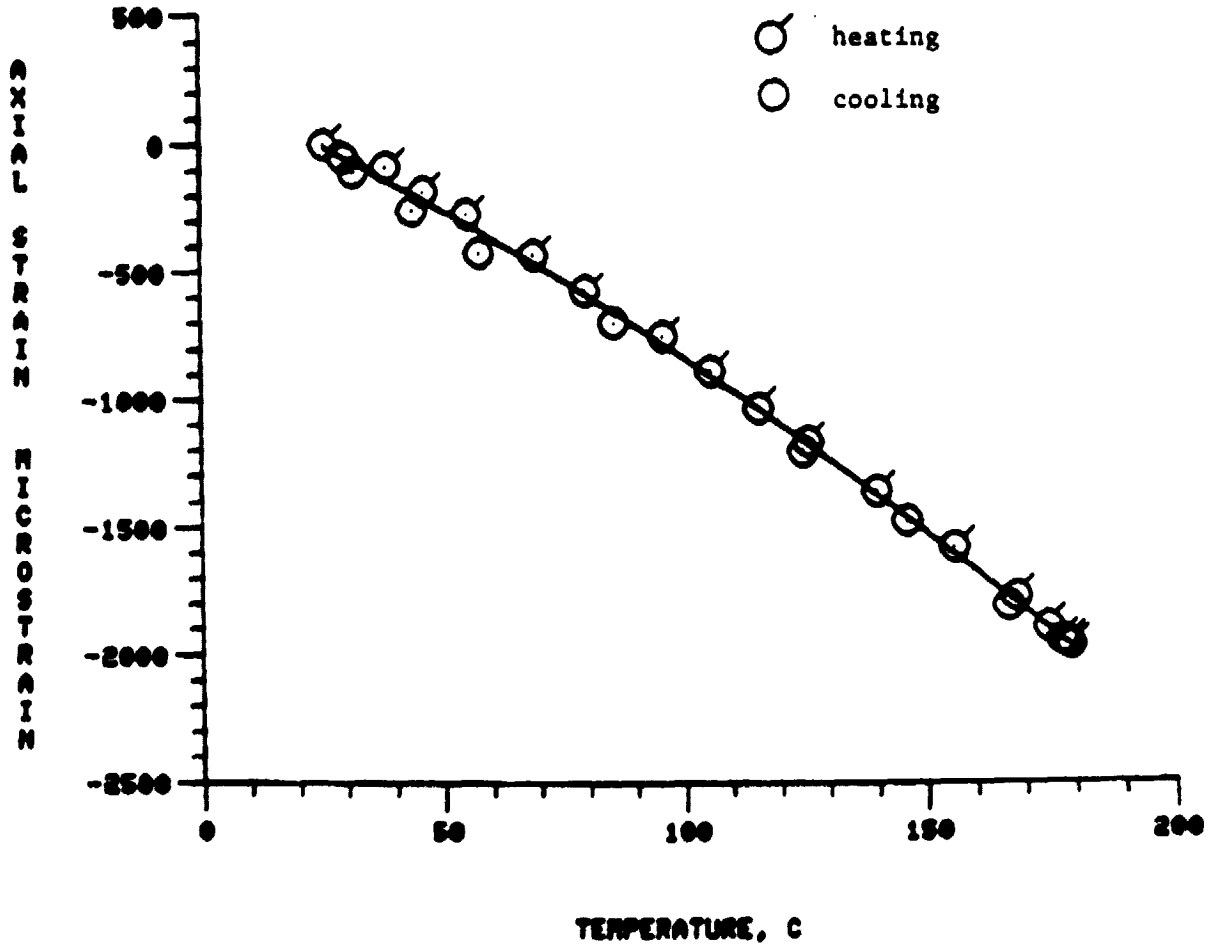

Fig. 6 Apparent Strain vs. Temperature, RT-180°C, Cycle 3

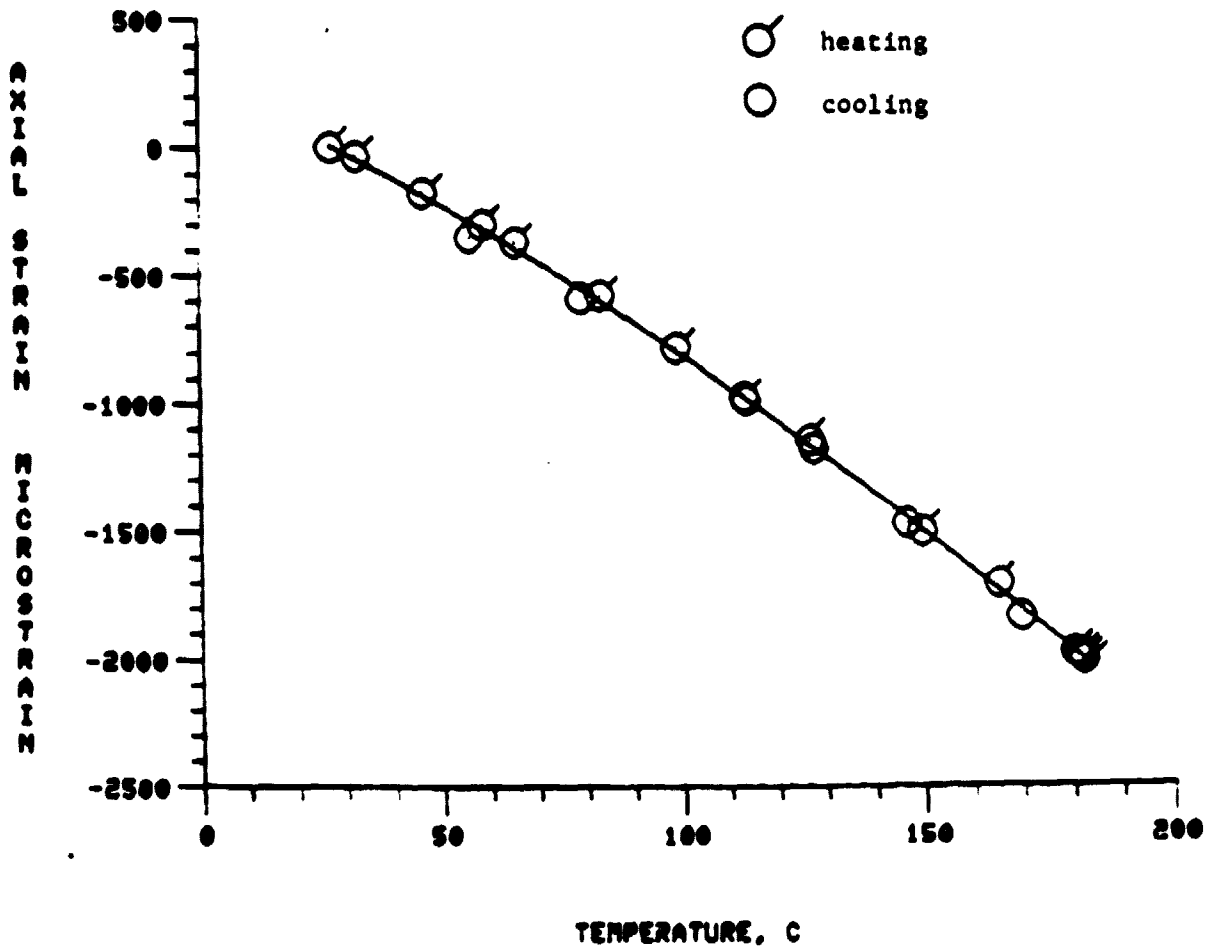

Fig. 7 Apparent Strain vs. Temperature, RT-180°C, Cycle 4

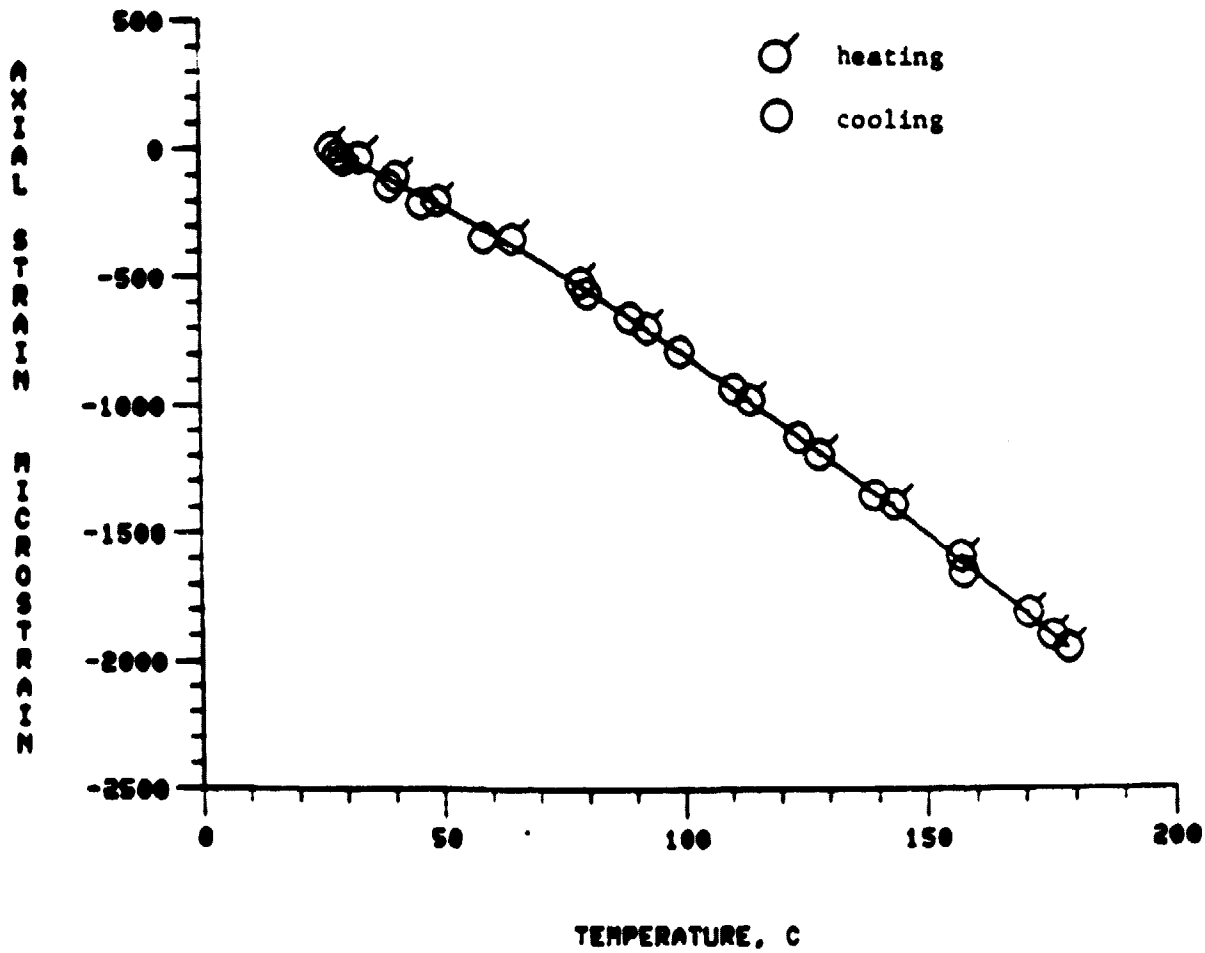

Fig. 8 Apparent Strain vs. Temperature, RT-180°C, Cycle 5

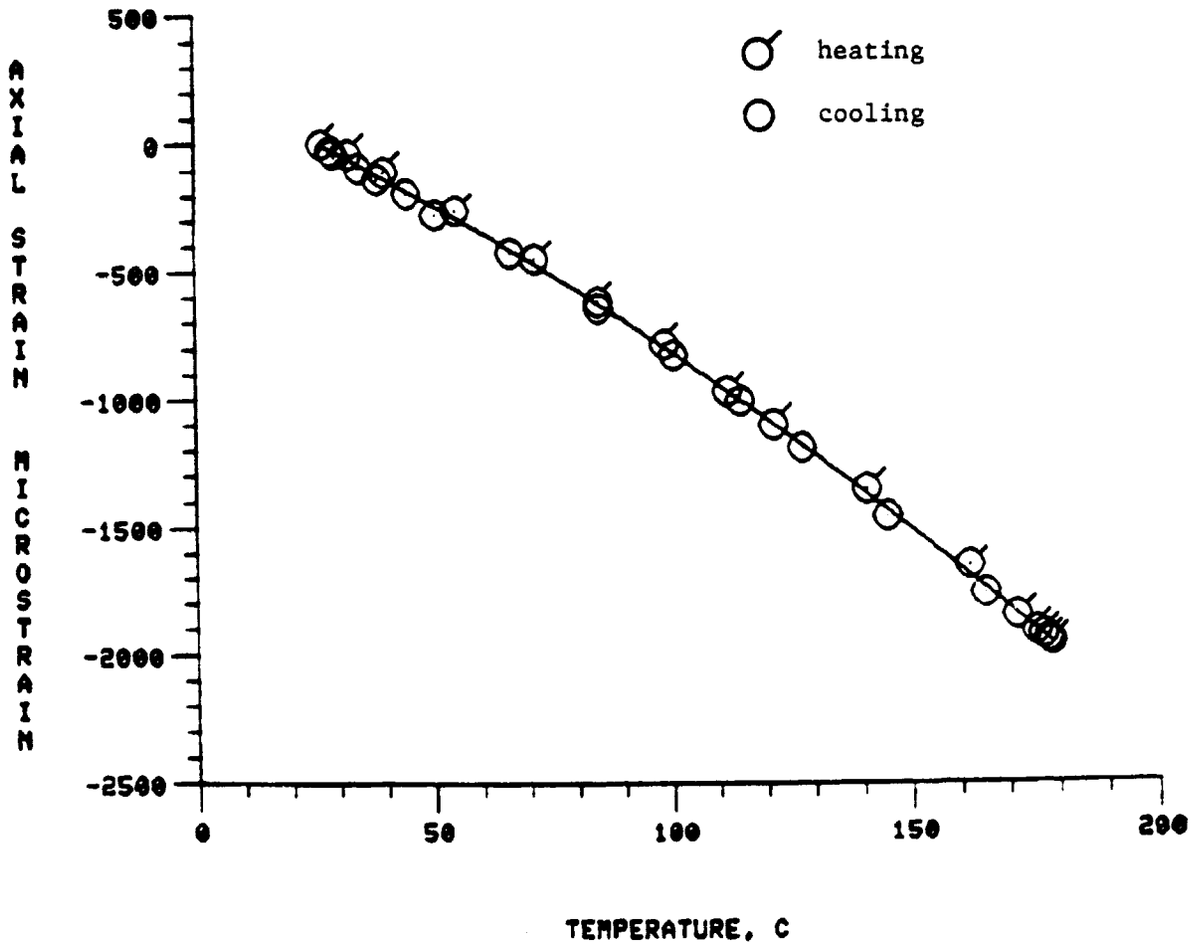

Fig. 9 Apparent Strain vs. Temperature, RT-180°C, Cycle 6

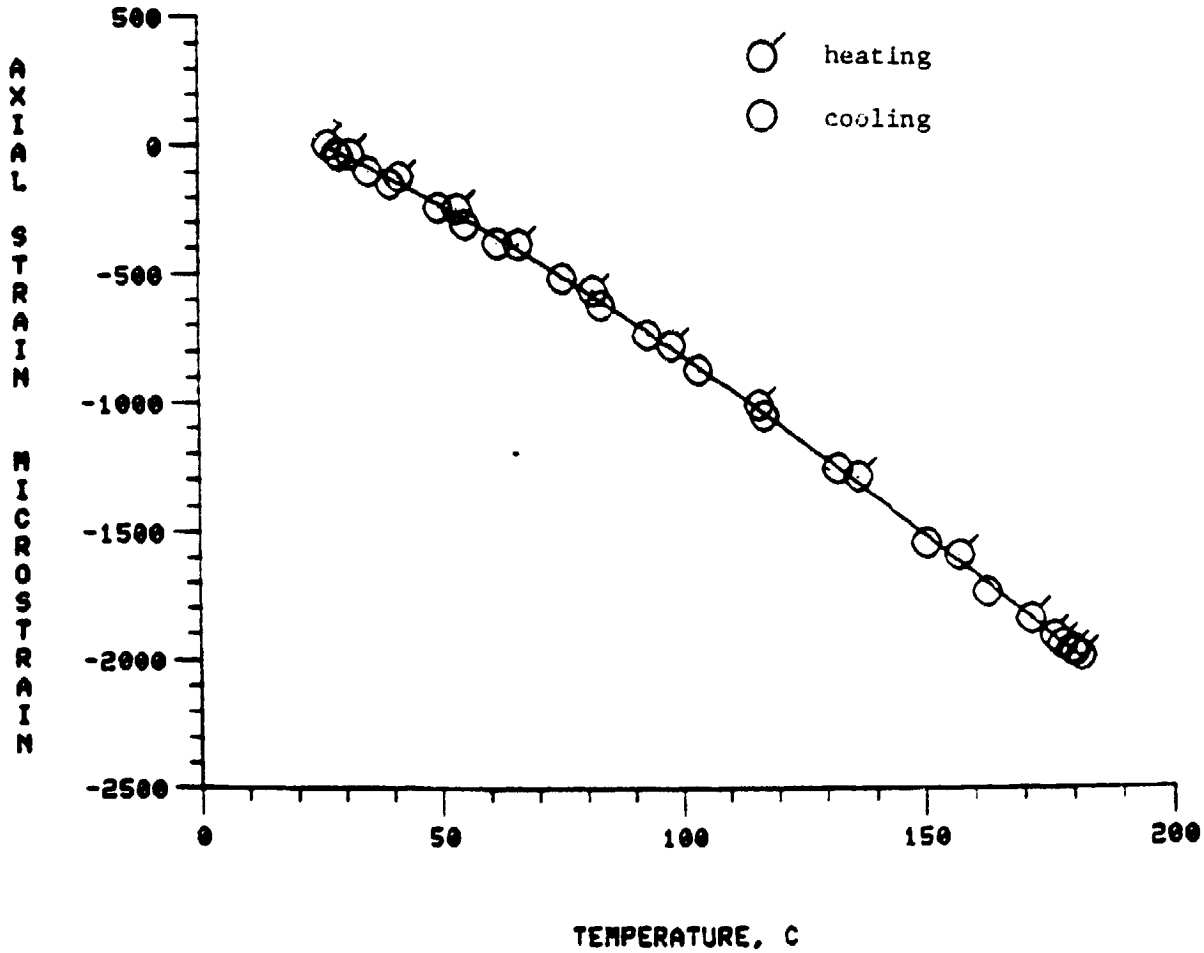

Fig. 10 Apparent Strain vs. Temperature, RT-180°C, Cycle 7

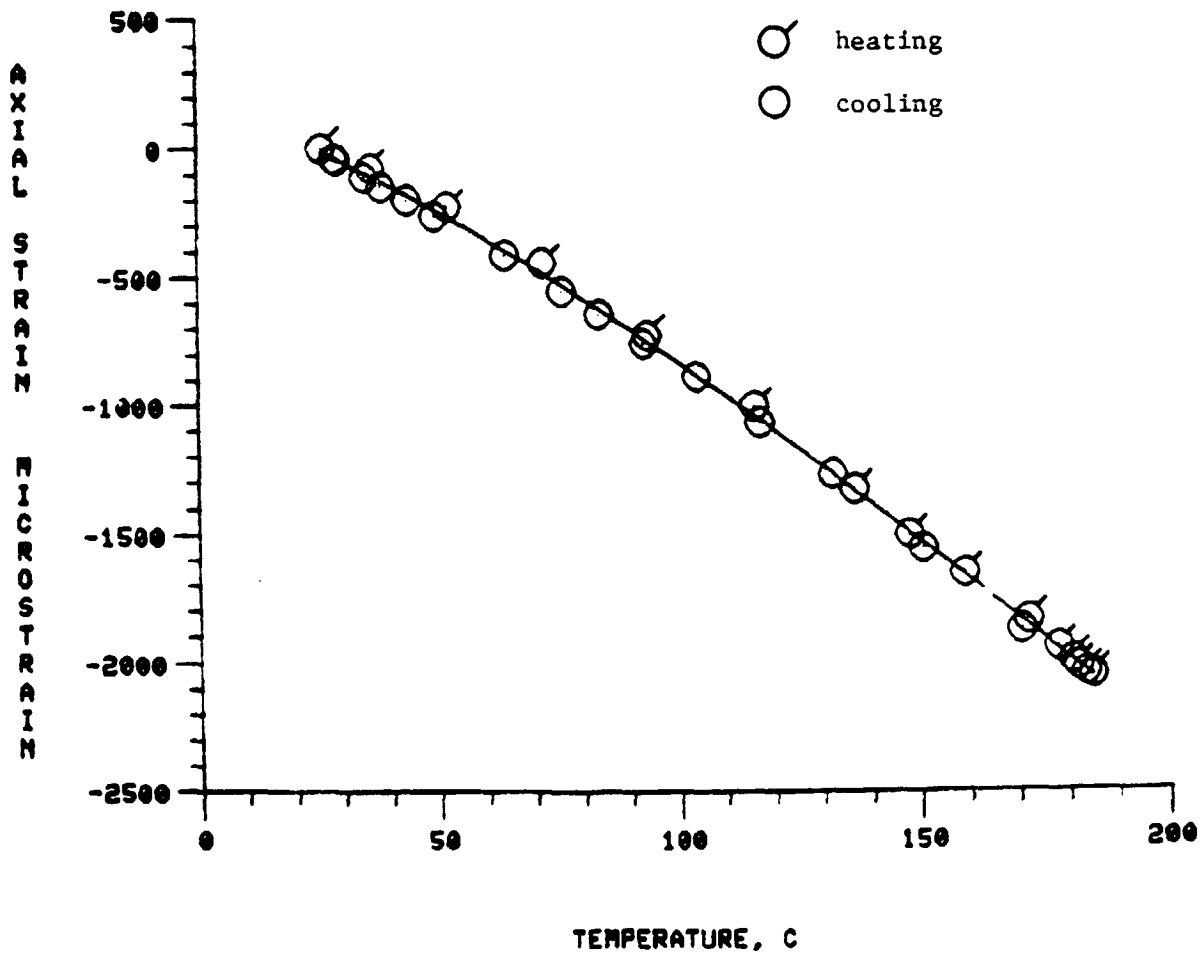

Fig. 11 Apparent Strain vs. Temperature, RT-180°C, Cycle 8

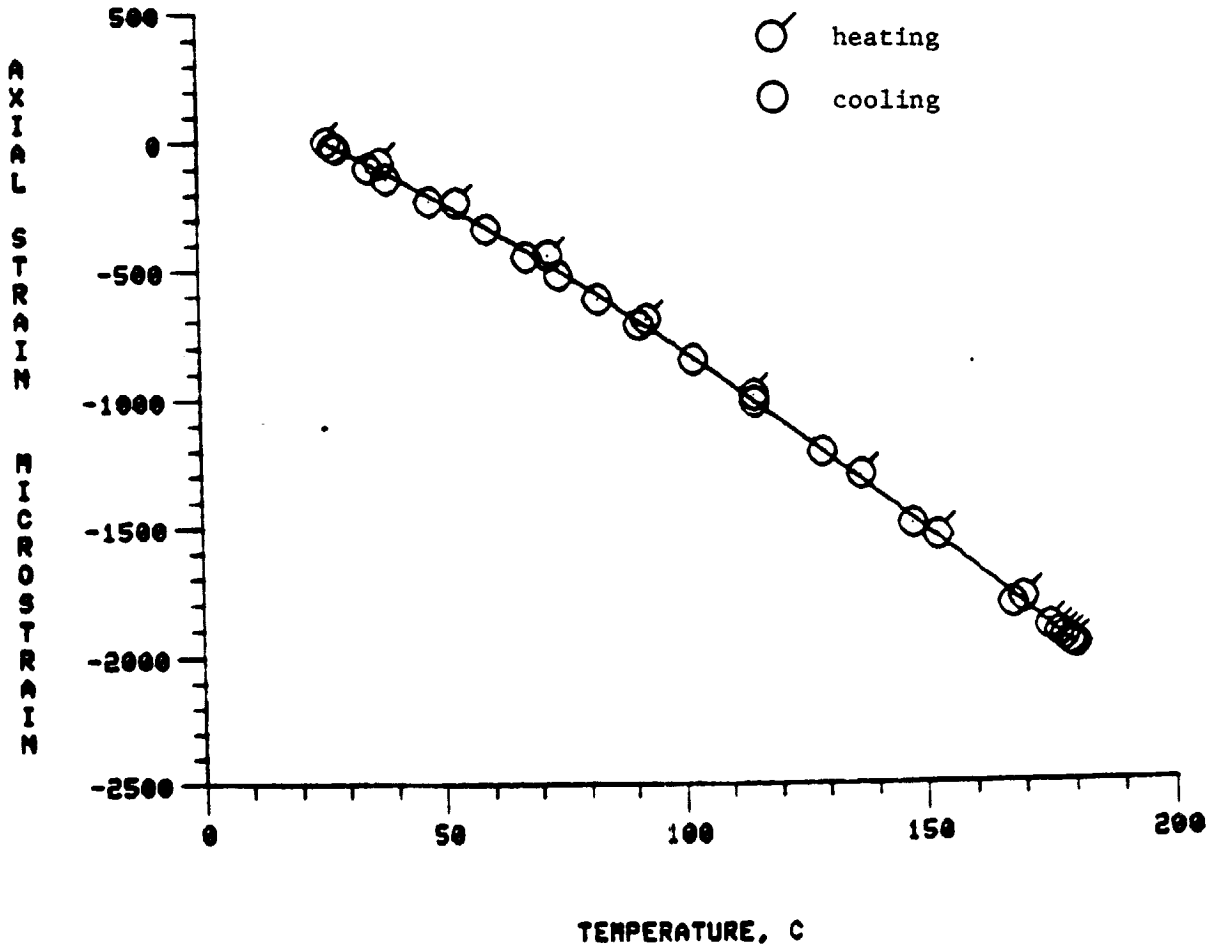

Fig. 12 Apparent Strain vs. Temperature, RT-180°C, Cycle 9

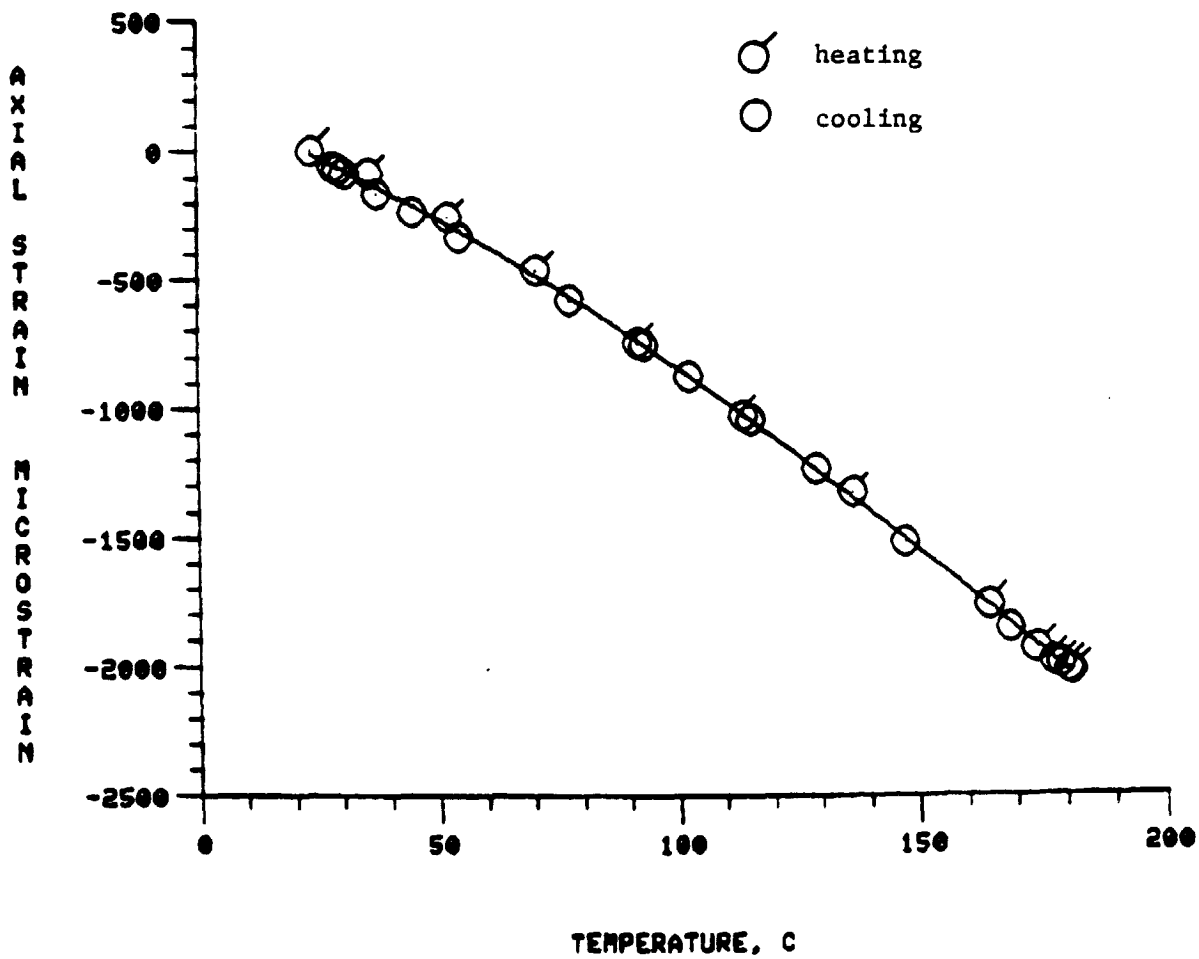

Fig. 13 Apparent Strain vs. Temperature, RT-180°C, Cycle 10

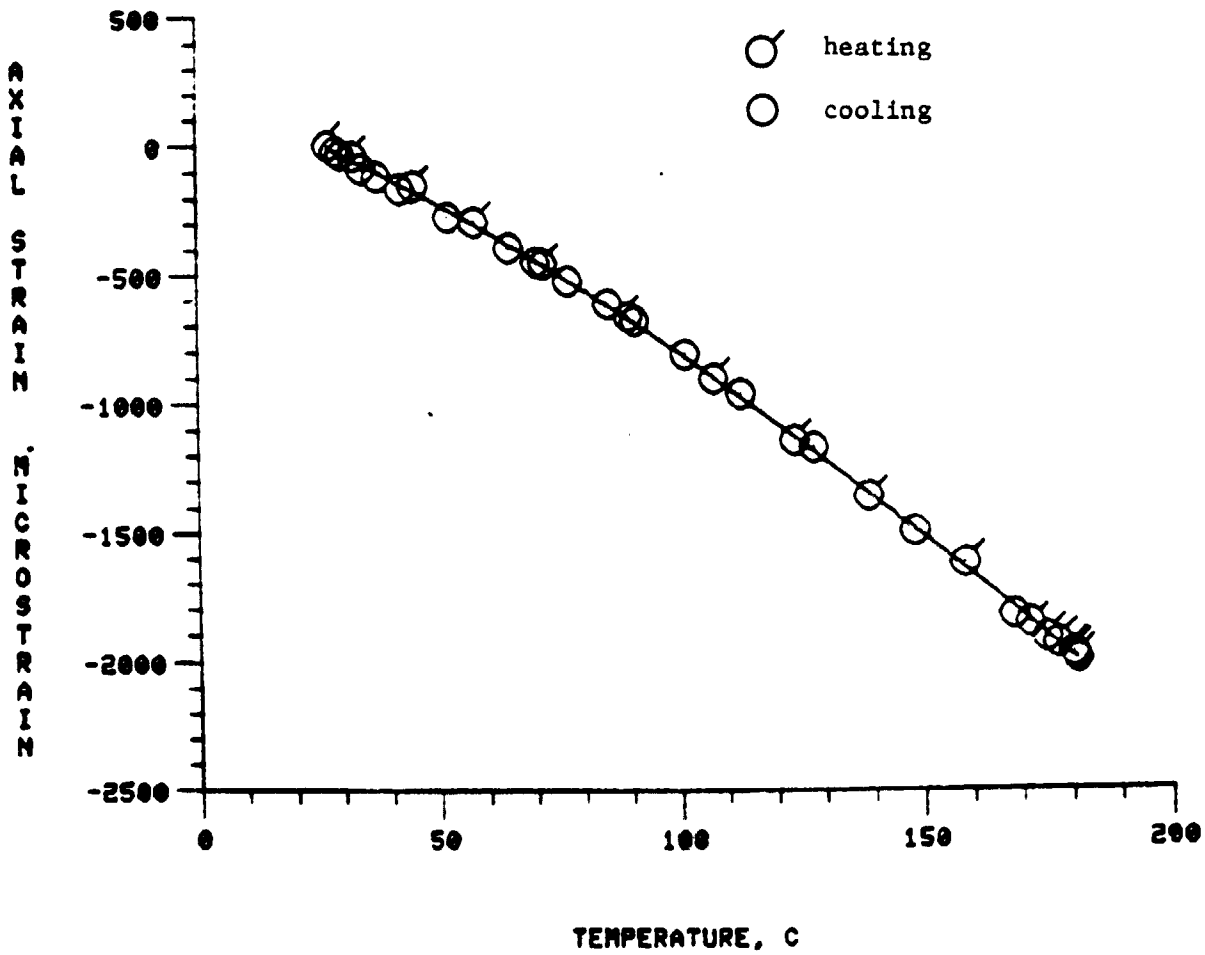

Fig. 14 Apparent Strain vs. Temperature, RT-180°C, Cycle 11

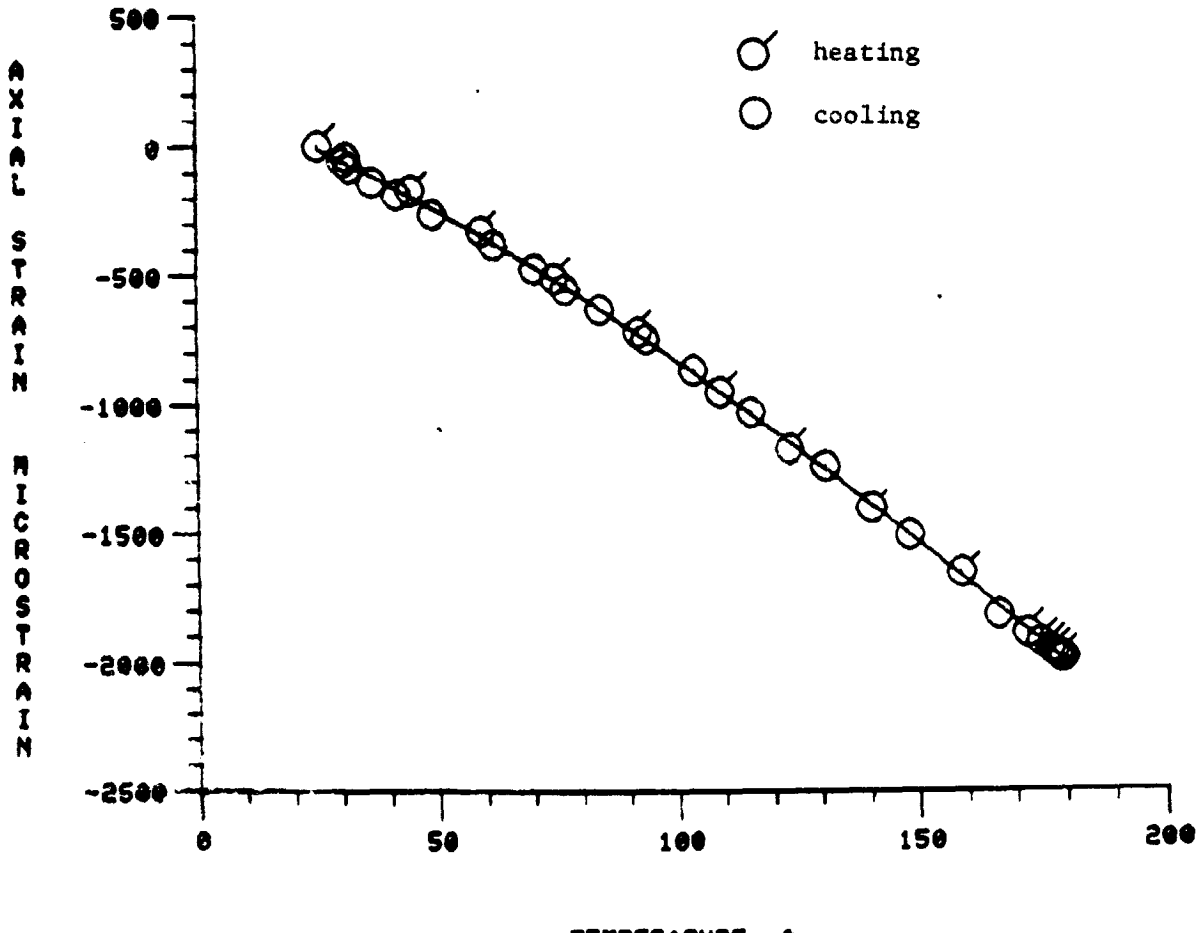

Fig. 15 Apparent Strain vs. Temperature, RT-180°C, Cycle 12

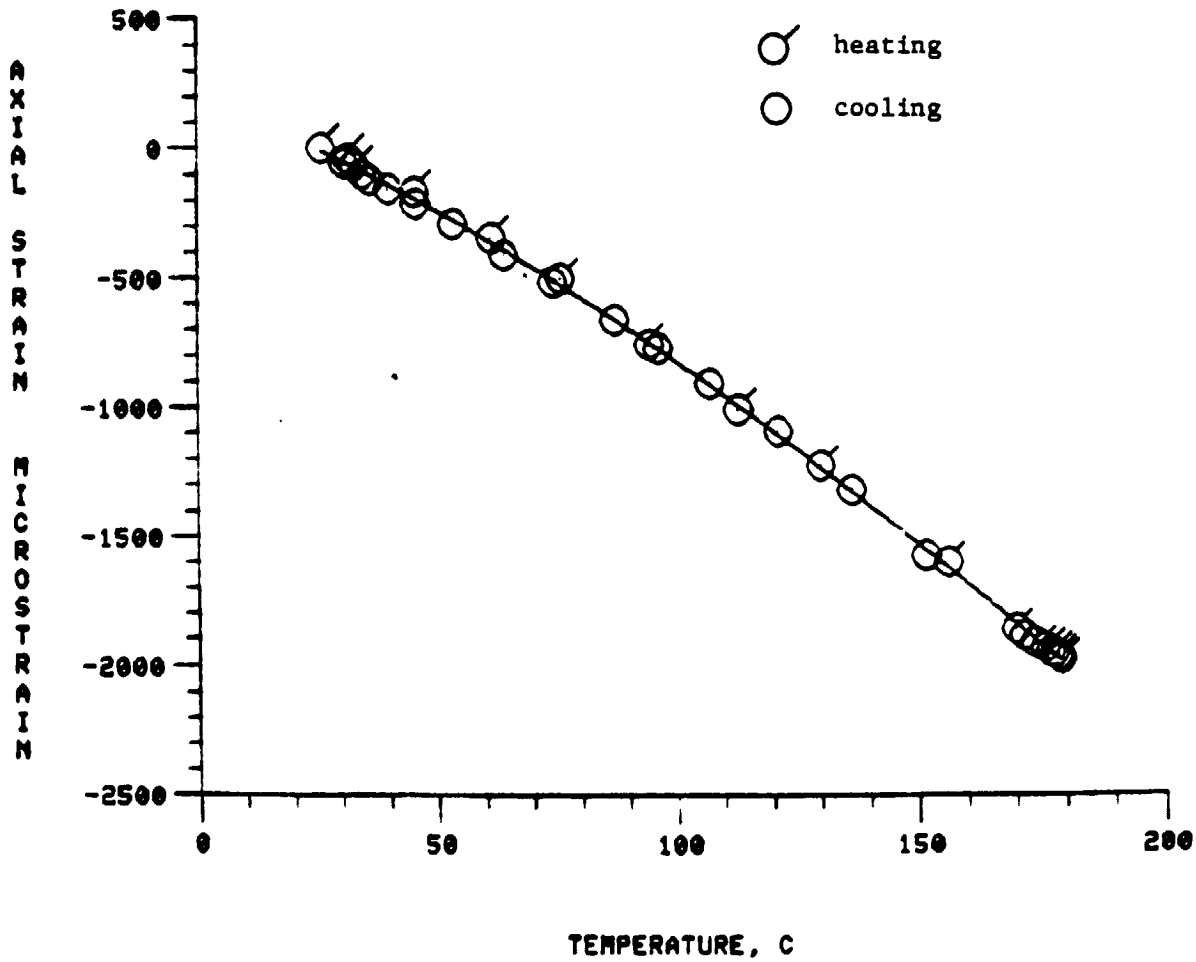

Fig. 16 Apparent Strain vs. Temperature, RT-180°C, Cycle 13

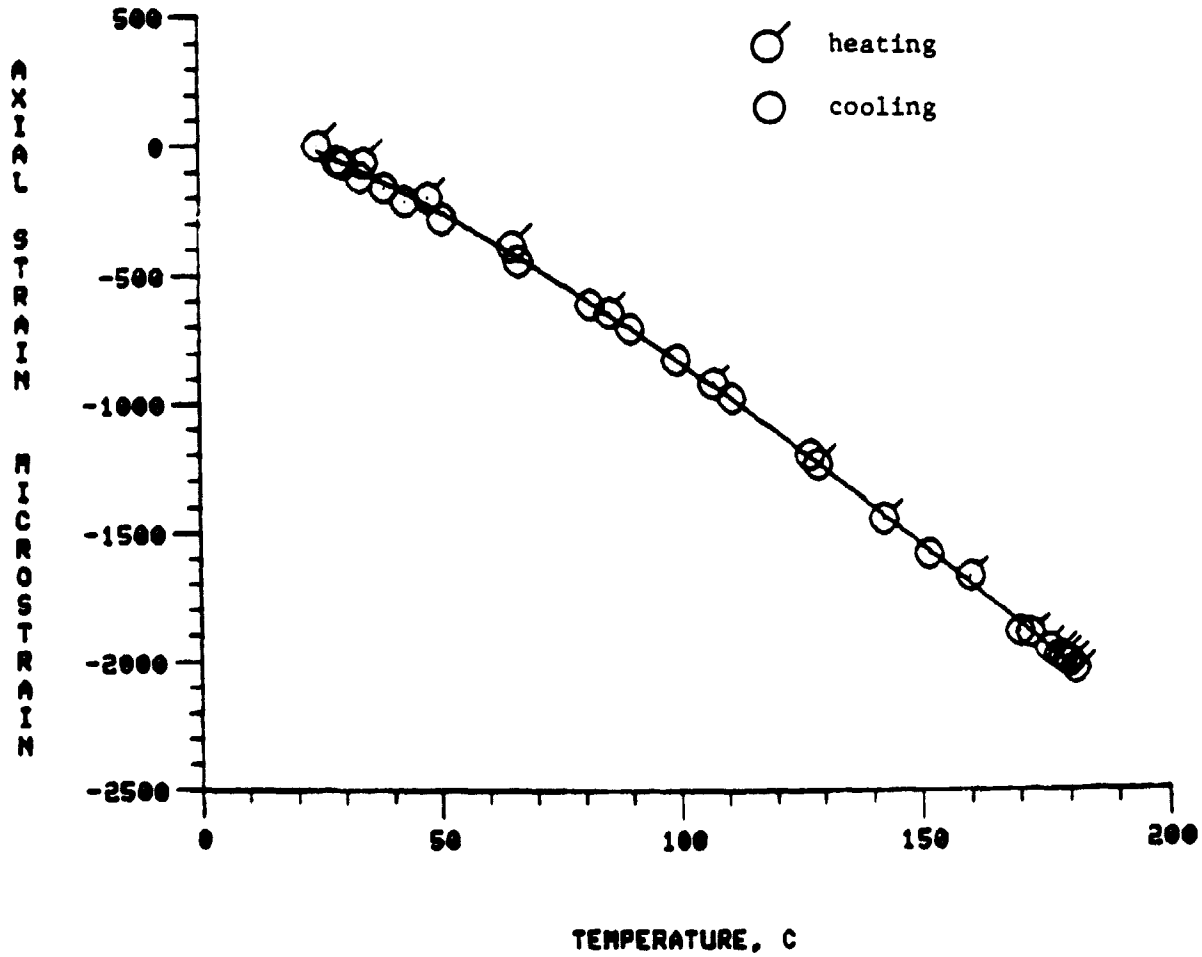

Fig. 17 Apparent Strain vs. Temperature, RT-180°C, Cycle 14

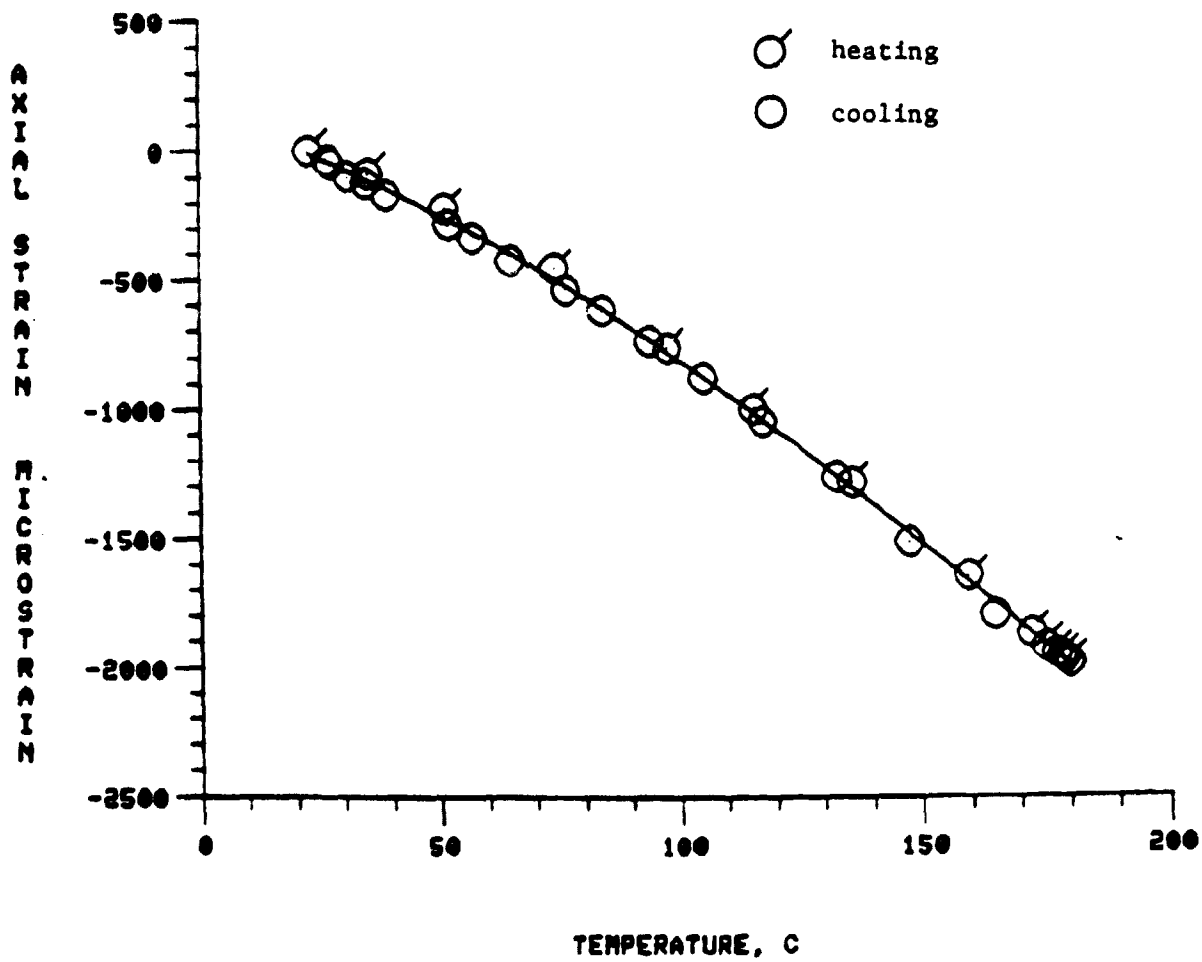

Fig. 18 Apparent Strain vs. Temperature, RT-180°C, Cycle 15

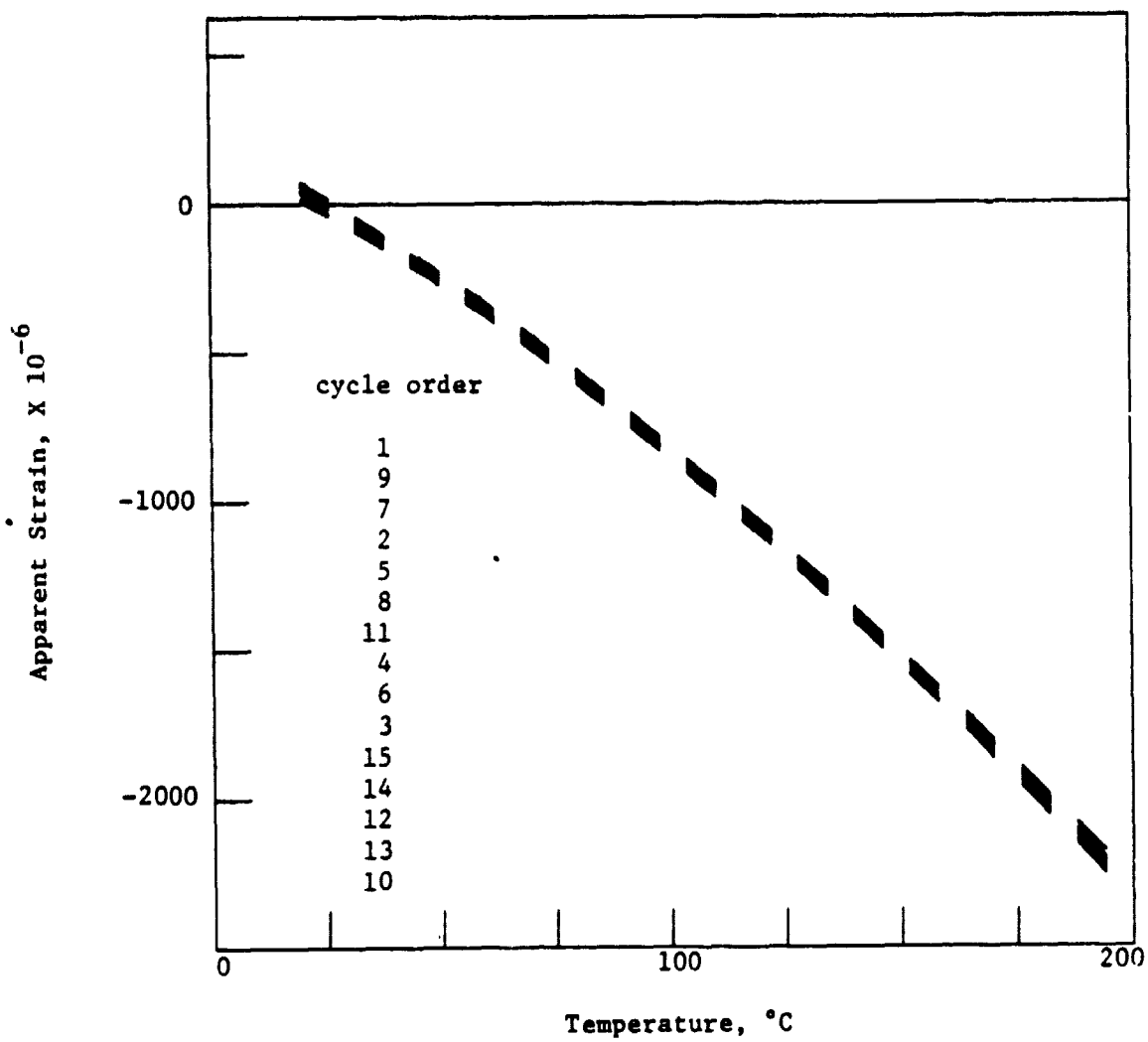

Fig. 19 Apparent Strain vs. Temperature, RT-180°C, Least-Squares Fit, All 15 Cycles

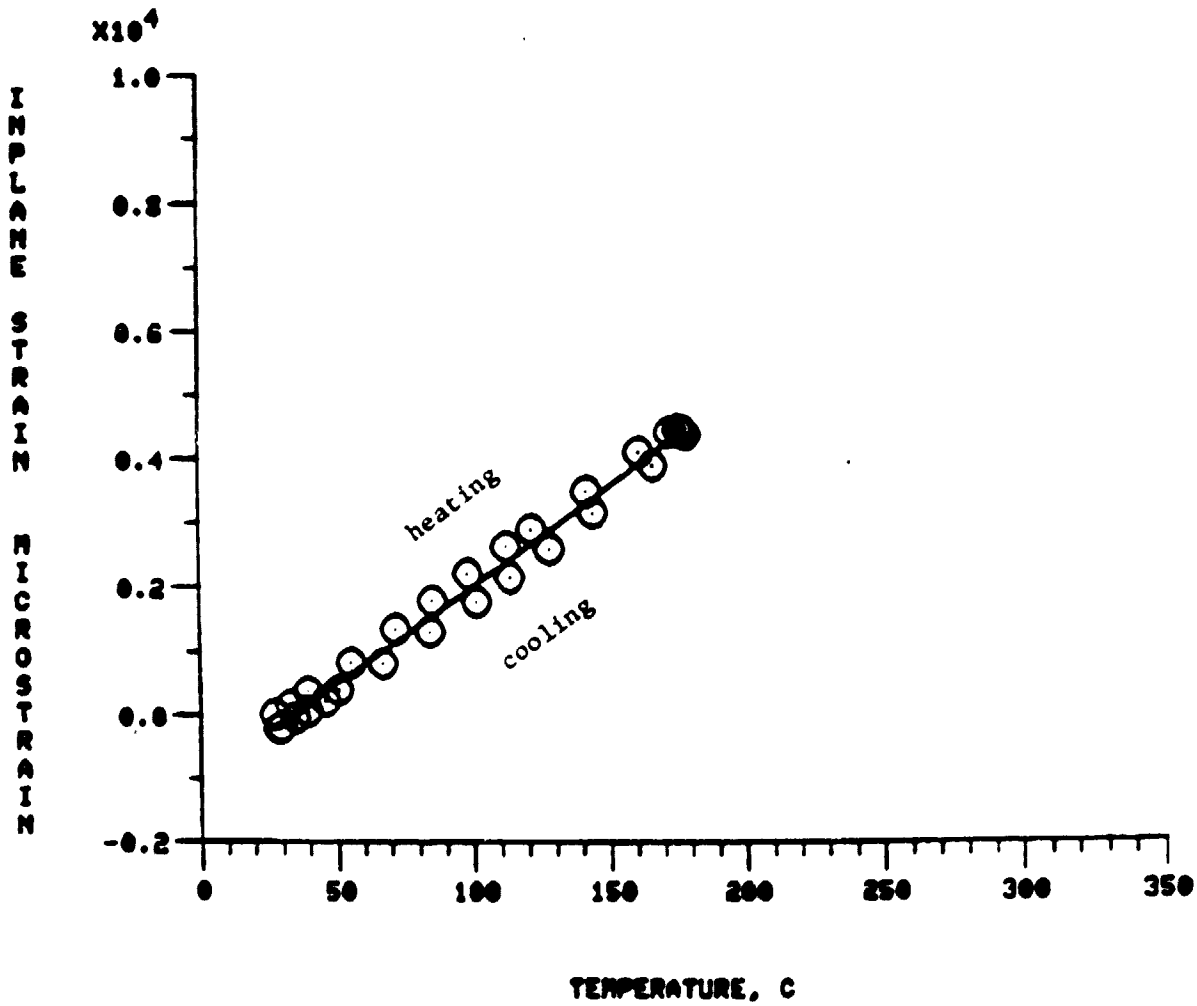

Fig. 20 Thermal Expansion of $[0_8^\circ]$ Laminate in Matrix Direction RT-180°C, Cycle 1

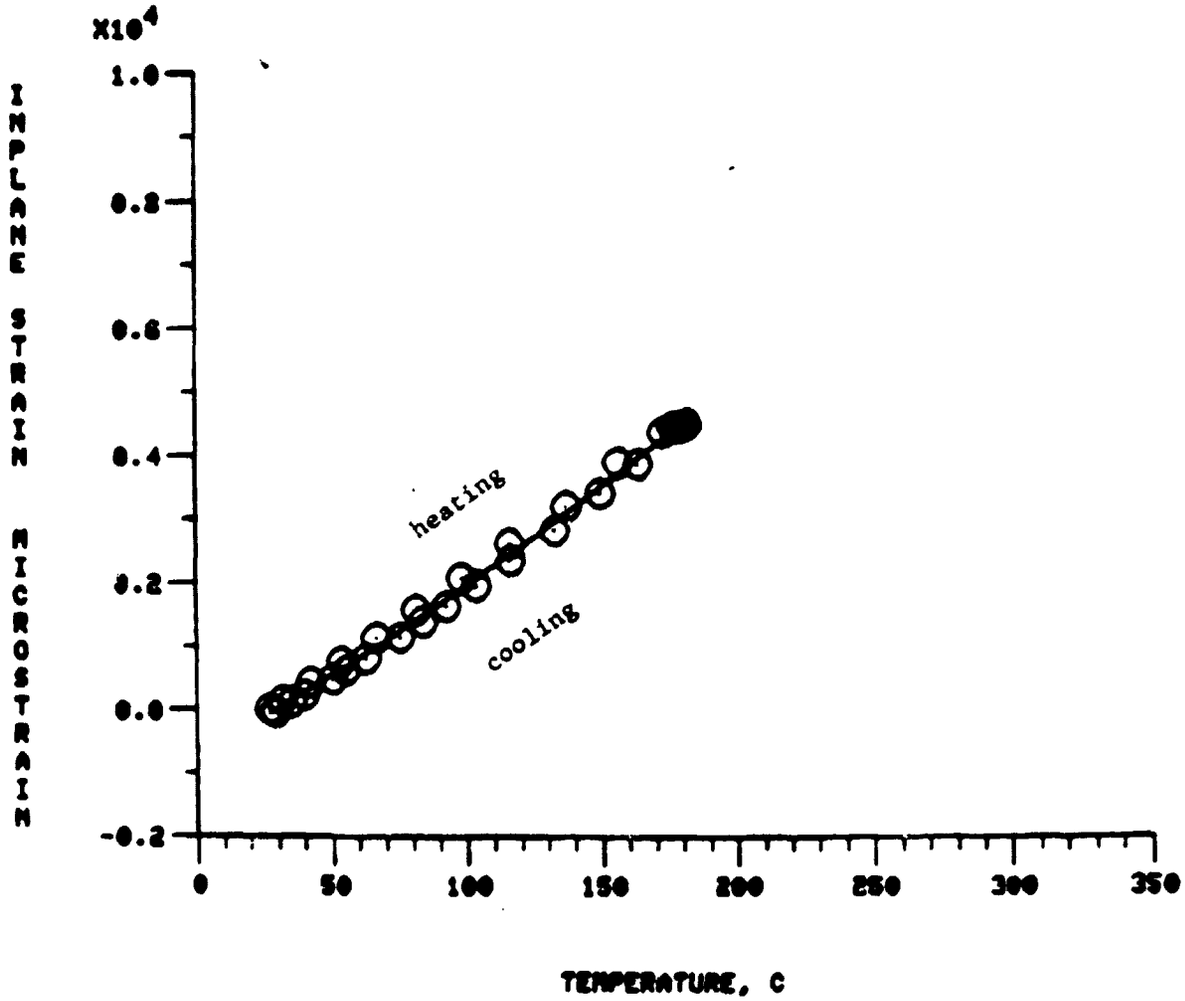

Fig. 21 Thermal Expansion of $[0^{\circ}_{8}]$ Laminate in Matrix Direction, RT-180°C, Cycle 2

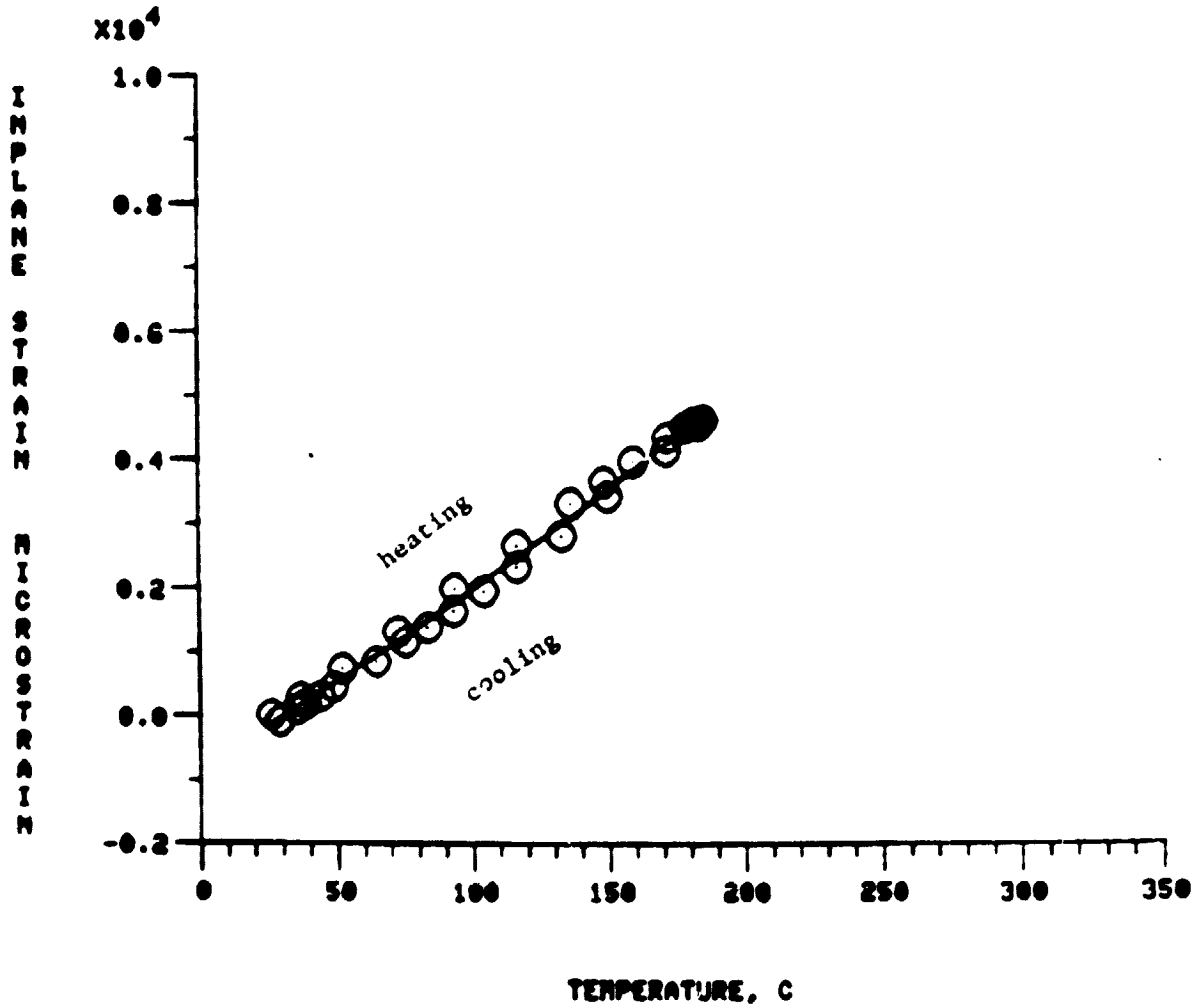

Fig. 22 Thermal Expansion of $[0_8^0]$ Laminate in Matrix Direction, RT-180°C, Cycle 3

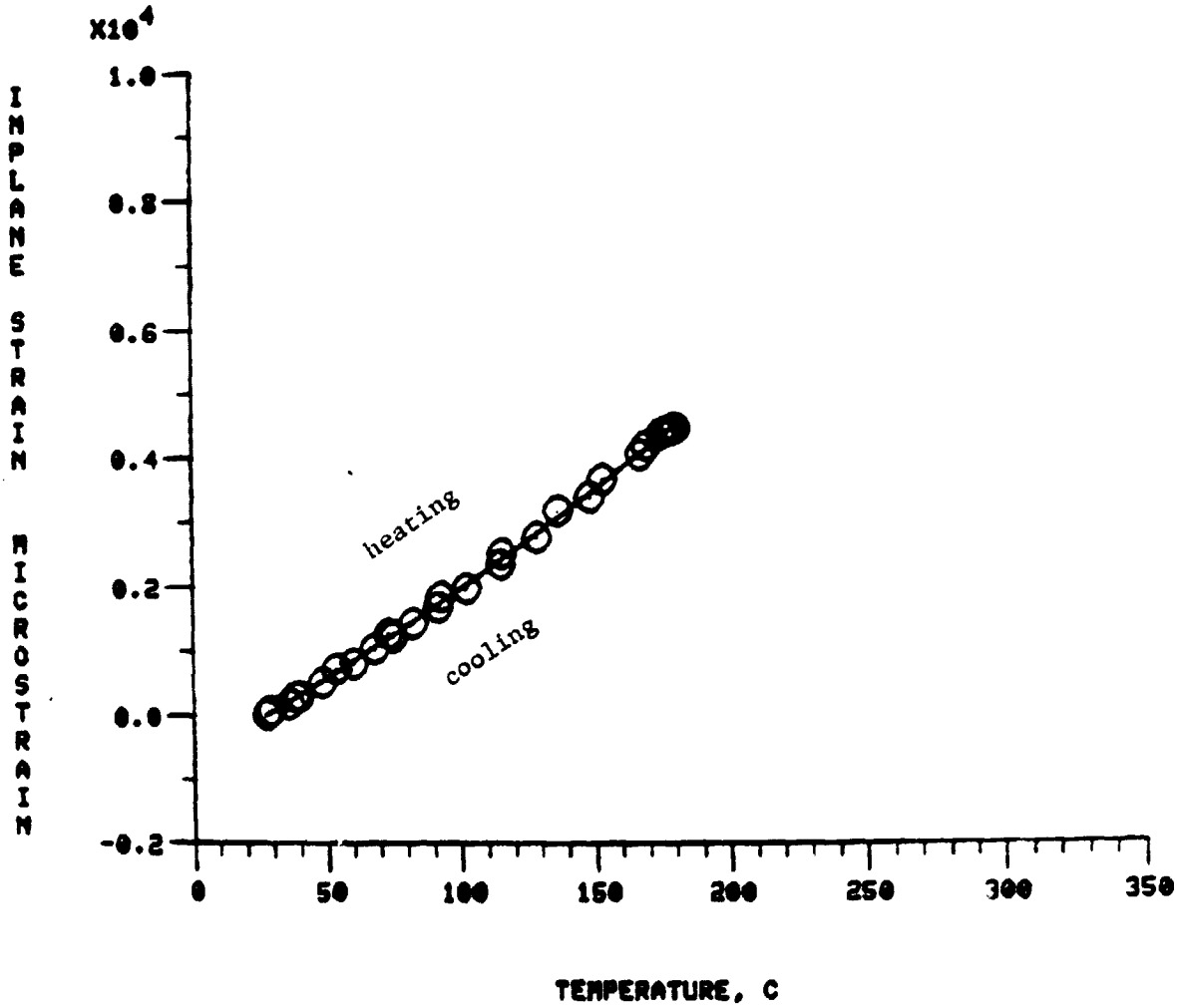

Fig. 23 Thermal Expansion of $[0_8^o]$ Laminate in Matrix Direction, RT-180°C, Cycle 4

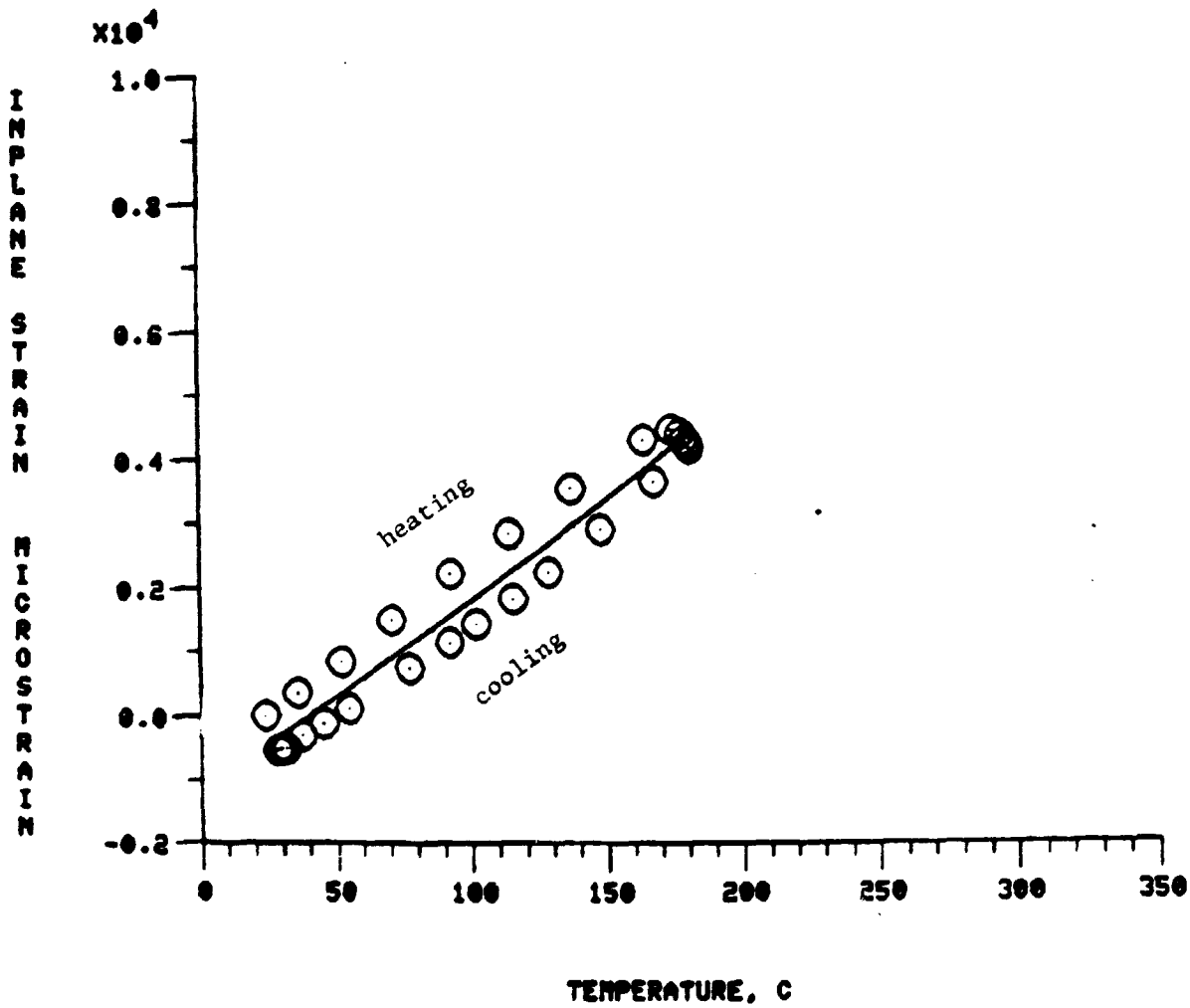

Fig. 24 Thermal Expansion of $[0^{\circ}_{8}]$ Laminate in Matrix Direction, RT-180°C, Cycle 5

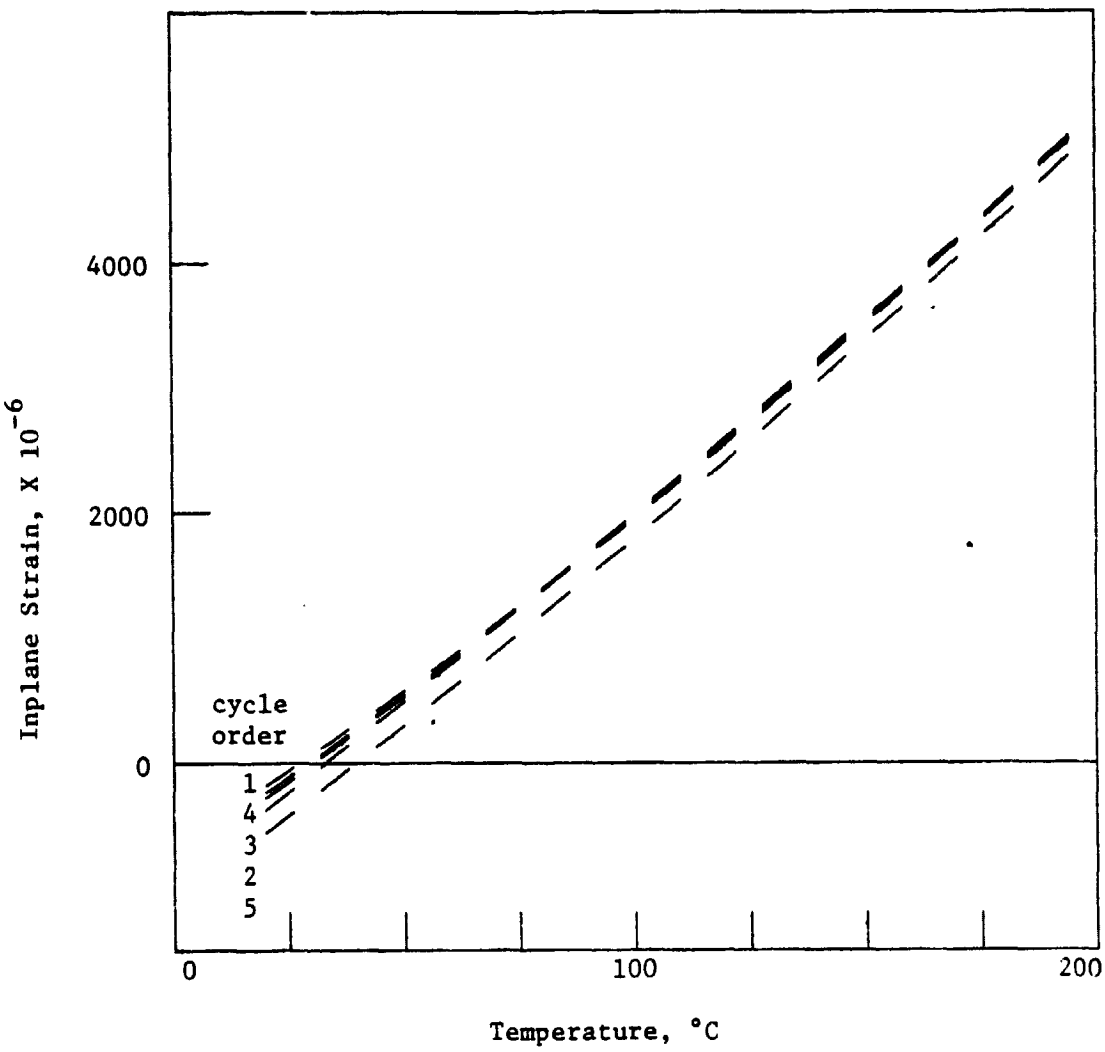

Fig. 25 Thermal Expansion of $[0_8^\circ]$ Laminate in Matrix Direction, RT-180°C, Least-Squares Fit, All 5 Cycles

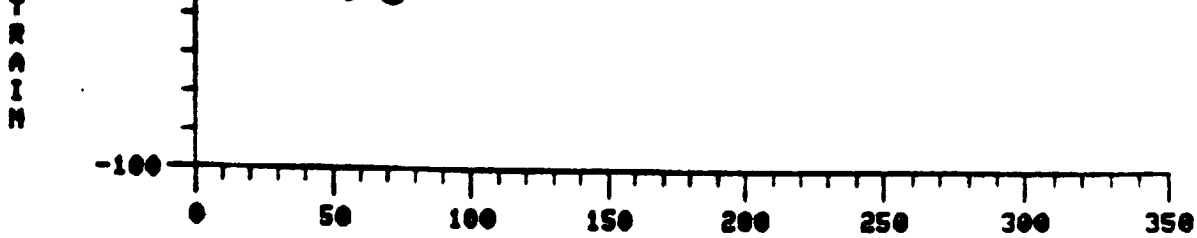

Fig. 26 Thermal Expansion of $[0_8^o]$ Laminate in Fiber Direction RT-180°C, Cycle 1

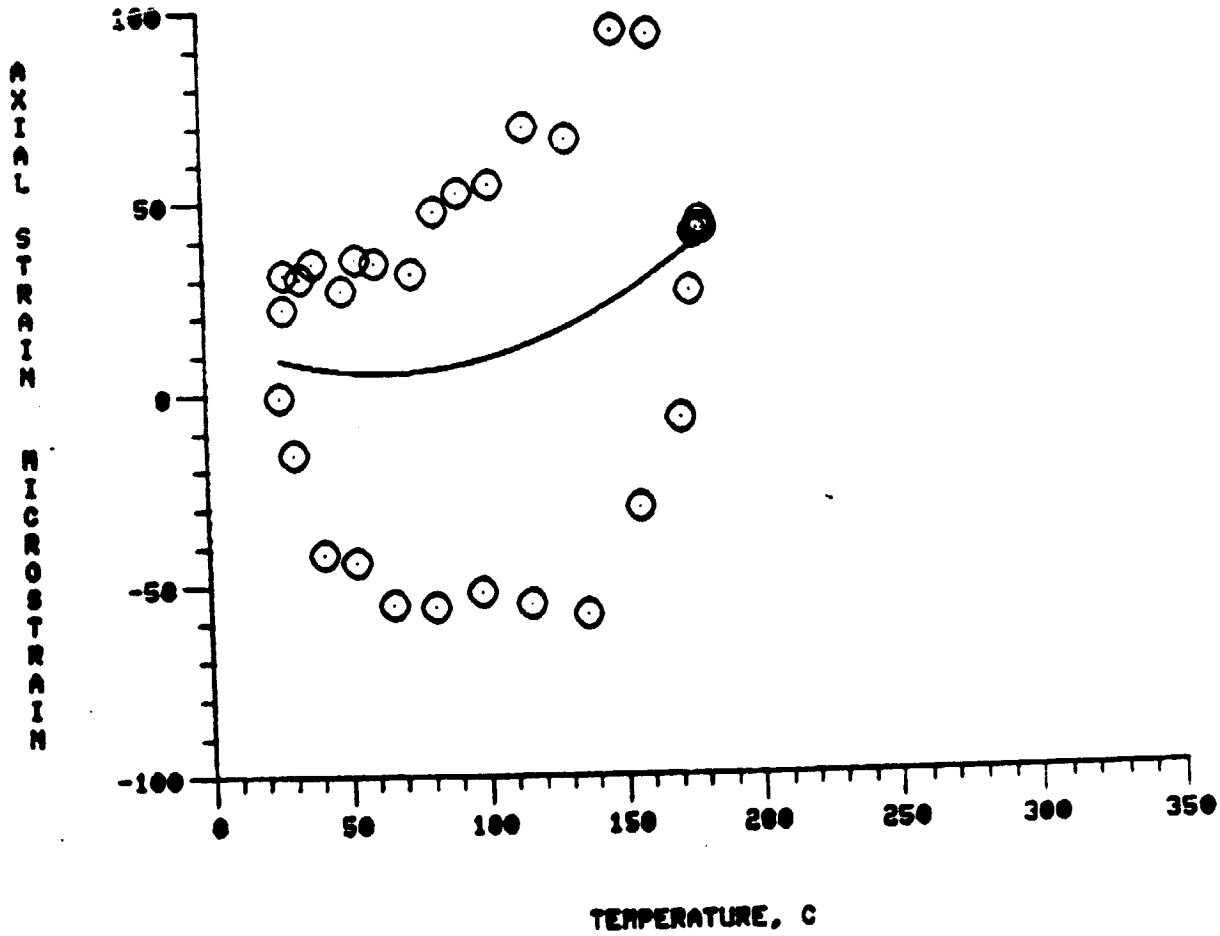

Fig. 27 Thermal Expansion of $[0_8^o]$ Laminate in Fiber Direction, RT-180°C, Cycle 2

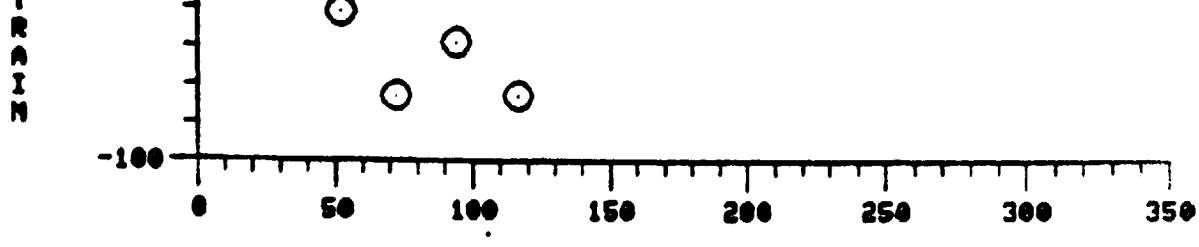

Fig. 28 Thermal Expansion of $[0_8^o]$ Laminate in Fiber Direction, RT-180°C, Cycle 3

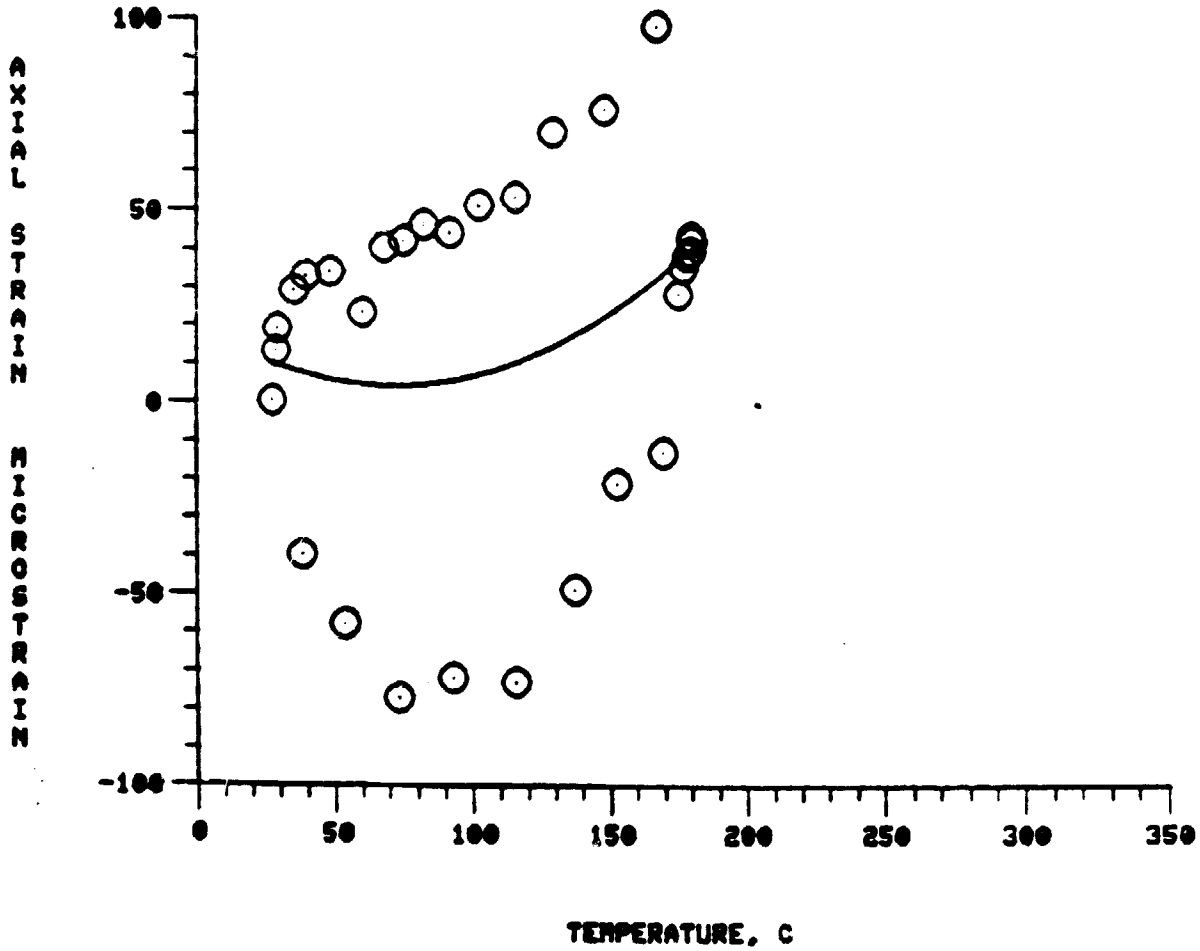

Fig. 29 Thermal Expansion of $[0_8^o]$ Laminate in Fiber Direction, RT-180°C, Cycle 4

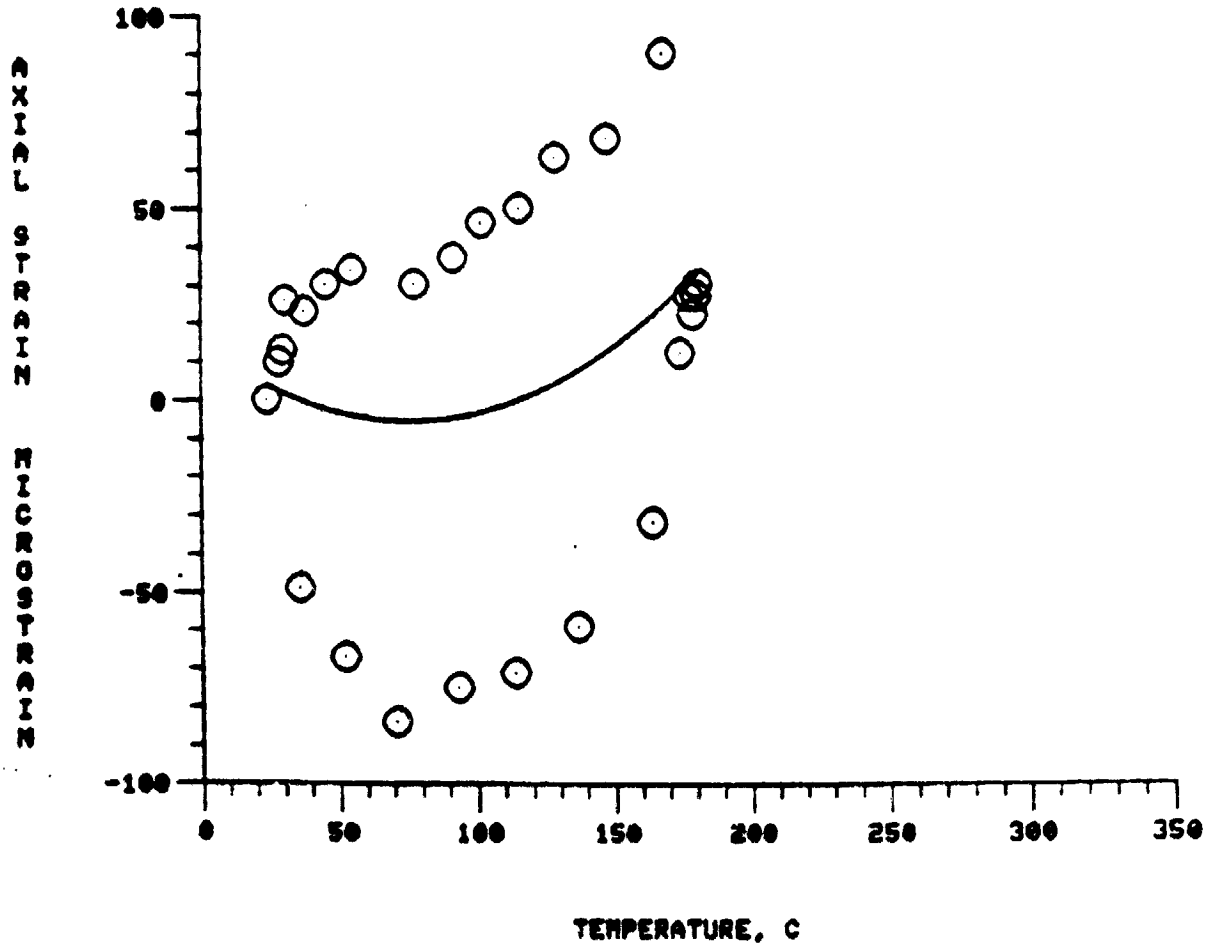

Fig. 30 Thermal Expansion of $[0_8^\circ]$ Laminate in Fiber Direction, RT-180°C, Cycle 5

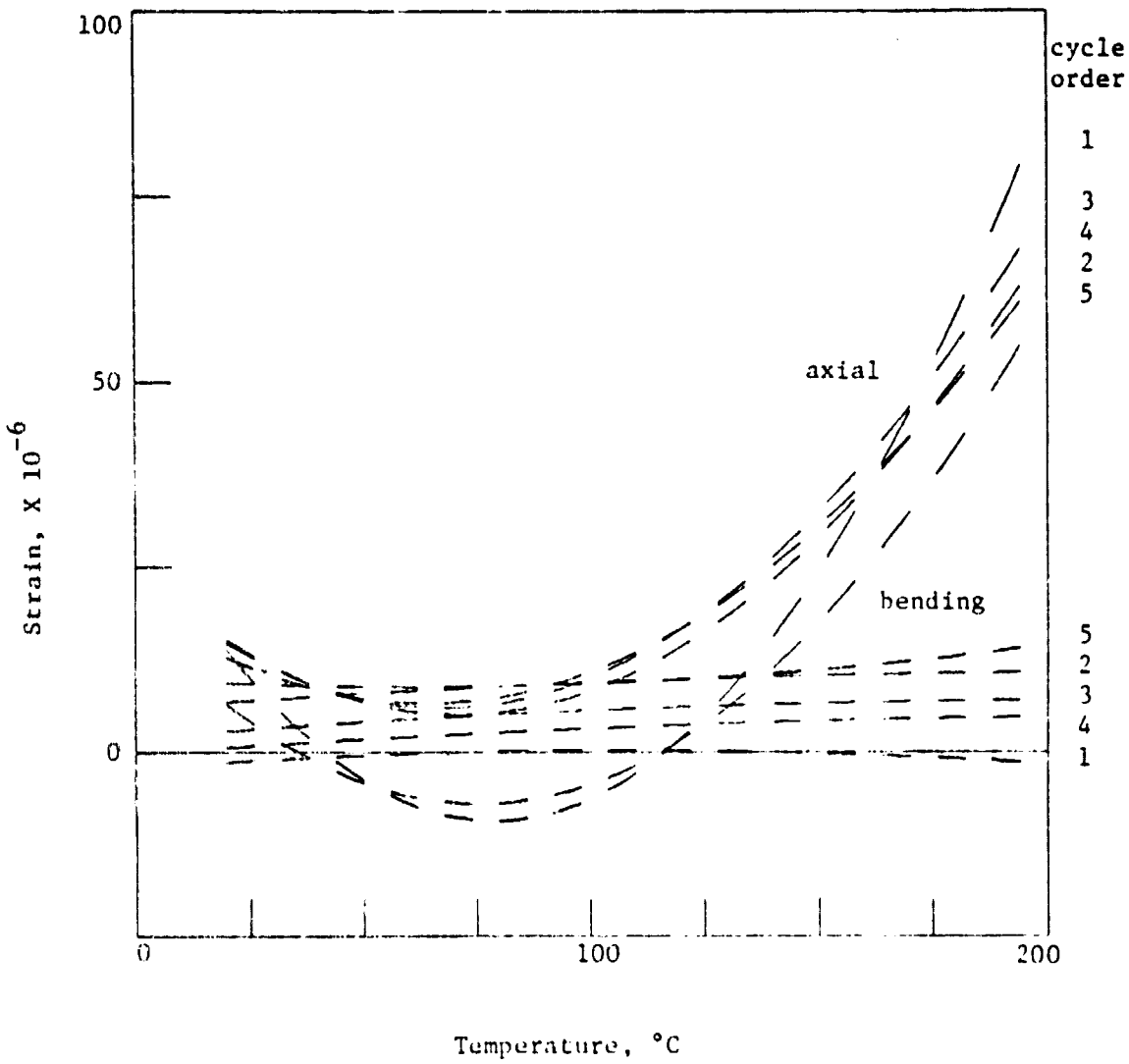

Fig. 31 Thermal Expansion of $[0_8^o]$ Laminate in Fiber Direction, RT-180°C, Least-Squares Fit, All 5 Cycles

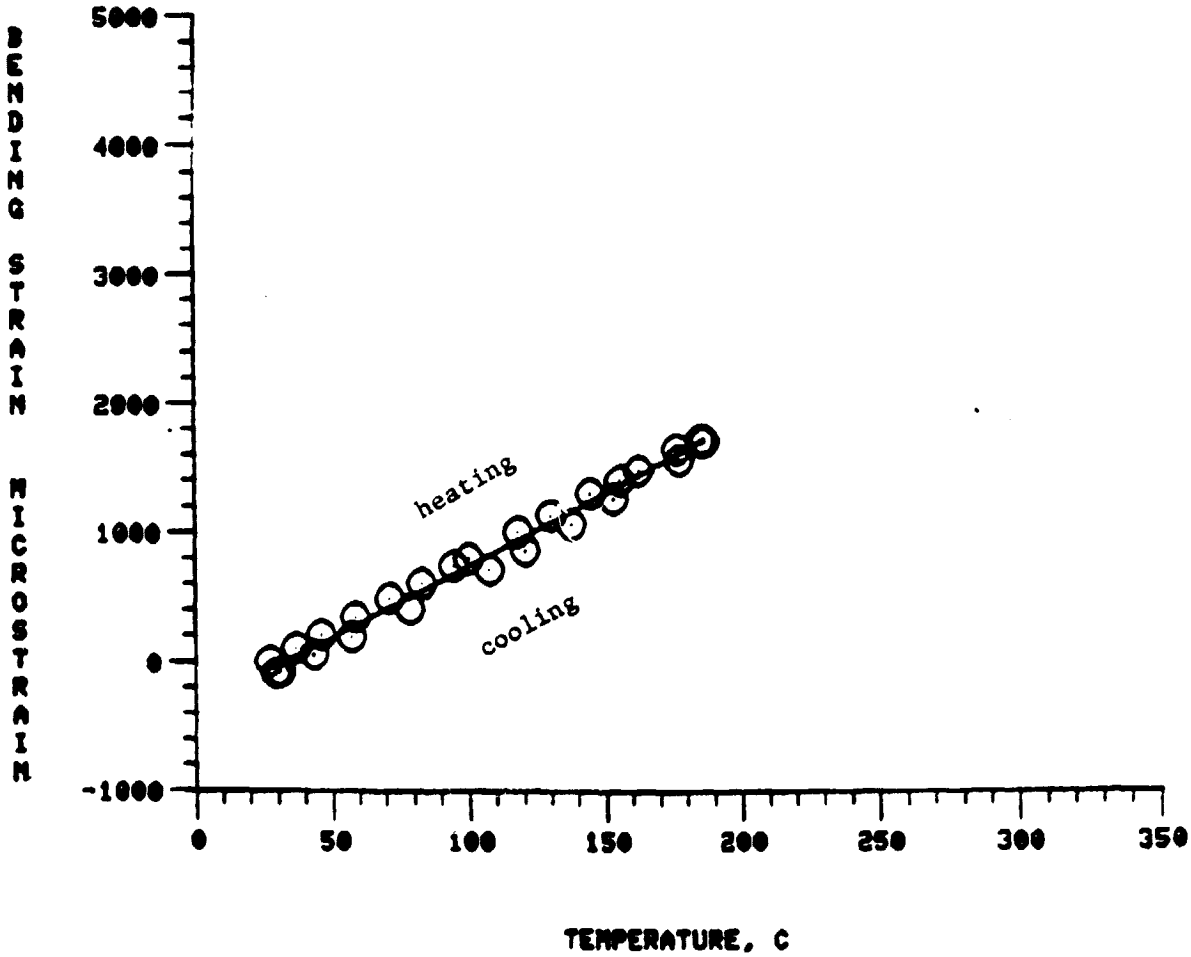

Fig. 32 Thermal Bending Strain, $[0_4^o/90_4^o]$ Laminate, RT-180°C, Cycle 1

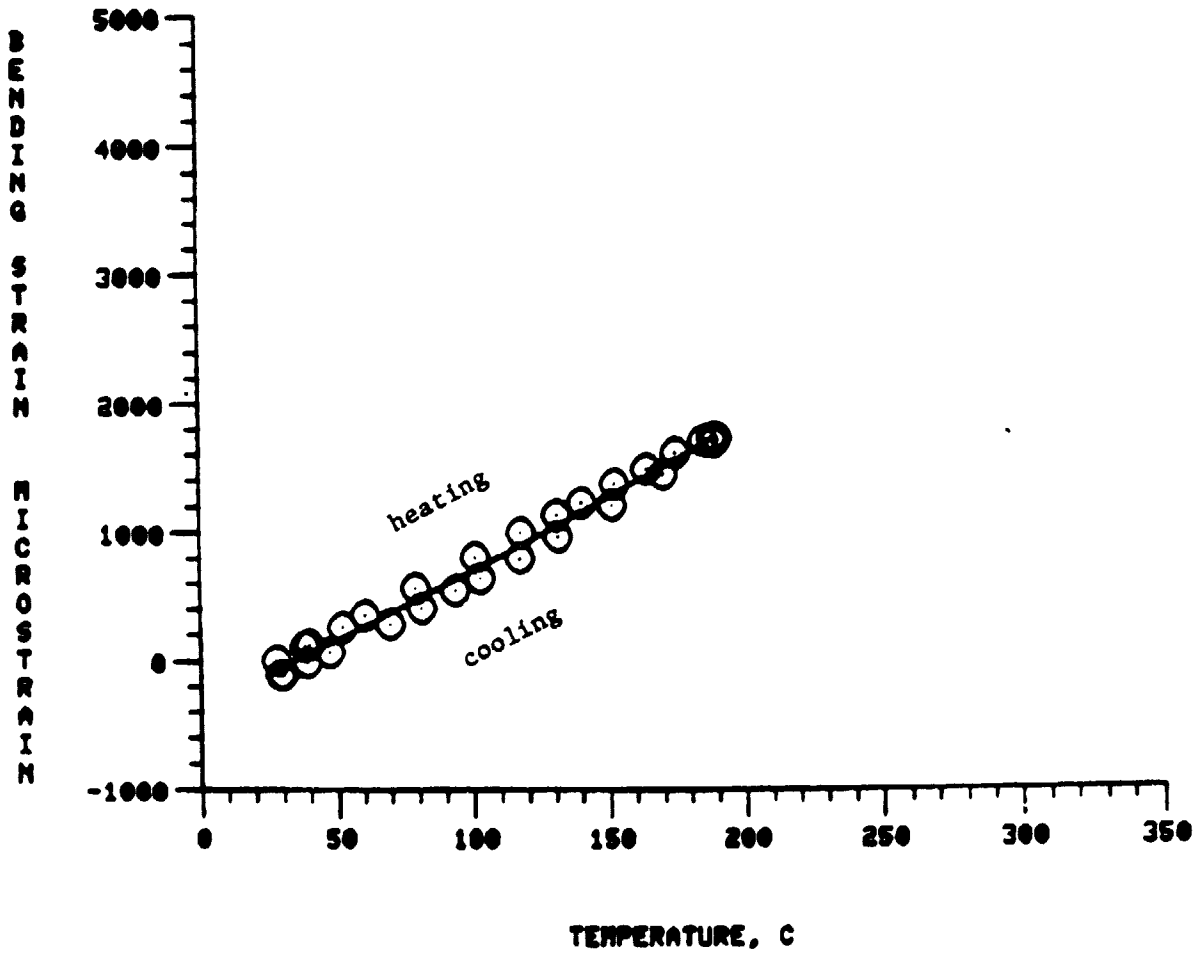

Fig. 33 Thermal Bending Strain, $[0_4^\circ/90_4^\circ]$ Laminate, RT-180°C, Cycle 2

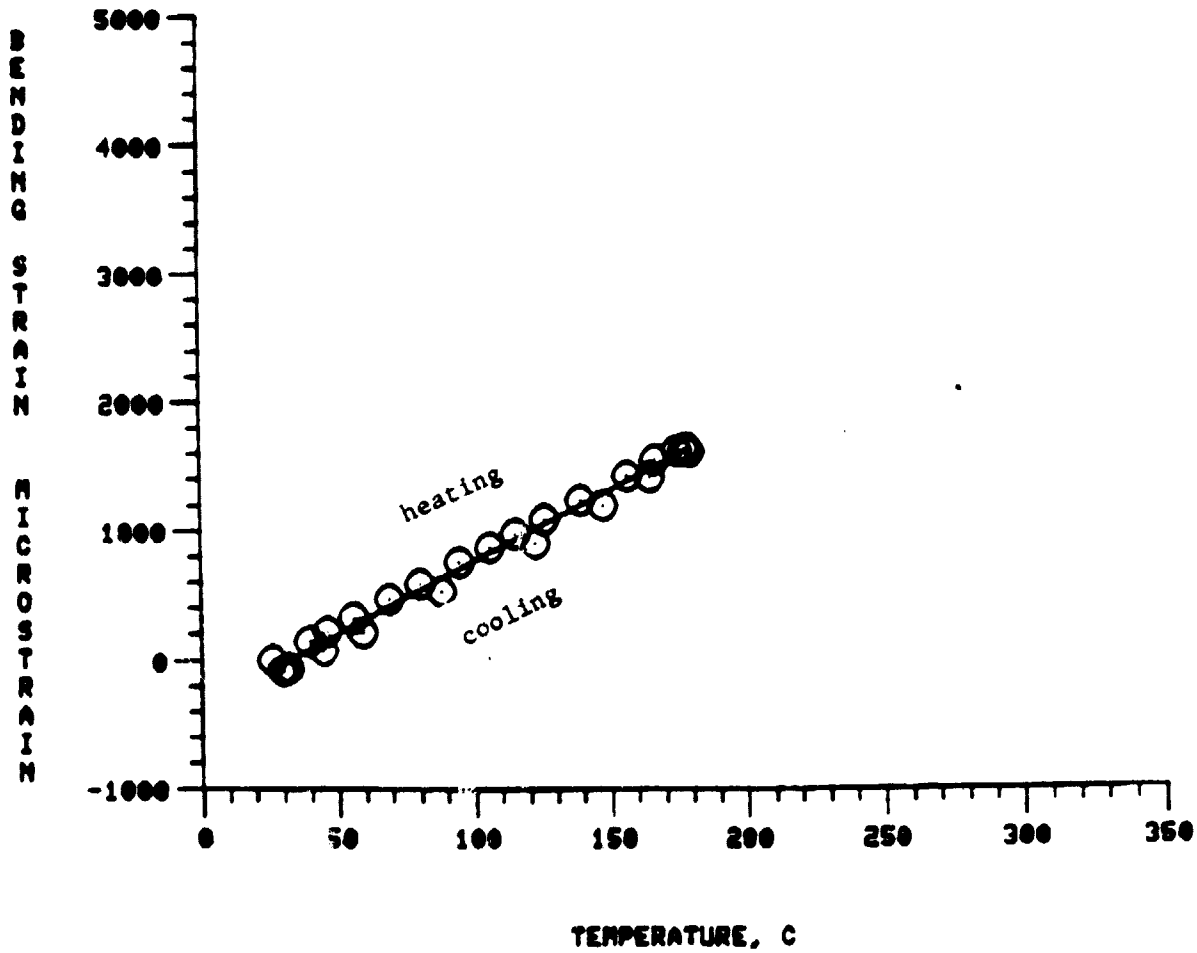

Fig. 34 Thermal Bending Strain, $[0_4^\circ/90_4^\circ]$ Laminate, RT-180°C, Cycle 3

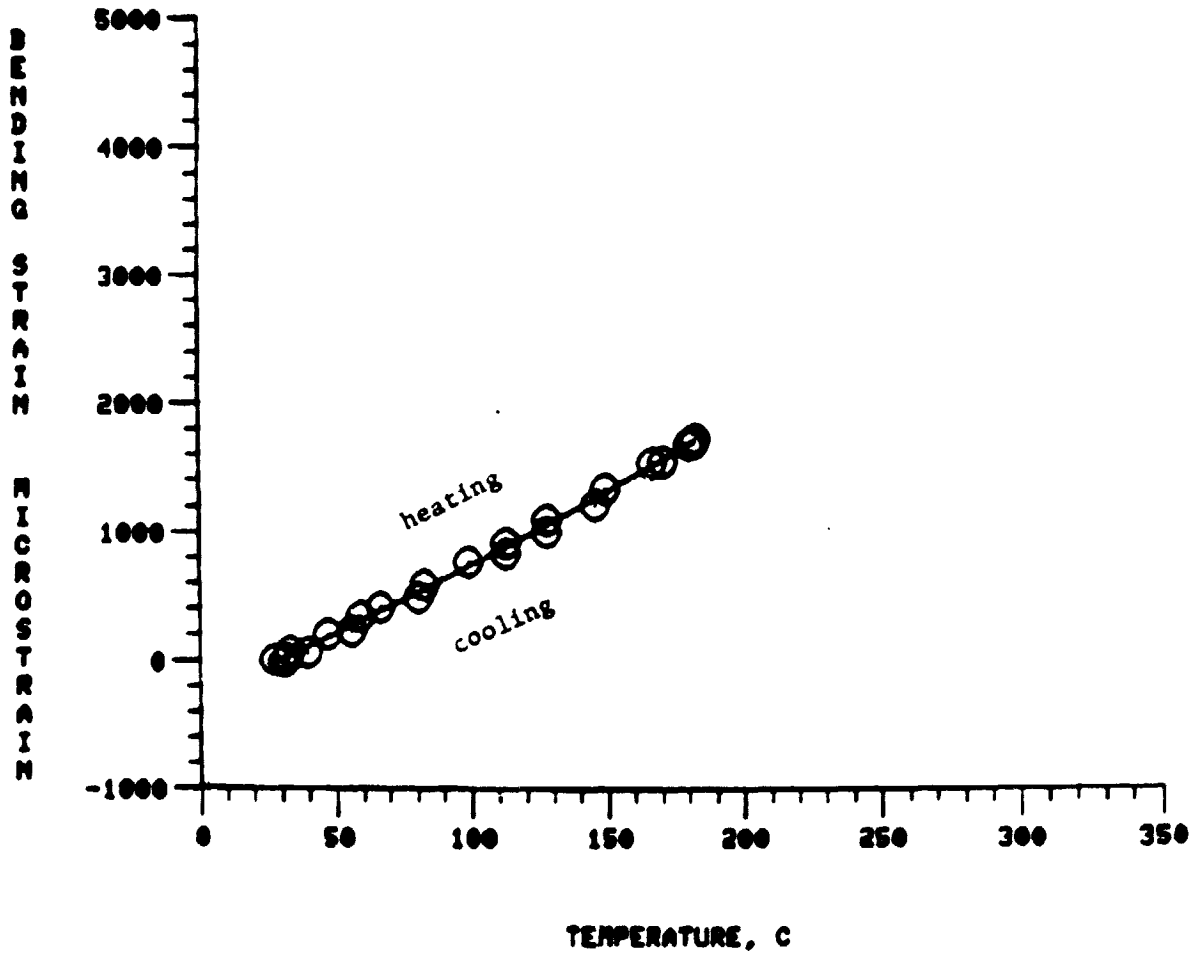

Fig. 35 Thermal Bending Strain, $[0_4^\circ/90_4^\circ]$ Laminate, RT-180°C, Cycle 4

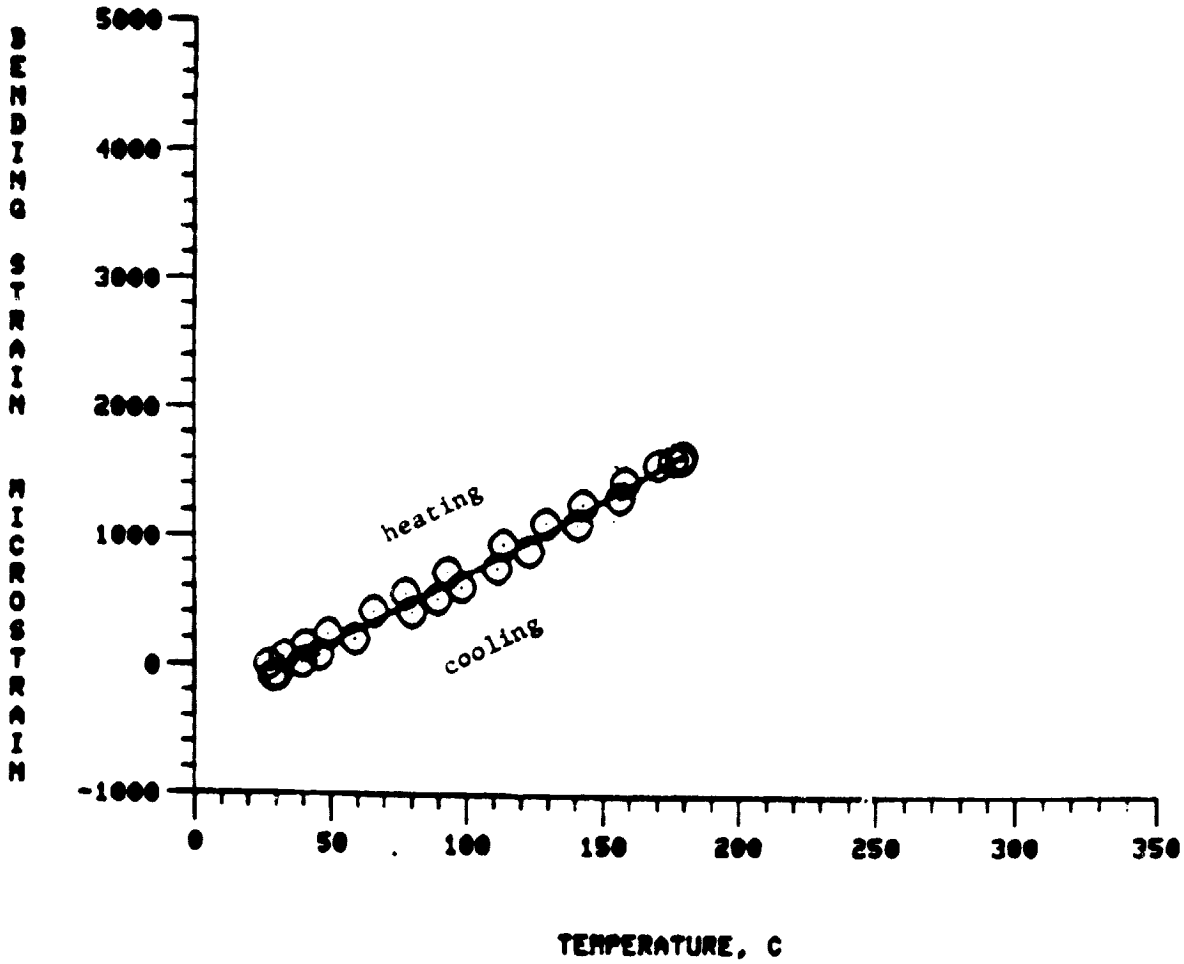

Fig. 36 Thermal Bending Strain, $[0^{\circ}_{4}/90^{\circ}_{4}]$ Laminate, RT-180°C, Cycle 5

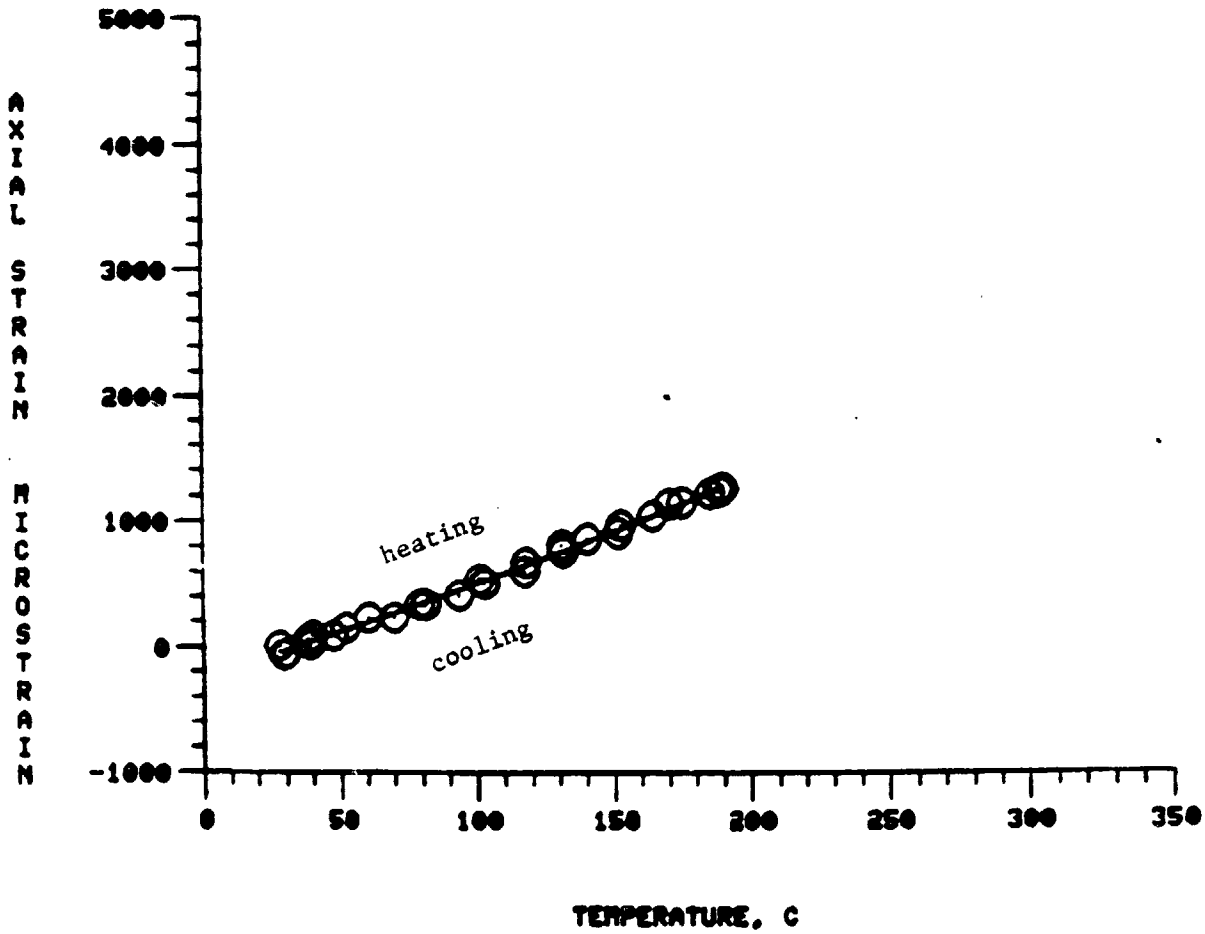

Fig. 37 Thermal Axial Strain, $[0_4^\circ/90_4^\circ]$ Laminate, RT-180°C, Cycle 1

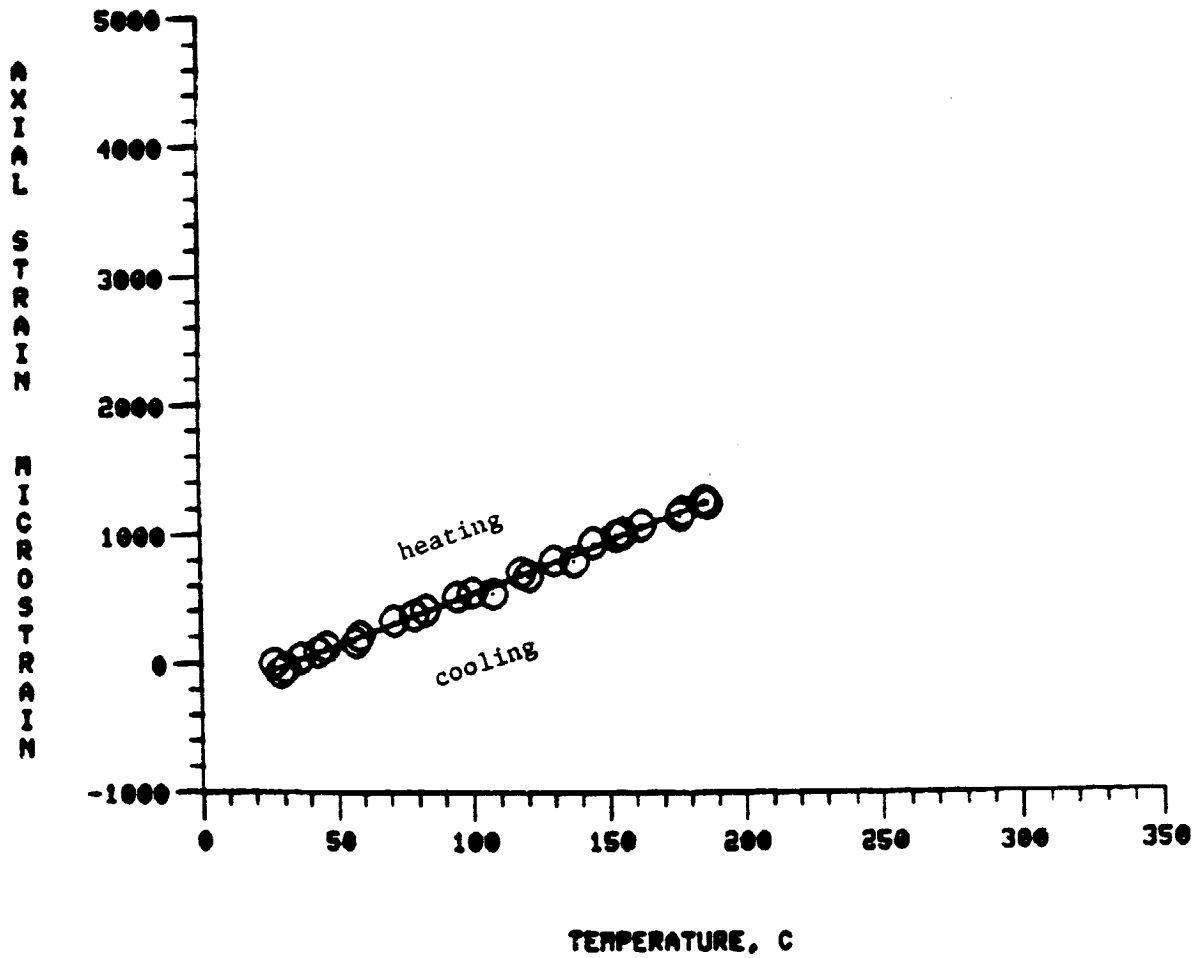

Fig. 38 Thermal Axial Strain, $[0_4^o/90_4^o]$ Laminate, RT-180°C, Cycle 2

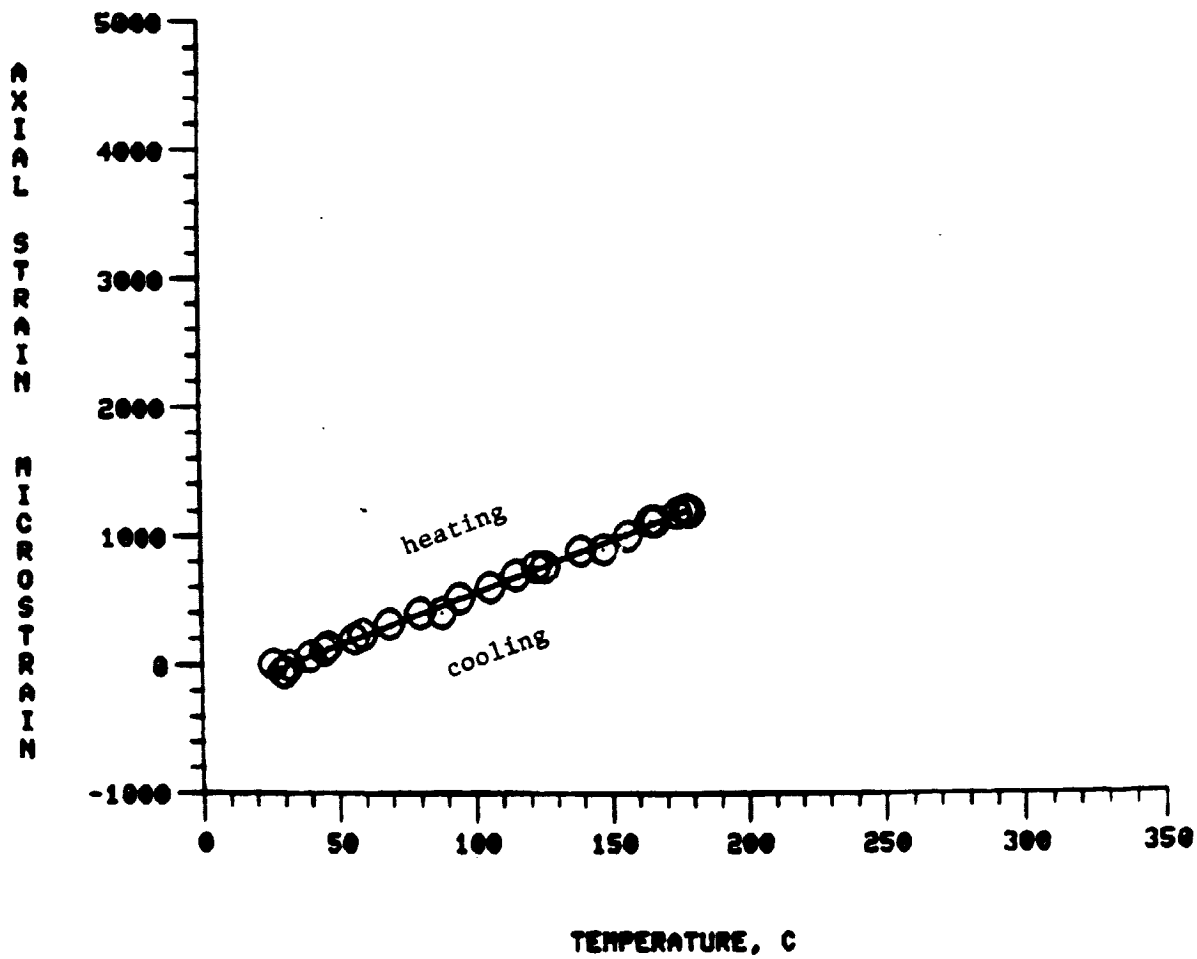

Fig. 39 Thermal Axial Strain, $[0^{\circ}_{4}/90^{\circ}_{4}]$ Laminate, RT-180°C, Cycle 3

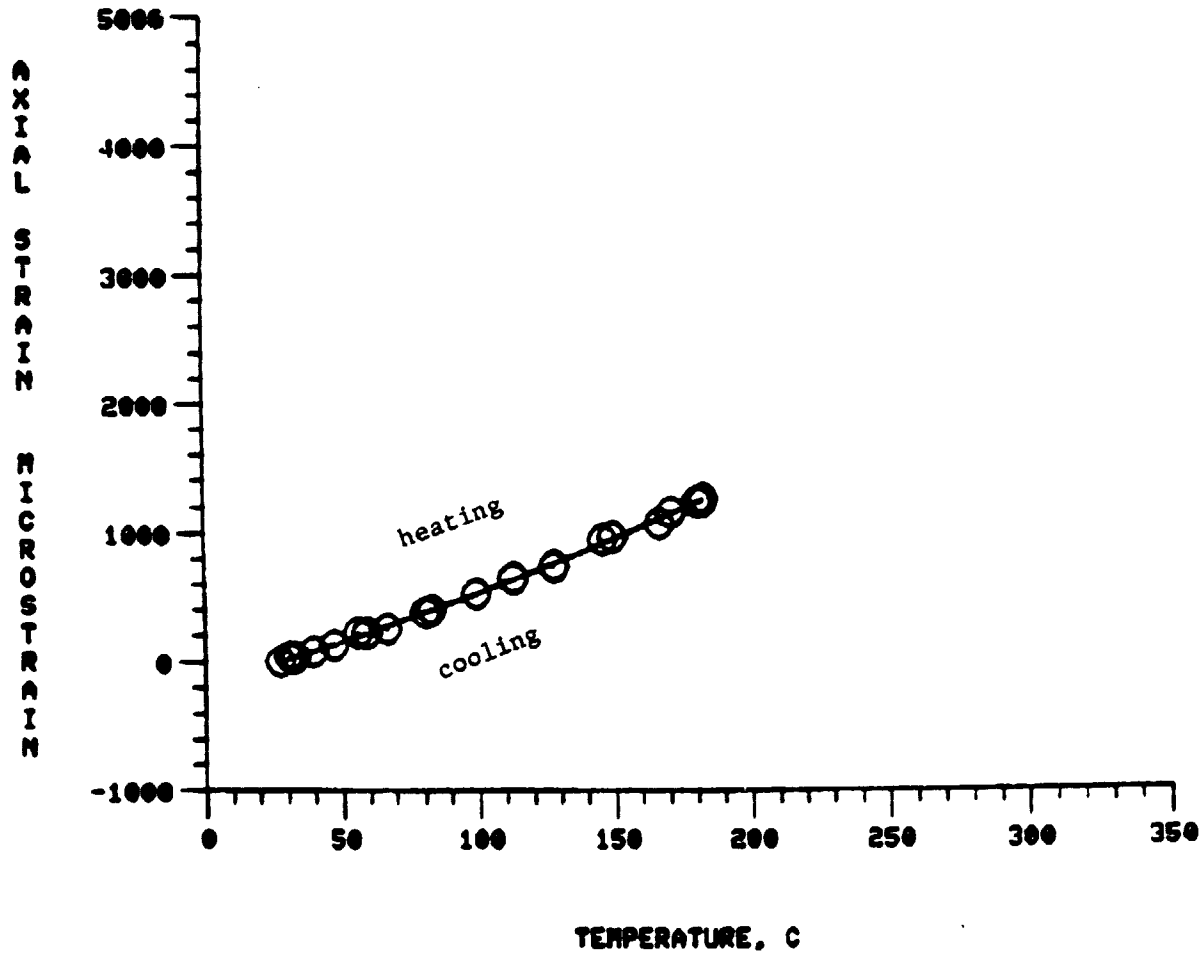

Fig. 40 Thermal Axial Strain, $[0^{\circ}_{4}/90^{\circ}_{4}]$ Laminate, RT-180°C, Cycle 4

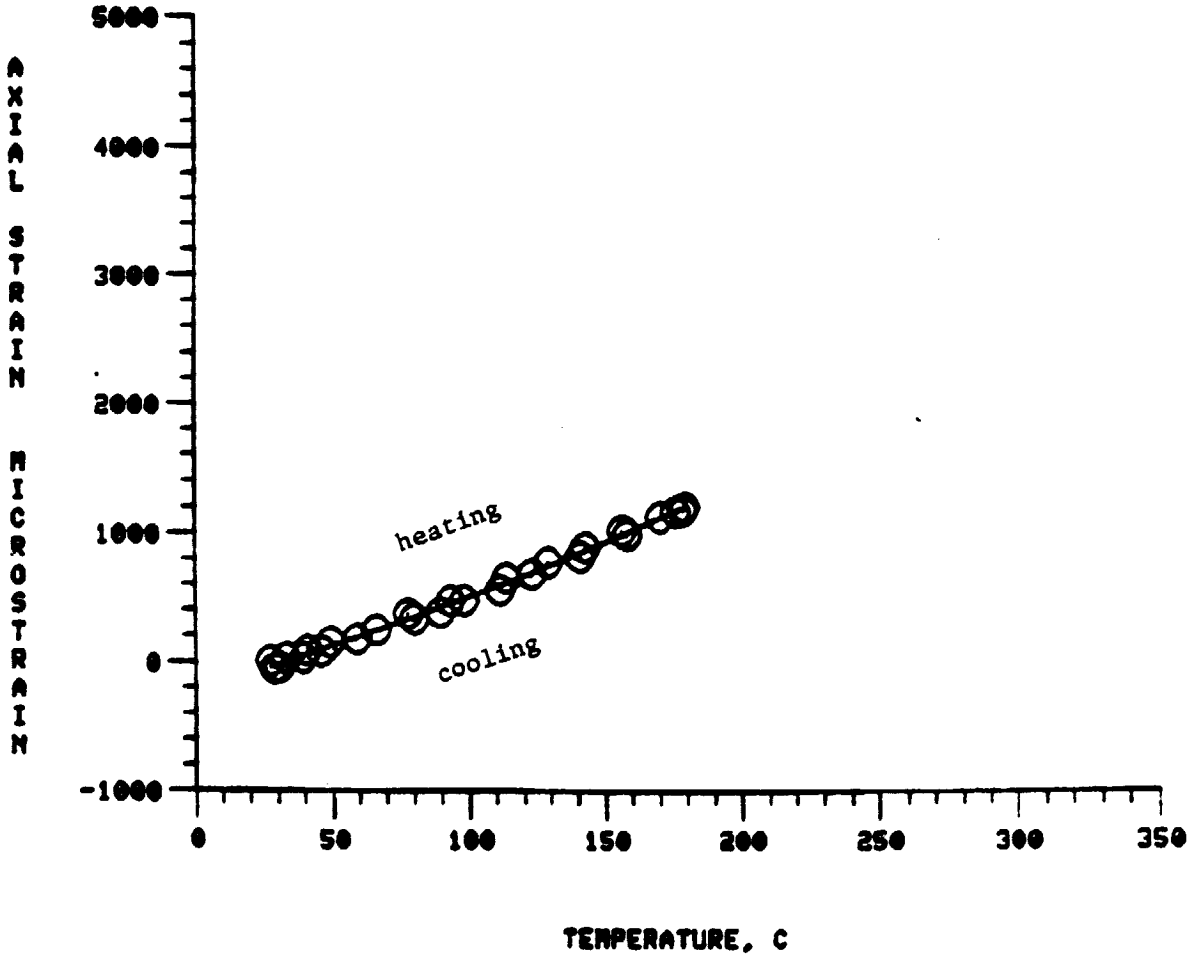

Fig. 41 Thermal Axial Strain, $[0^{\circ}_{4}/90^{\circ}_{4}]$ Laminate, RT-180°C, Cycle 5

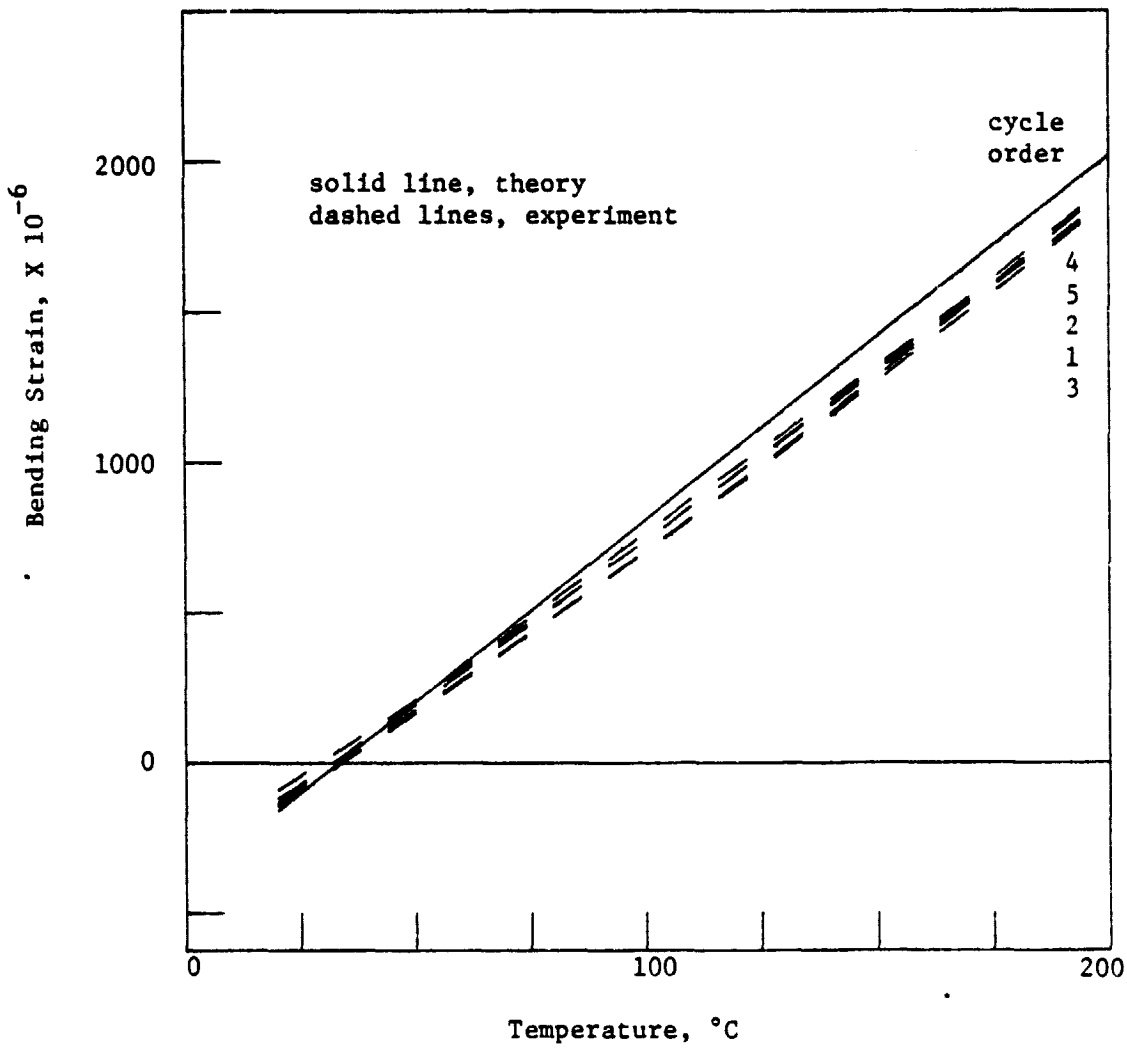

Fig. 42 Least-Square Thermal Bending Strains and Theoretical Prediction, $[0^\circ_4/90^\circ_4]$ Laminate, RT-180°C

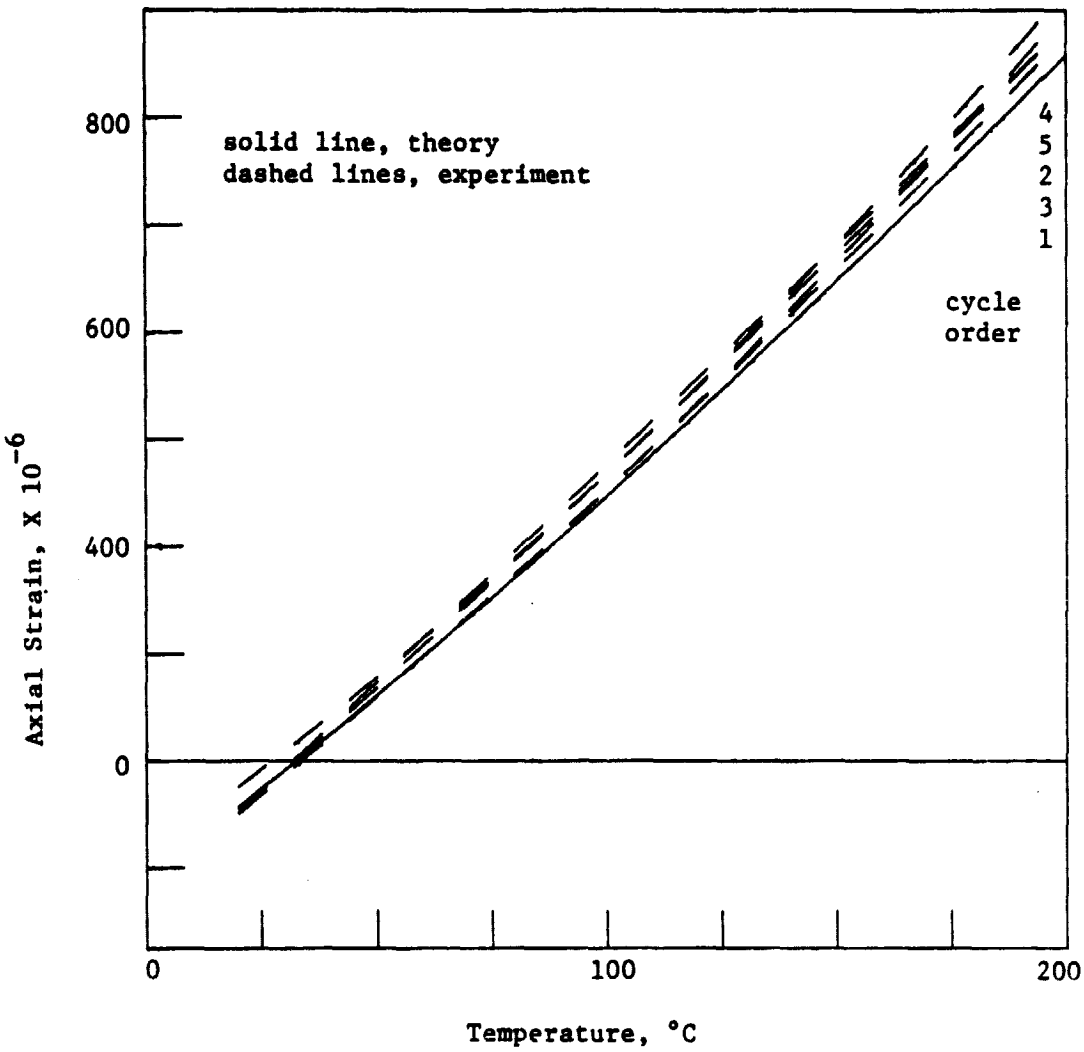

Fig. 43 Least-Squares Thermal Axial Strains and Theoretical Prediction, $[0^\circ_4/90^\circ_4]$ Laminate, RT-180°C

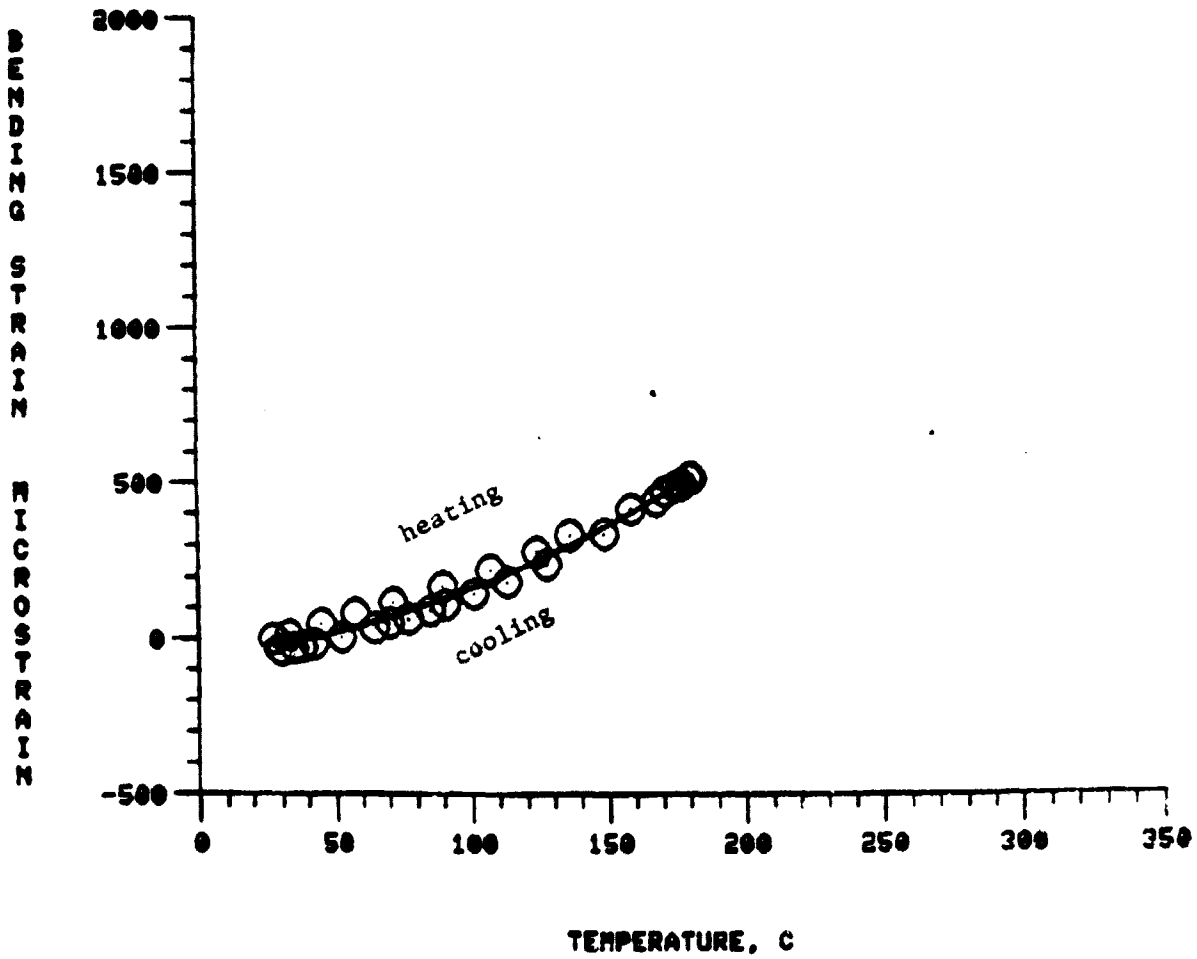

Fig. 44 Thermal Bending Strain, $[0_2^\circ/90_2^\circ]$ Laminate. RT-180°C, Cycle 1

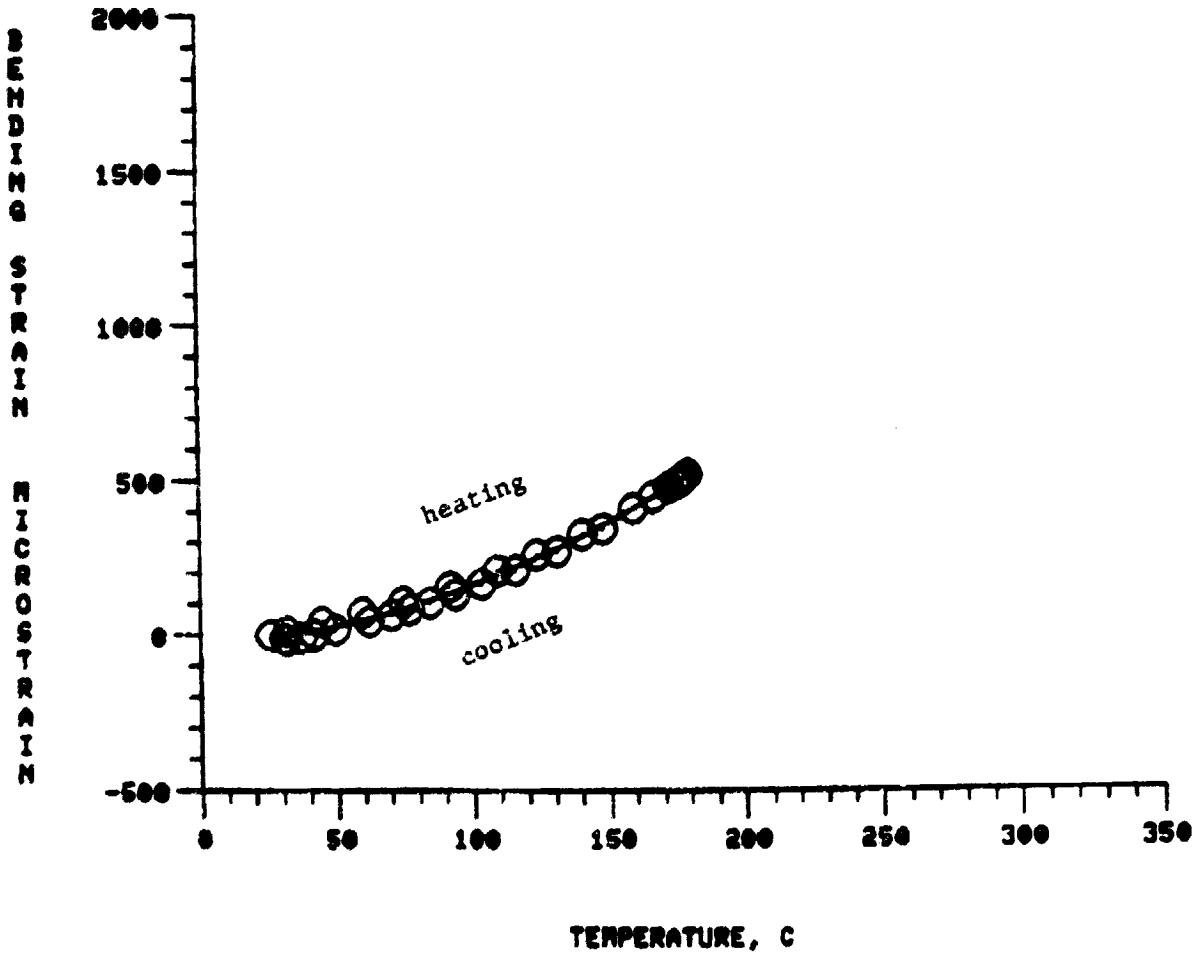

Fig. 45 Thermal Bending Strain, $[0_2^\circ/90_2^\circ]$ Laminate, RT-180°C, Cycle 2

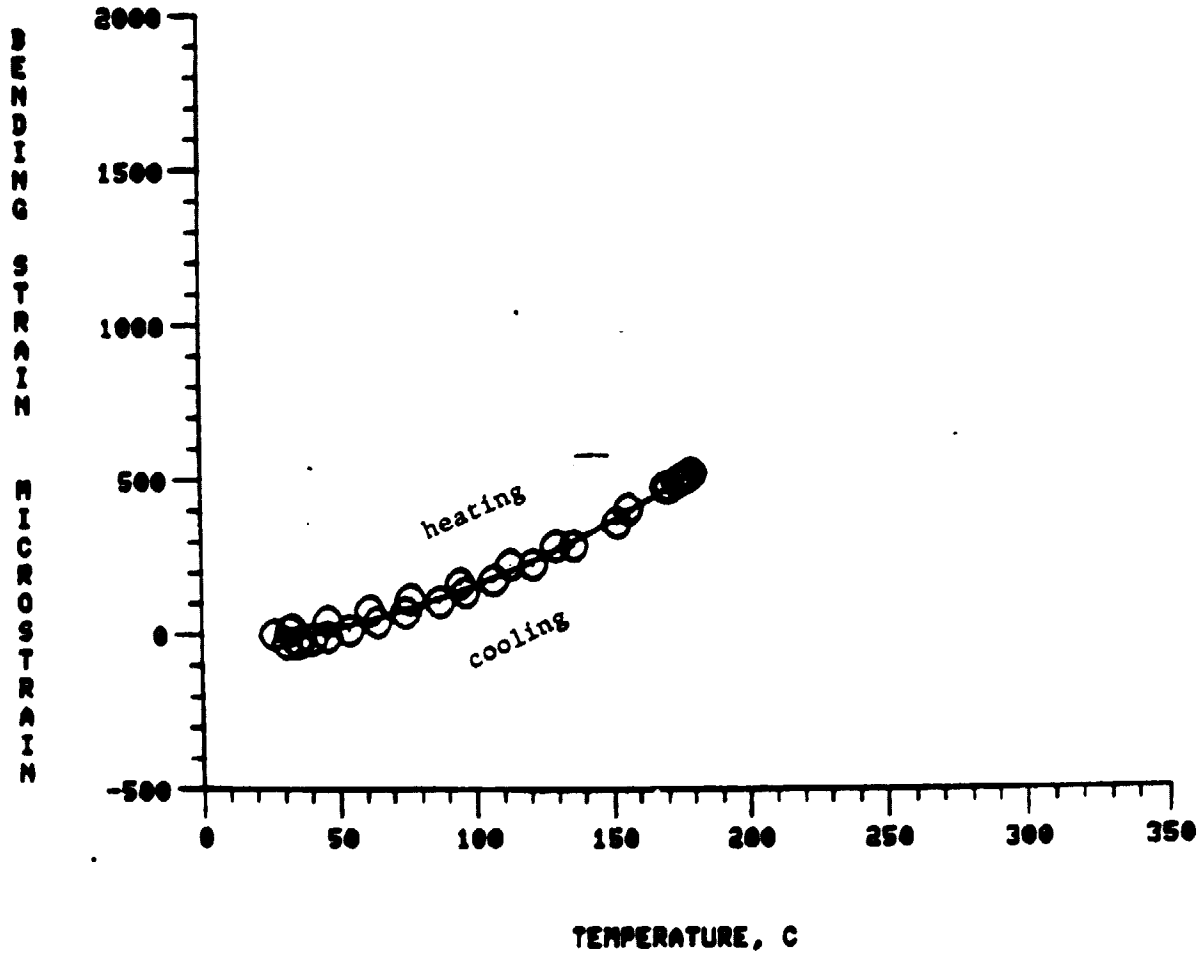

Fig. 46 Thermal Bending Strain, $[0_2^\circ/90_2^\circ]$ Laminate, RT-180°C, Cycle 3

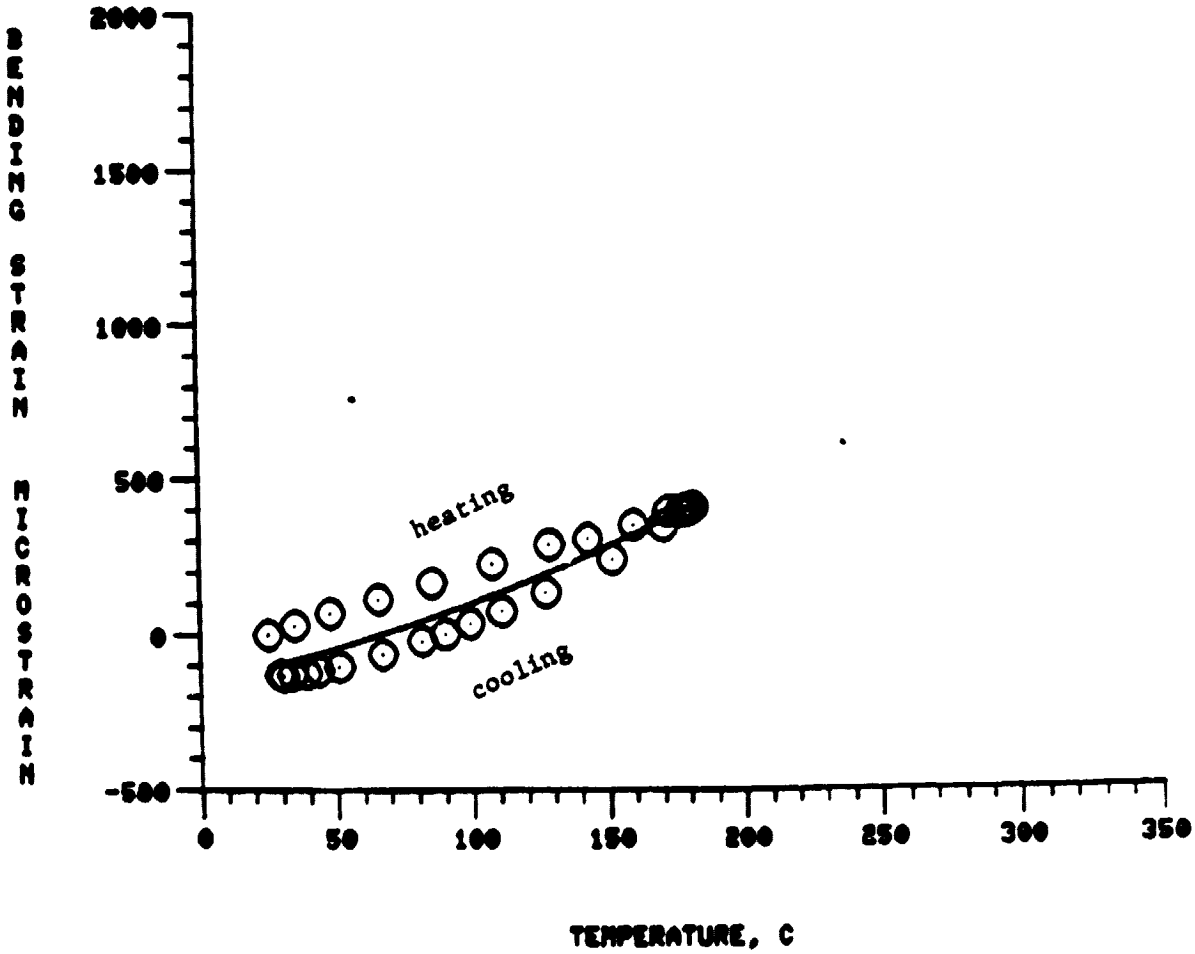

Fig. 47 Thermal Bending Strain, $[0_2^\circ/90_2^\circ]$ Laminate, RT-180°C, Cycle 4

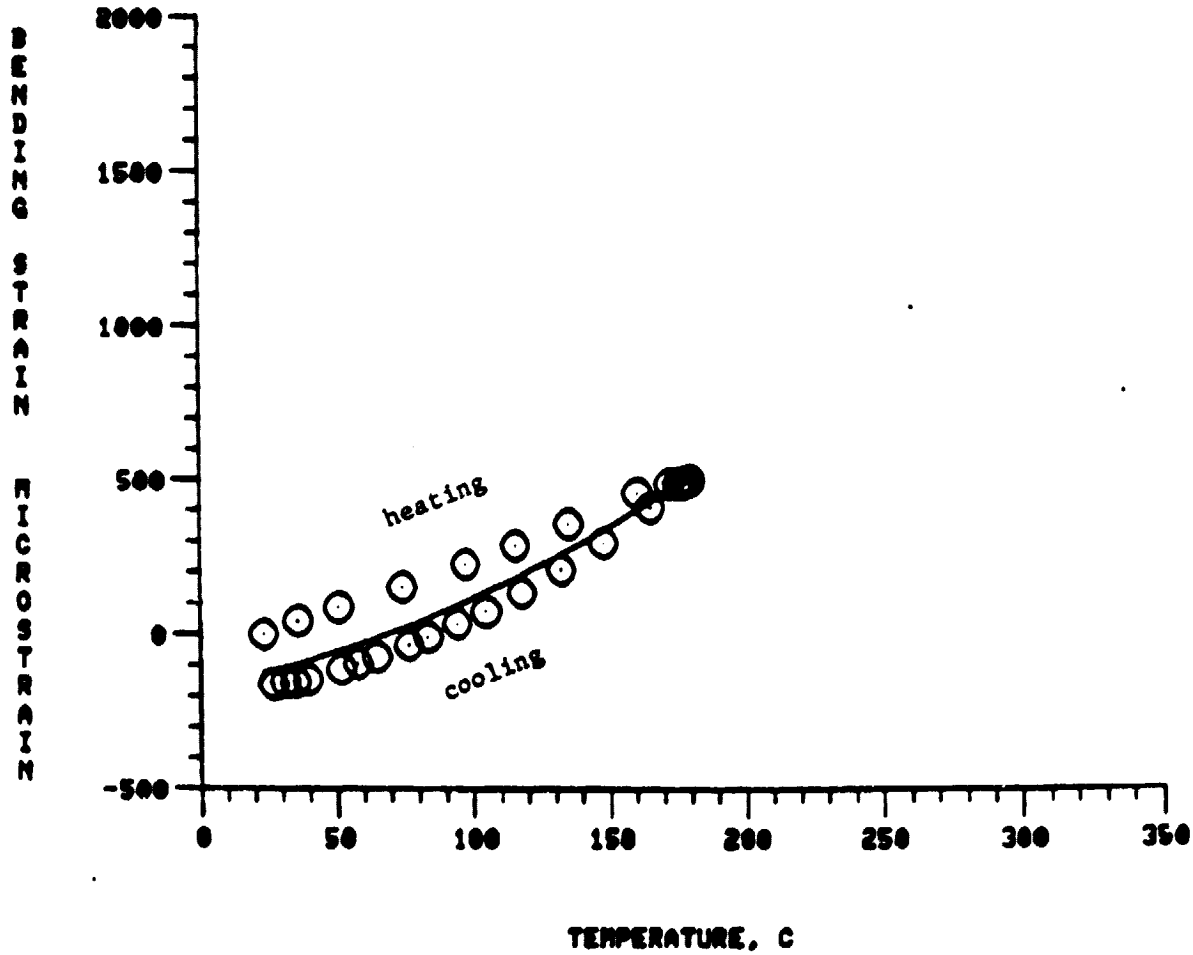

Fig. 48 Thermal Bending Strain, $[0_2^o/90_2^o]$ Laminate, RT-180°C, Cycle 5

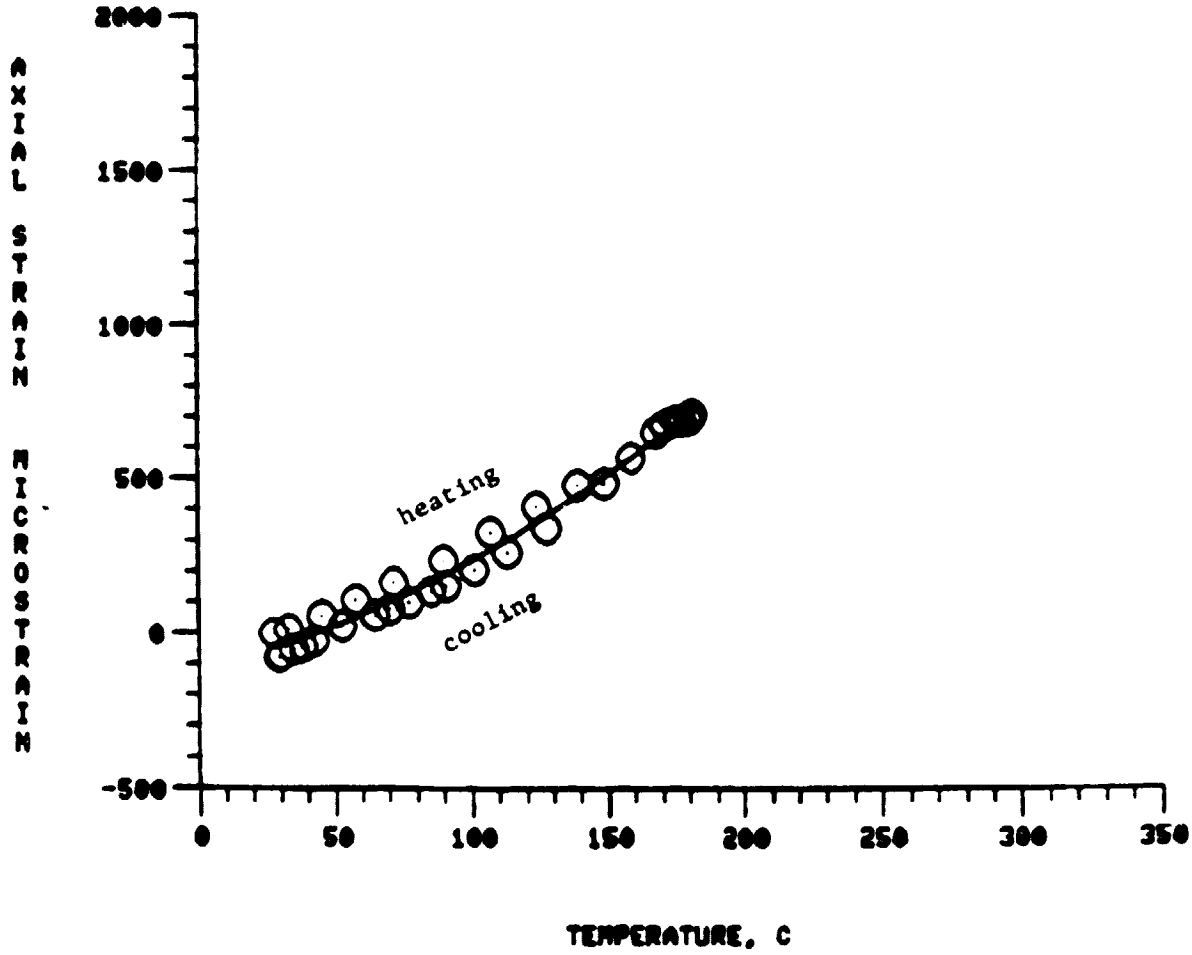

Fig. 49 Thermal Axial Strain, $[0_2^\circ/90_2^\circ]$ Laminate, RT-180°C, Cycle 1

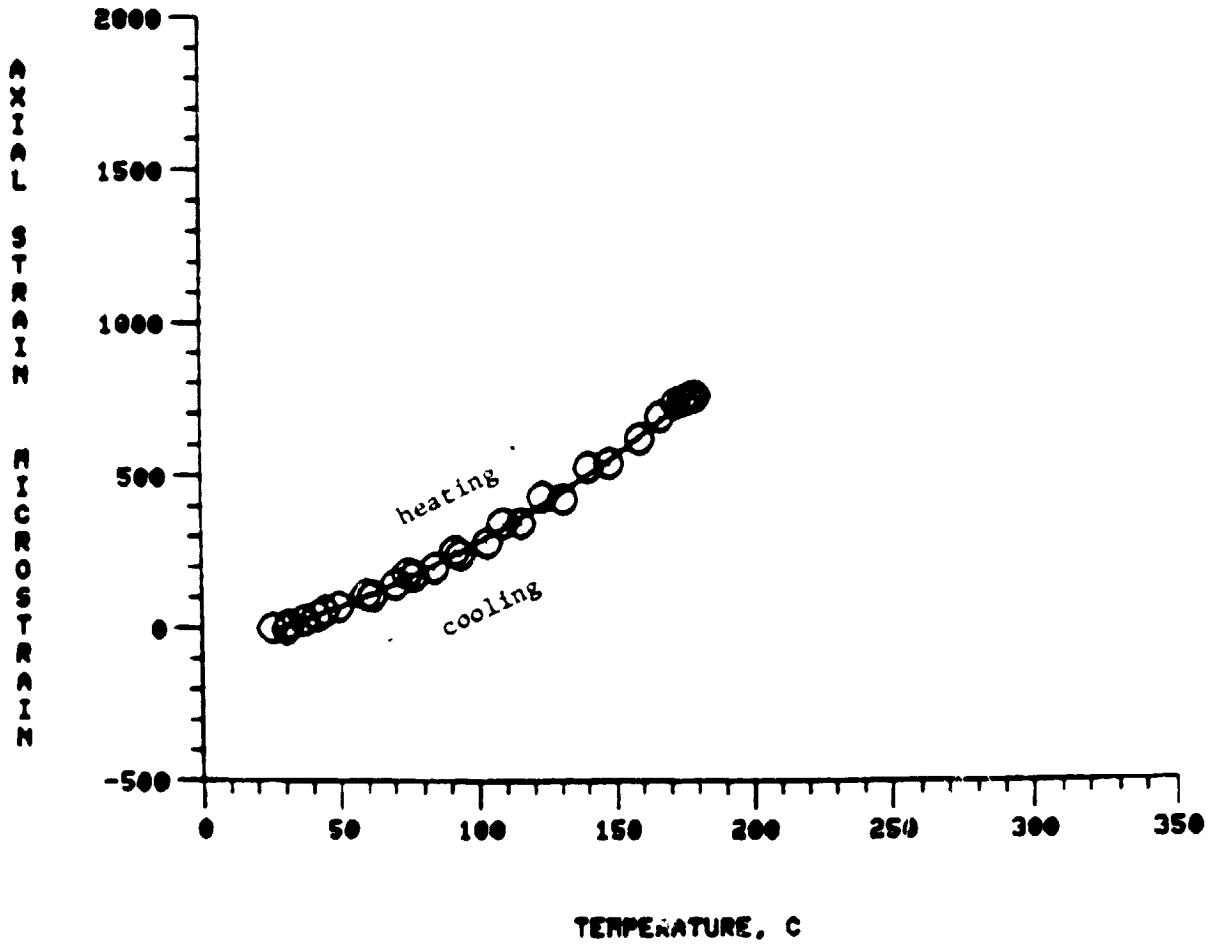

Fig. 50 Thermal Axial Strain, $[0^\circ_2/90^\circ_2]$ Laminate
RT-180°C, Cycle 2

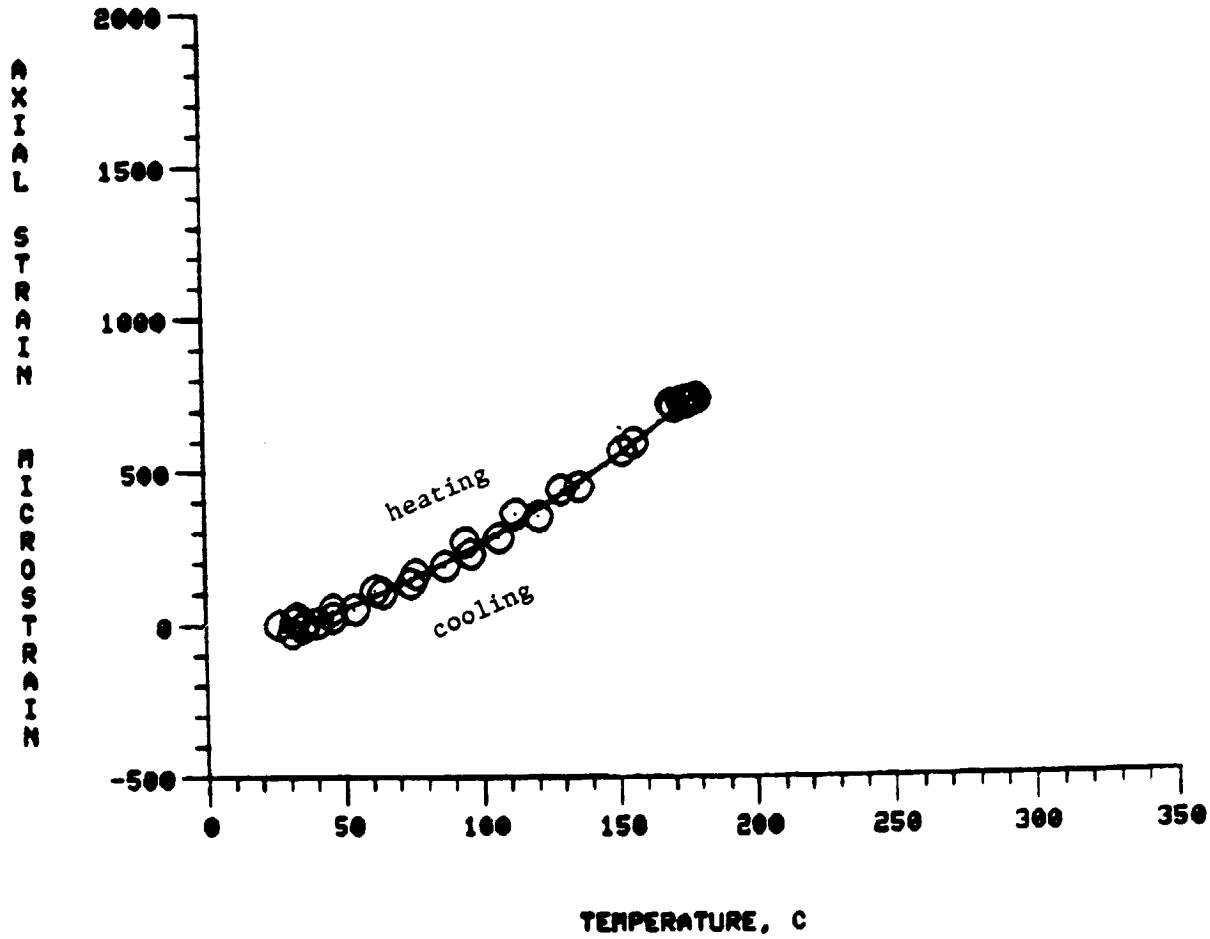

Fig. 51 Thermal Axial Strain, $[0_2^o/90_2^o]$ Laminate, RT-180°C, Cycle 3

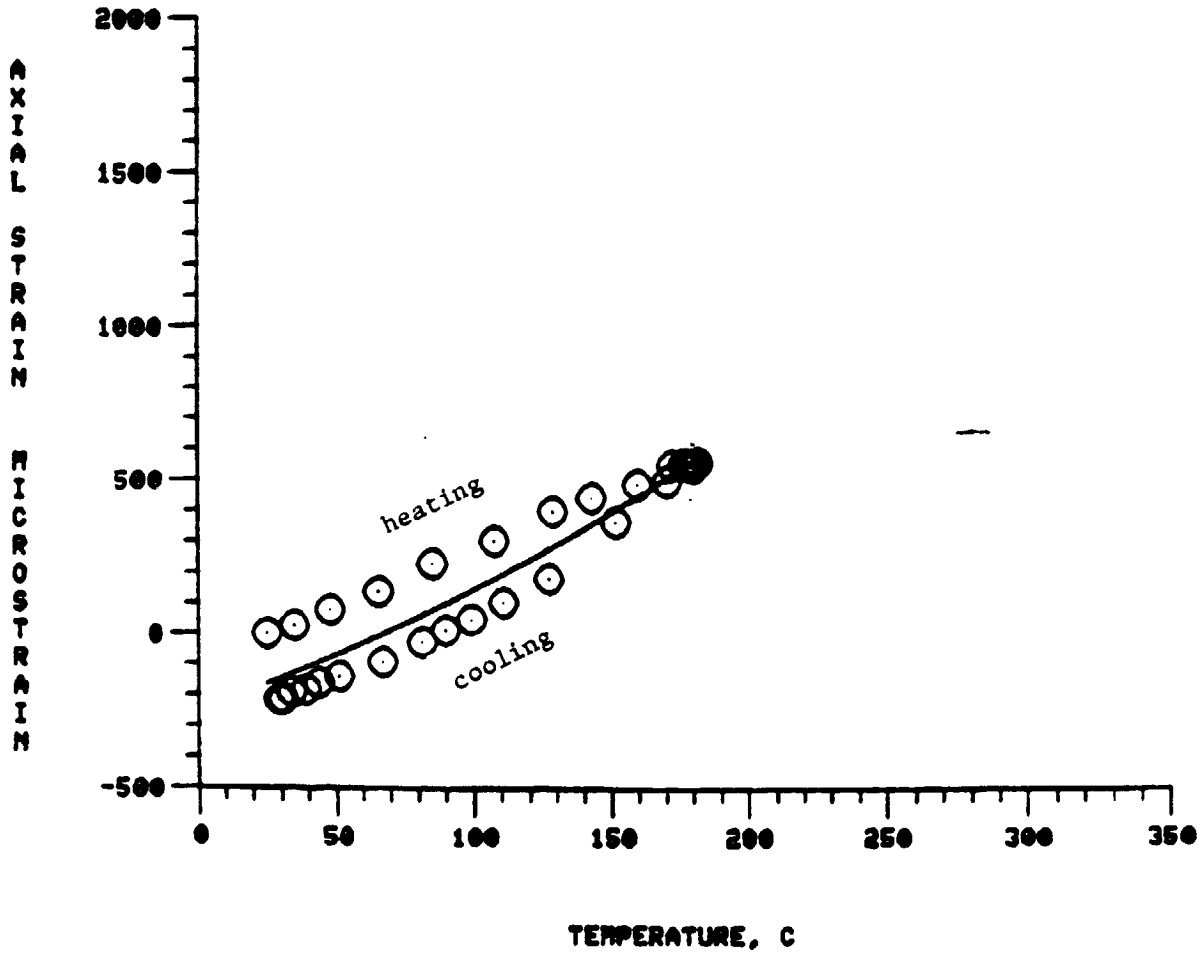

Fig. 52 Thermal Axial Strain, $[0_2^o/90_2^o]$ Laminate, RT-180°C, Cycle 4

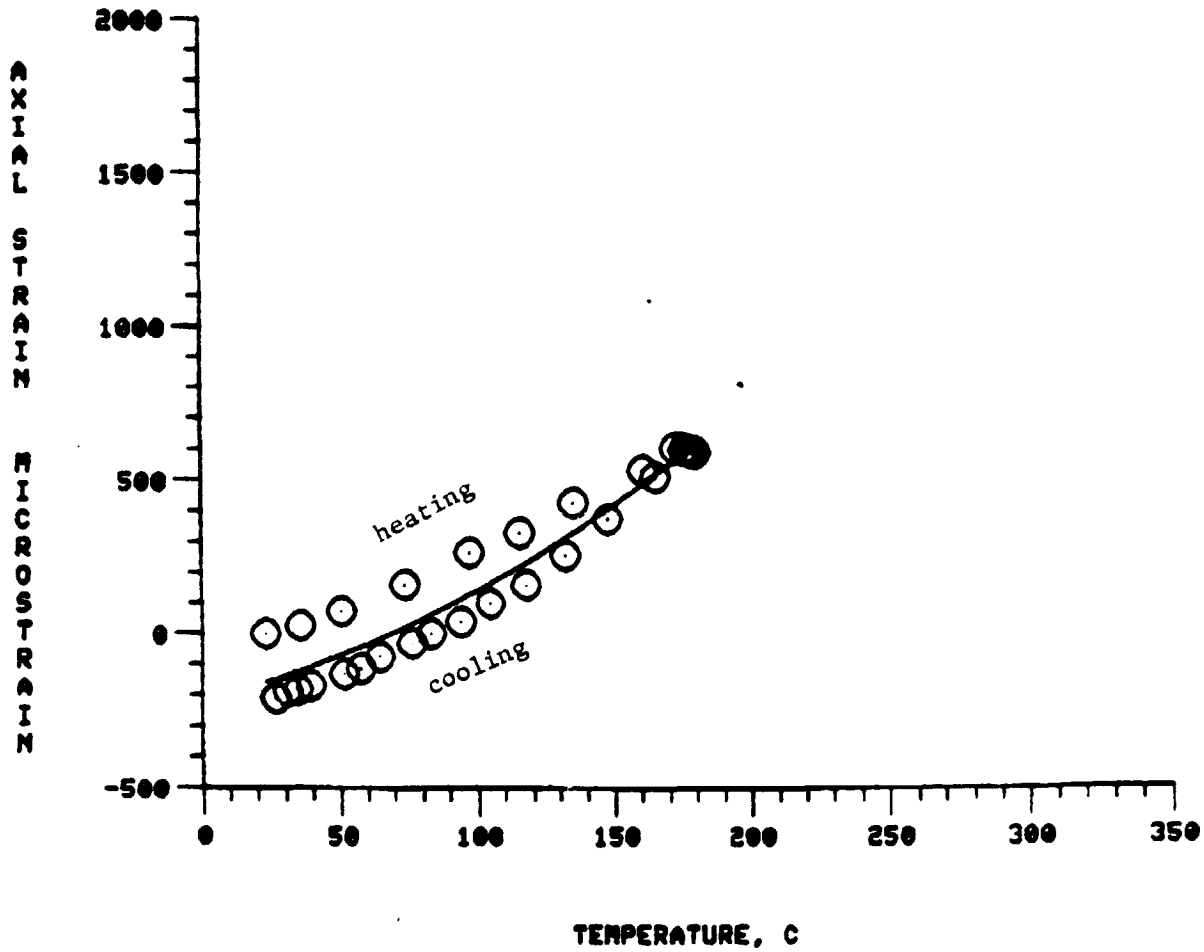

Fig. 53 Thermal Axial Strain, $[0^{\circ}_{2}/90^{\circ}_{2}]$ Laminate, RT-180°C, Cycle 5

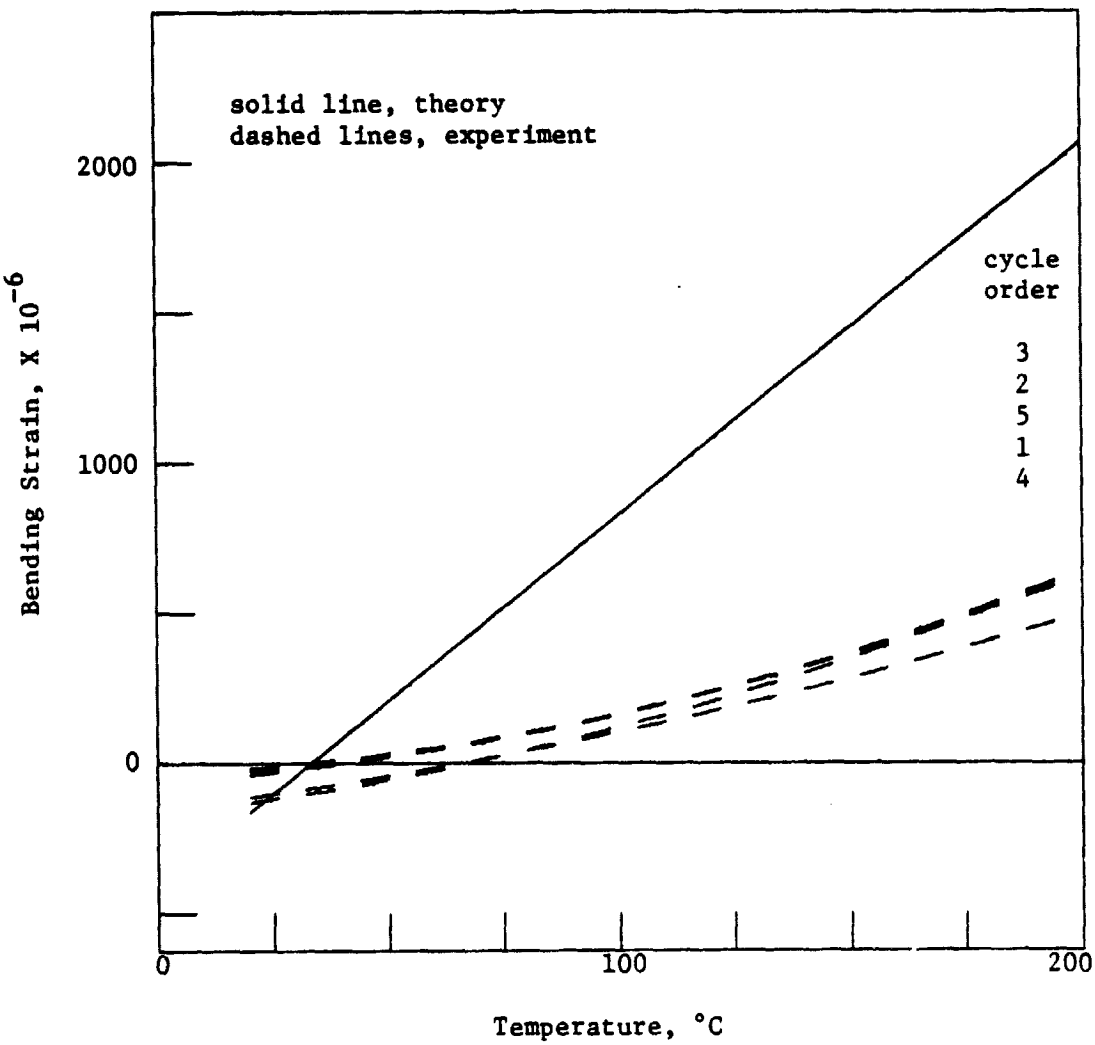

Fig. 54 Least-Squares, Thermal Bending Strains and Theoretical Prediction, $[0^\circ_2/90^\circ_2]$ Laminate, RT-180°C

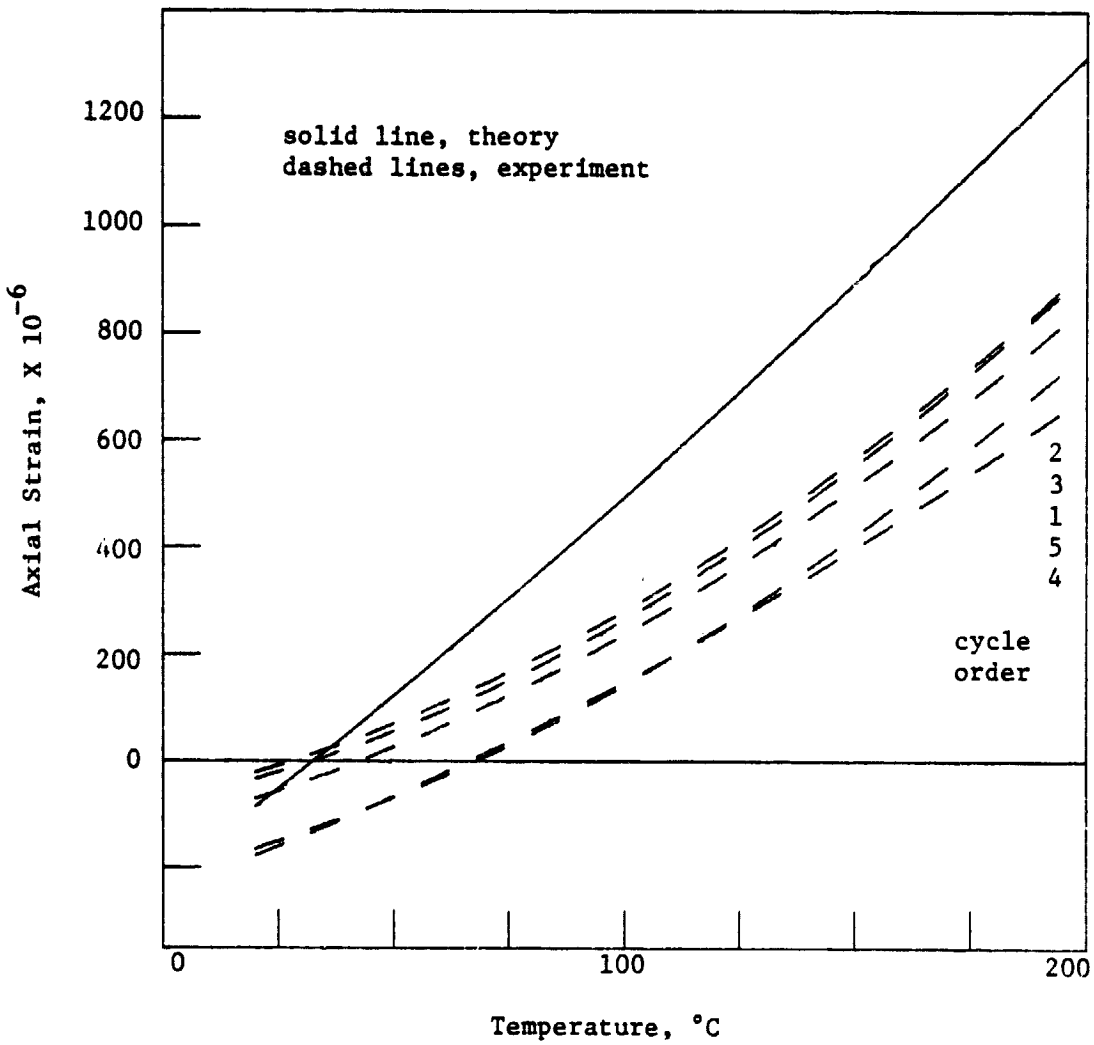

Fig. 55 Least-Squares Thermal Axial Strains and Theoretical Prediction, $[0^{\circ}_2/90^{\circ}_2]$ Laminate, RT-180°C

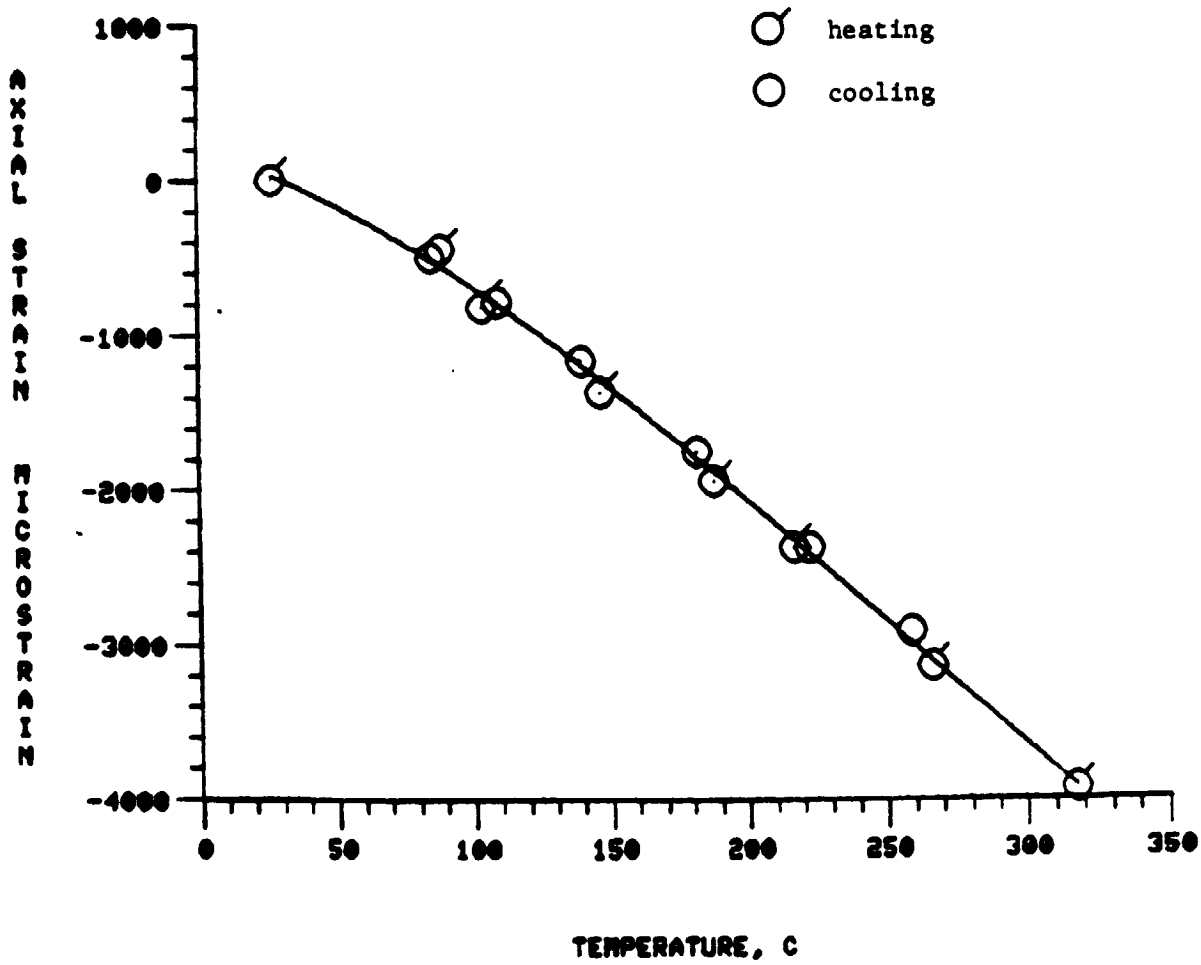

Fig. 56 Apparent Strain vs. Temperature, RT-315°C, Cycle 1

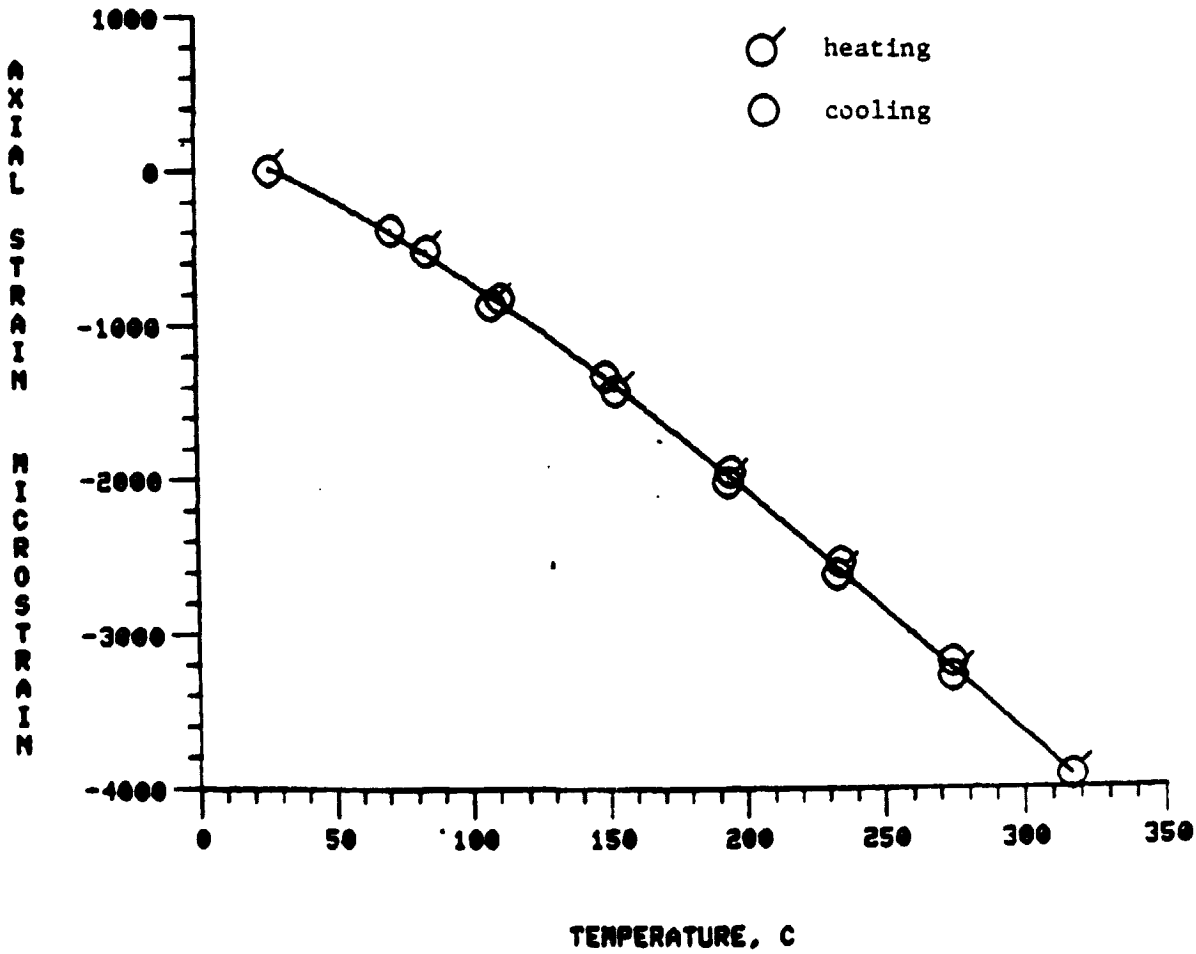

Fig. 57 Apparent Strain vs. Temperature, RT-315°C, Cycle 2

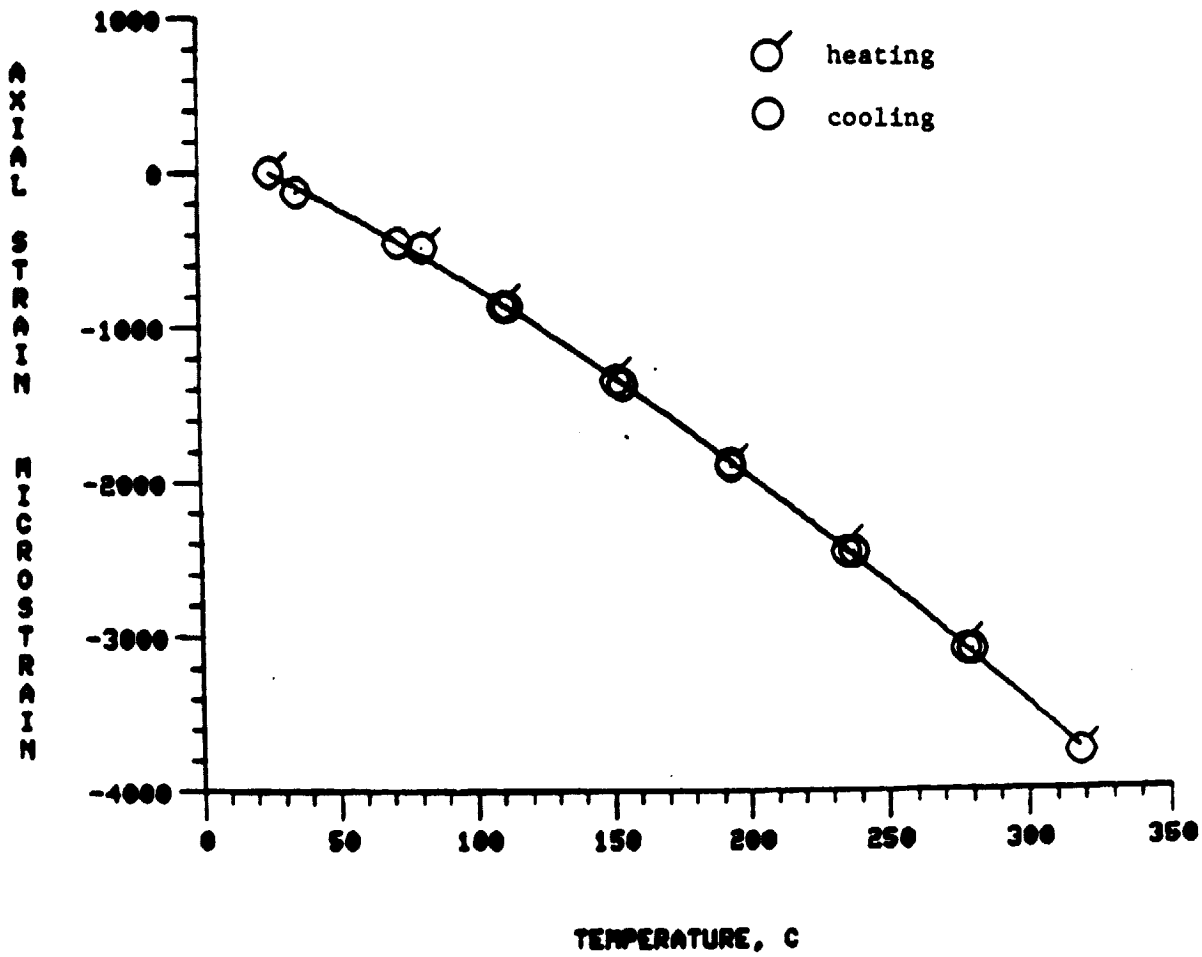

Fig. 58 Apparent Strain vs. Temperature, RT-315°C, Cycle 3

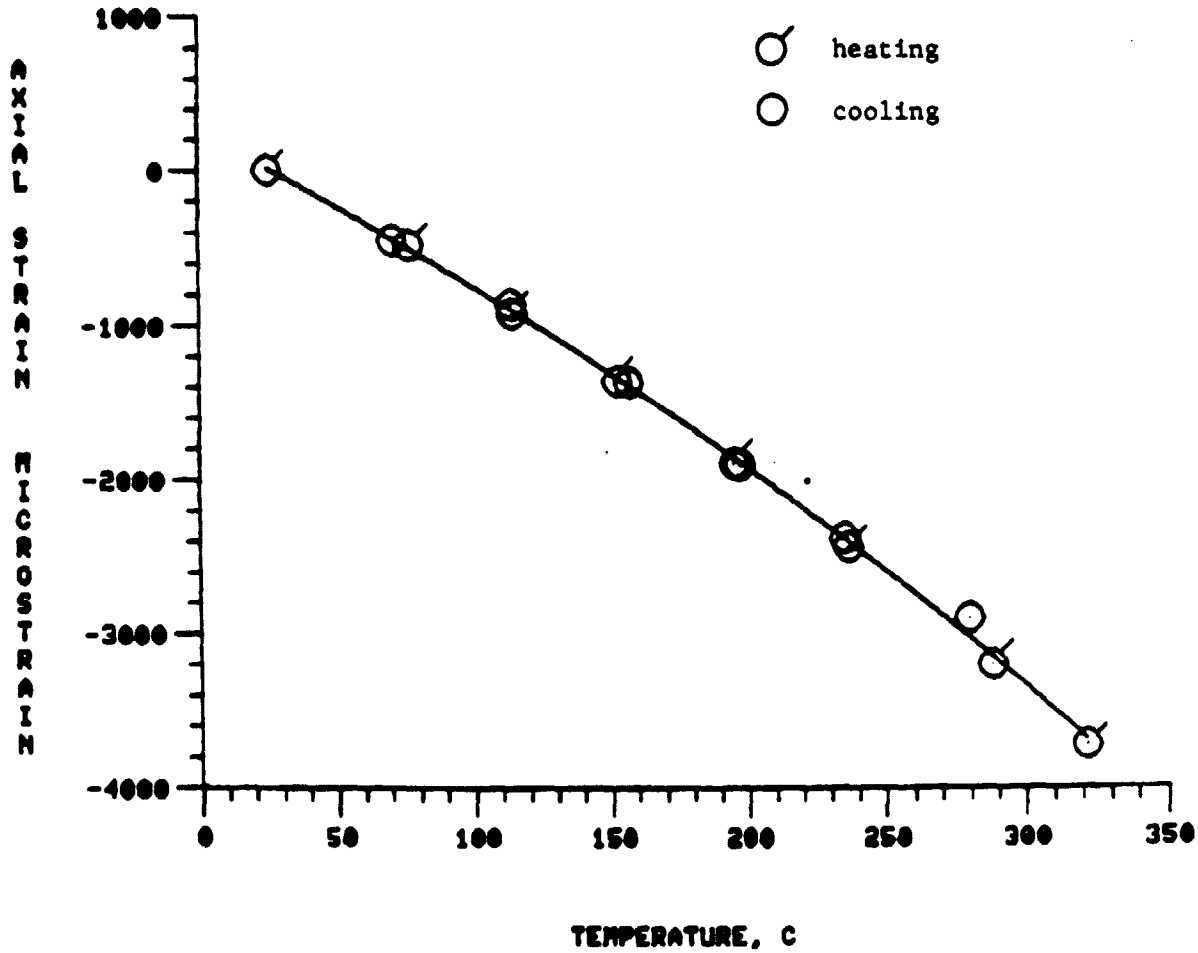

Fig. 59 Apparent Strain vs. Temperature, RT-315°C, Cycle 4

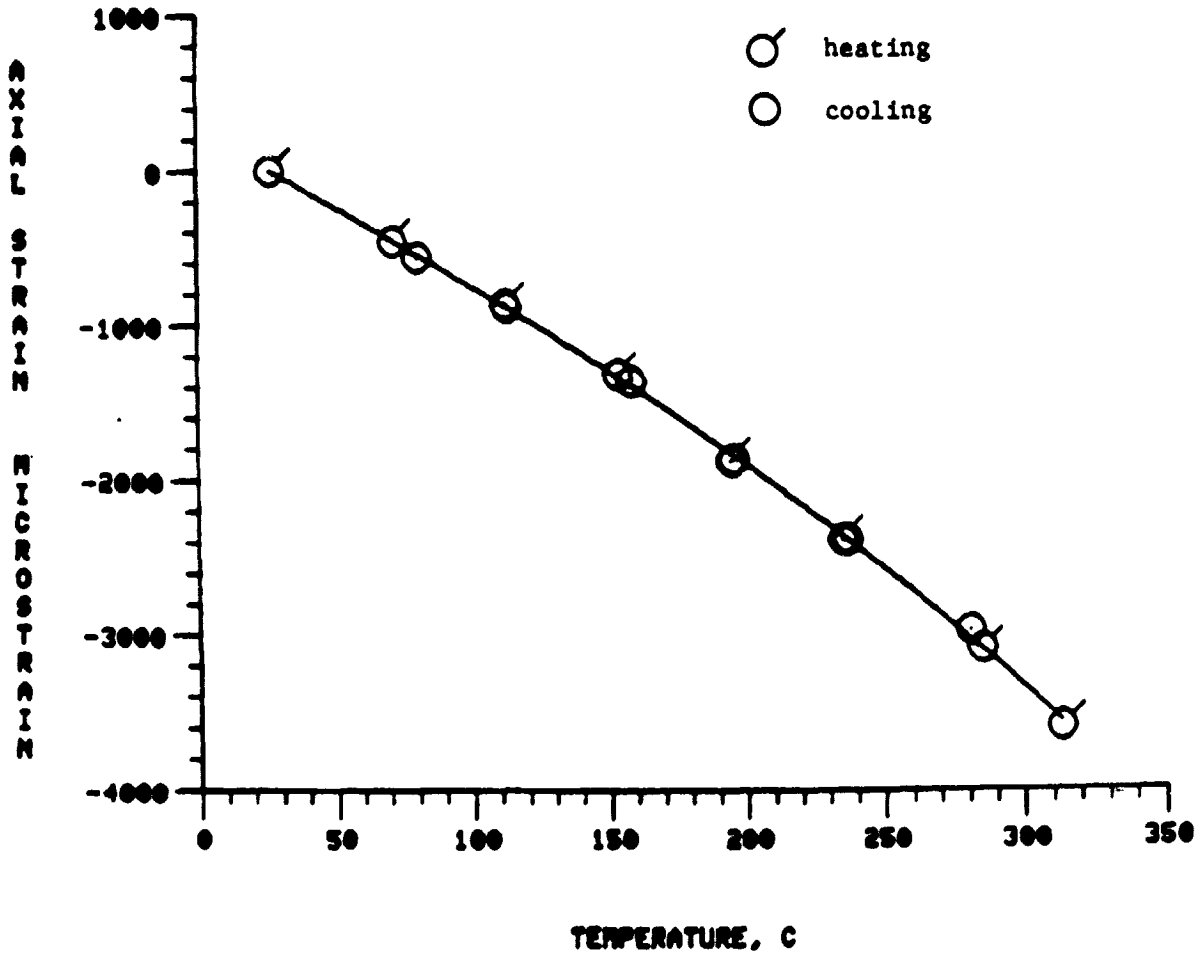

Fig. 60 Apparent Strain vs. Temperature, RT-315°C, Cycle 5

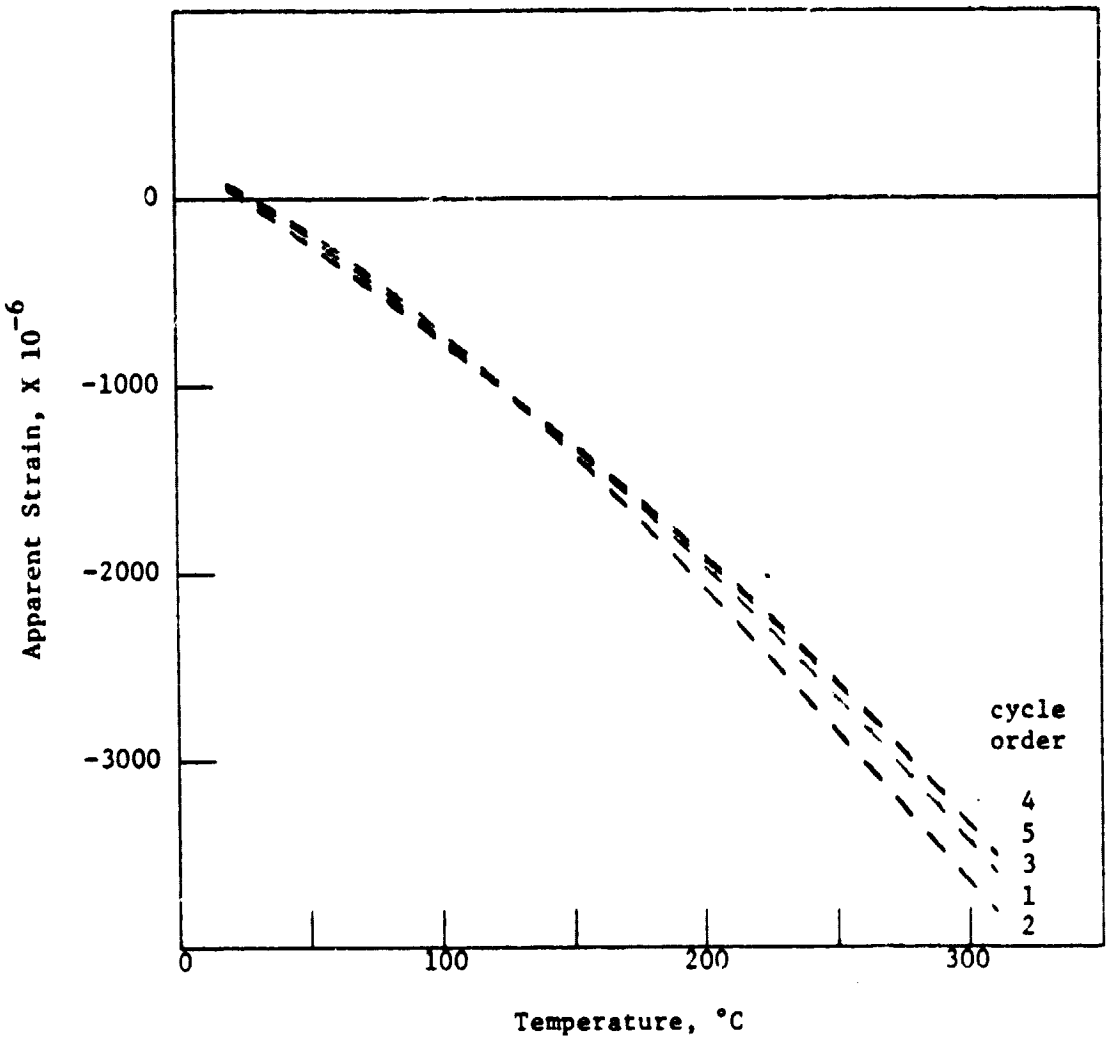

Fig. 61 Apparent Strain vs. Temperature, RT-315°C, Least-Squares Fit, All 5 Cycles

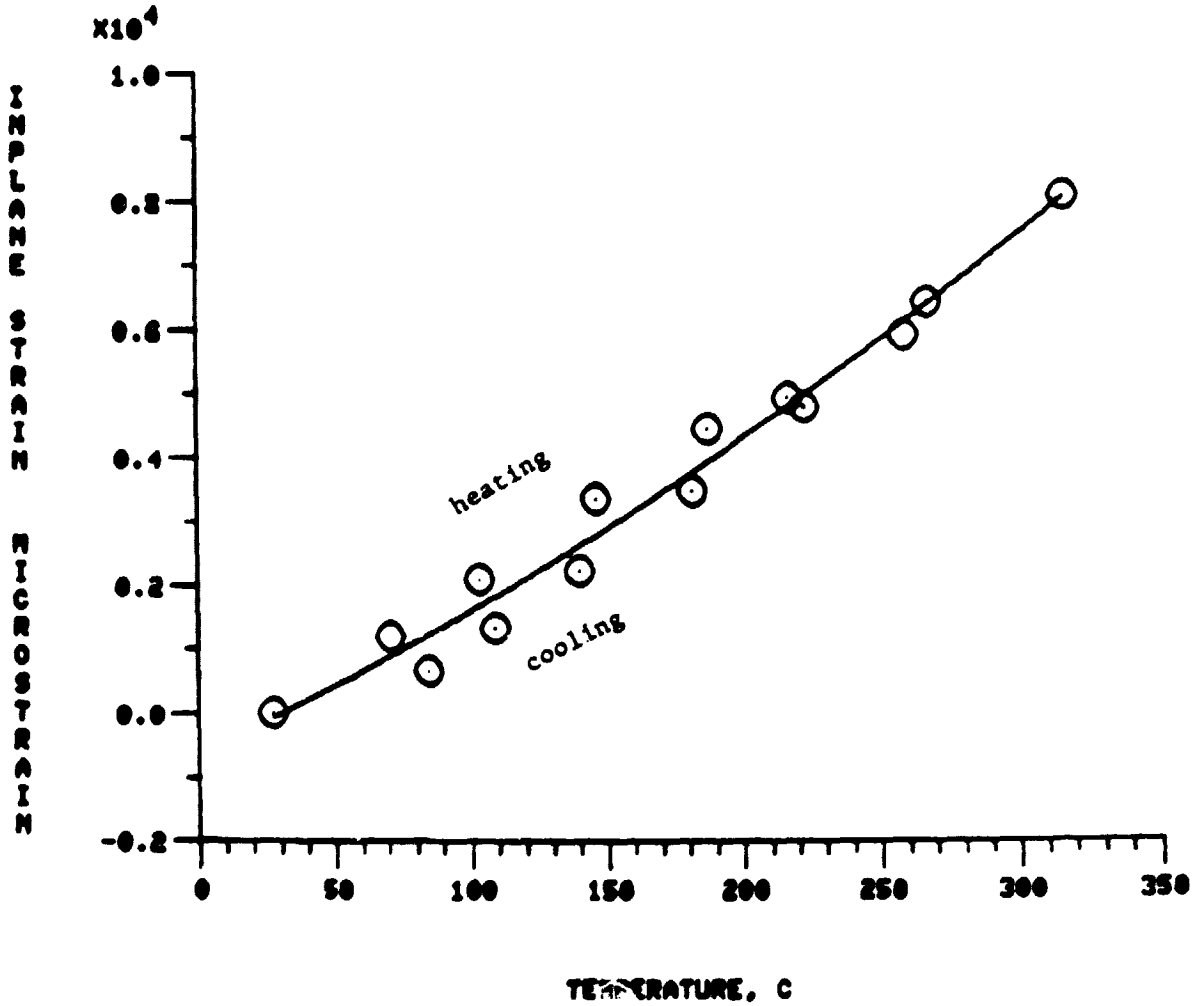

Fig. 62 Thermal Expansion of $[0_8^o]$ Laminate in Matrix Direction, RT-315°C, Cycle 1

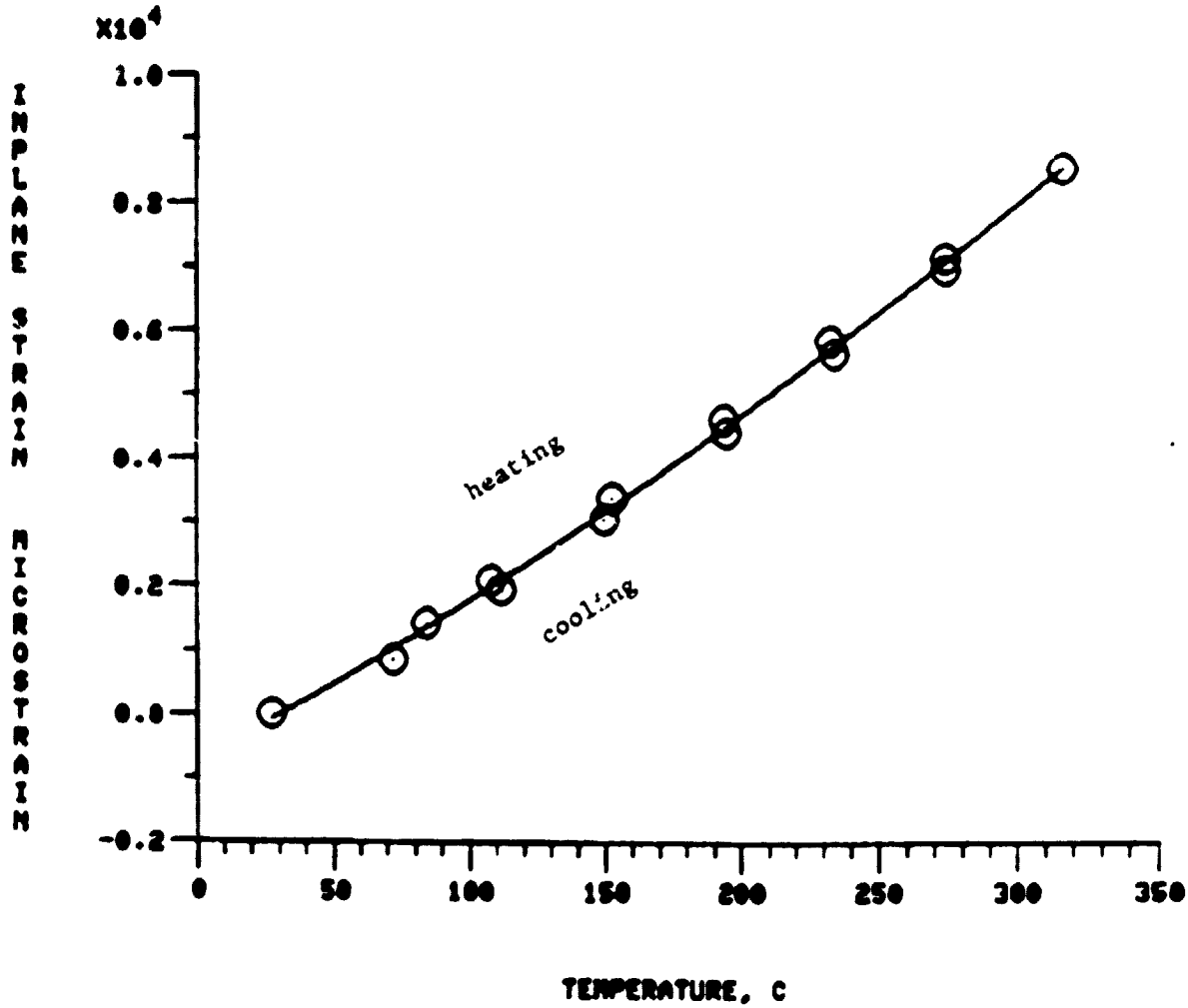

Fig. 63 Thermal Expansion of $[0_8^\circ]$ Laminate in Matrix Direction. RT-315°C, Cycle 2

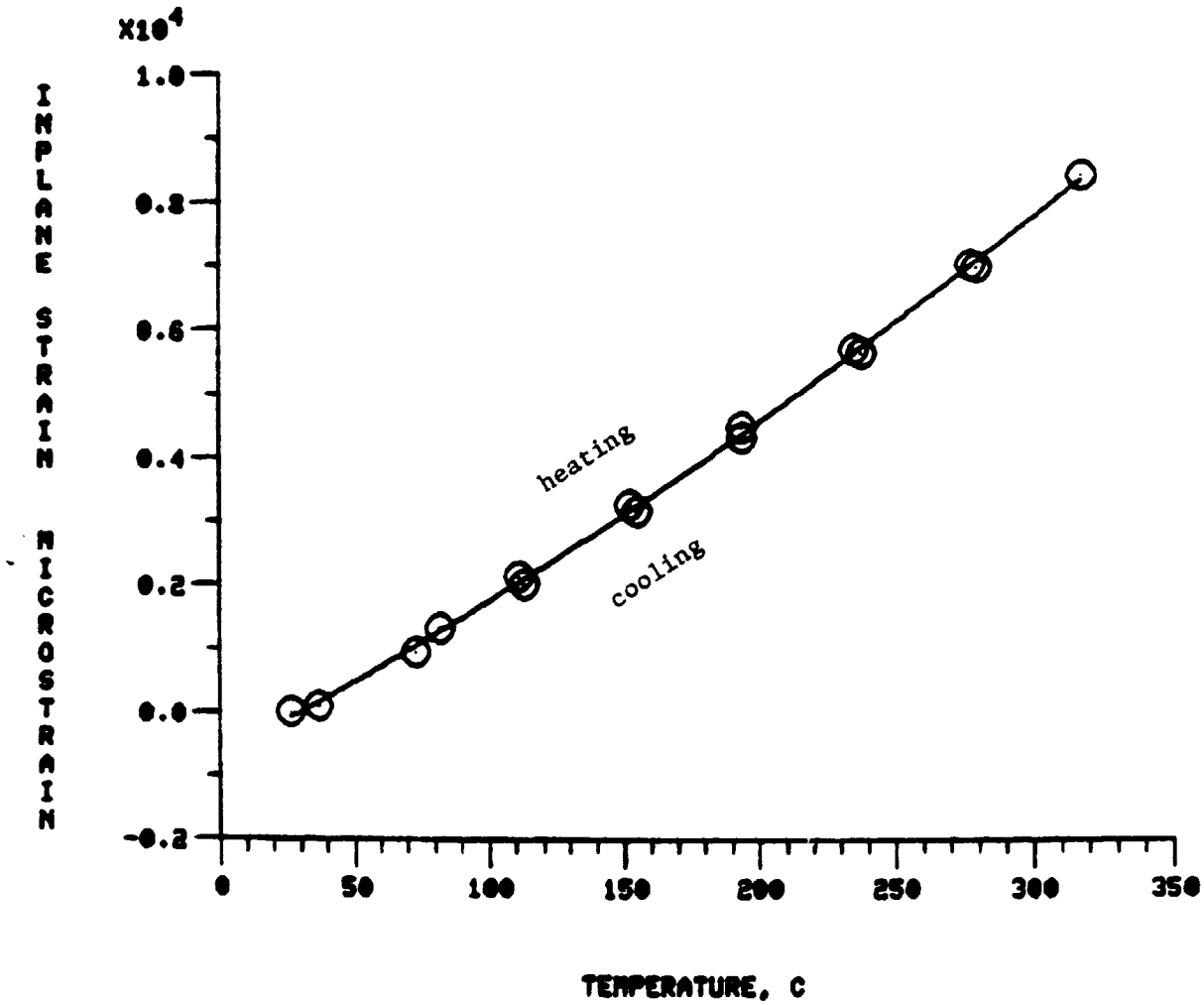

Fig. 64 Thermal Expansion of $[0_8^o]$ Laminate in Matrix Direction, RT-315°C, Cycle 3

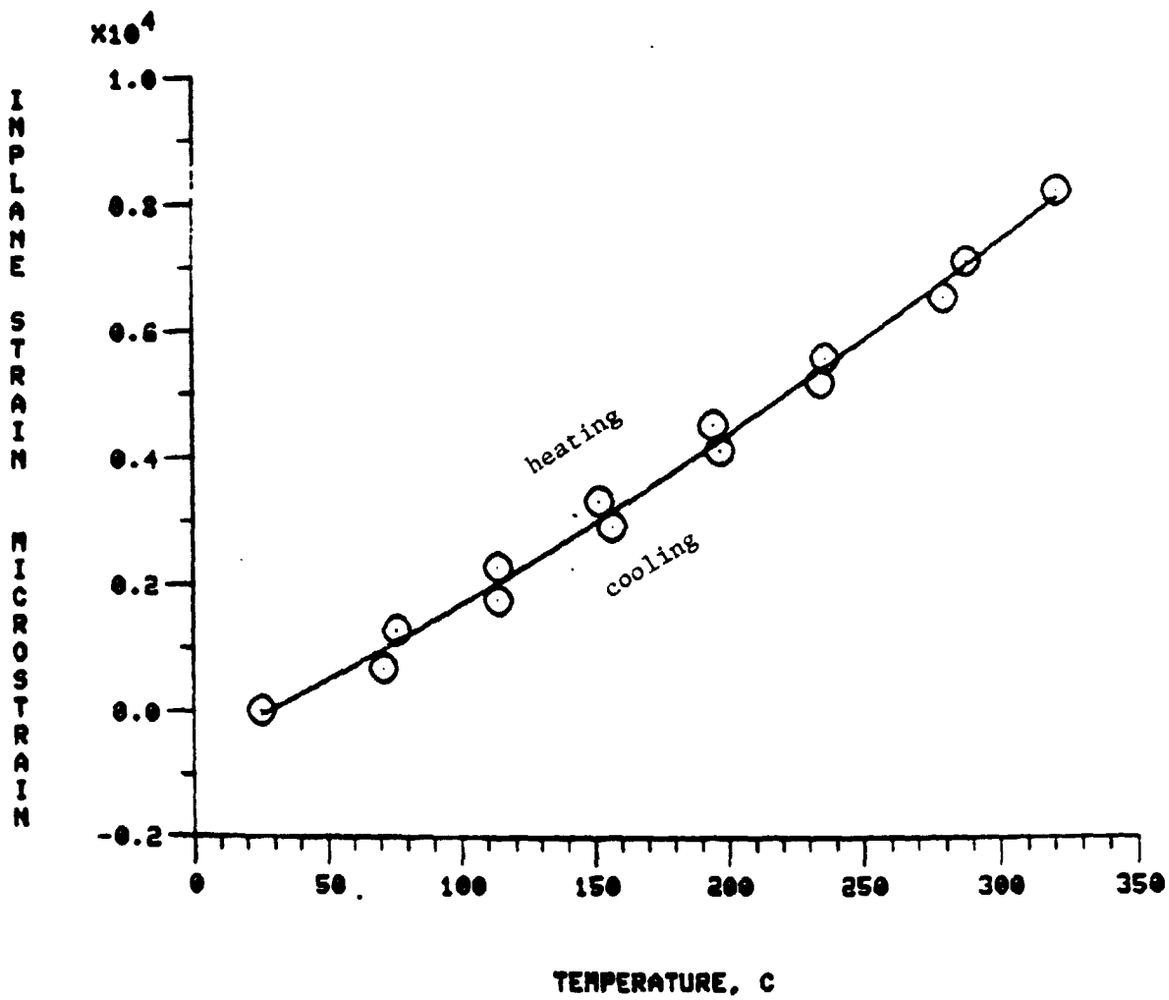

Fig. 65 Thermal Expansion of $[0^{\circ}_{8}]$ Laminate in Matrix Direction, RT-315°C, Cycle 4

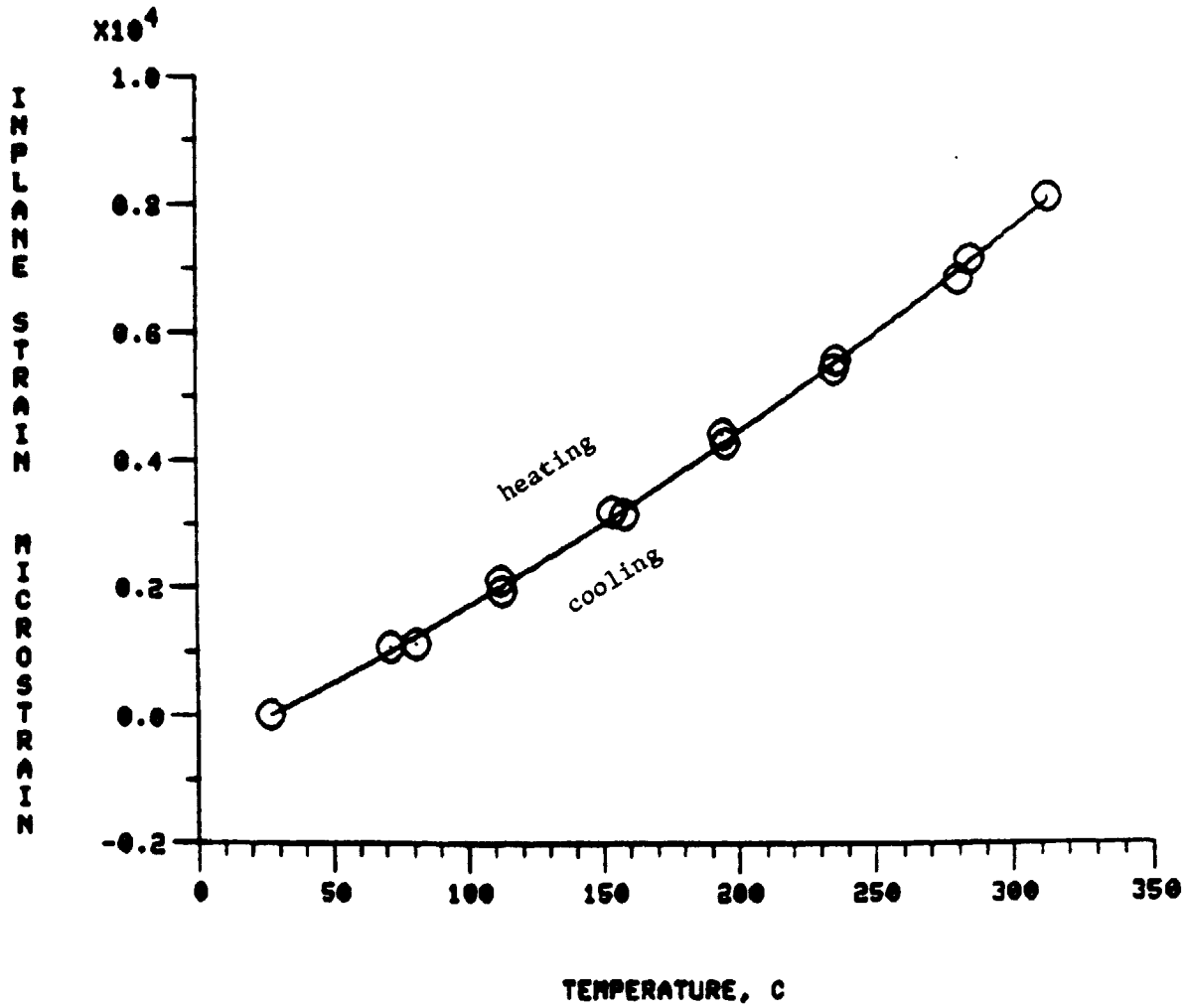

Fig. 66 Thermal Expansion of $[0_8^o]$ Laminate in Matrix Direction, RT-315°C, Cycle 5

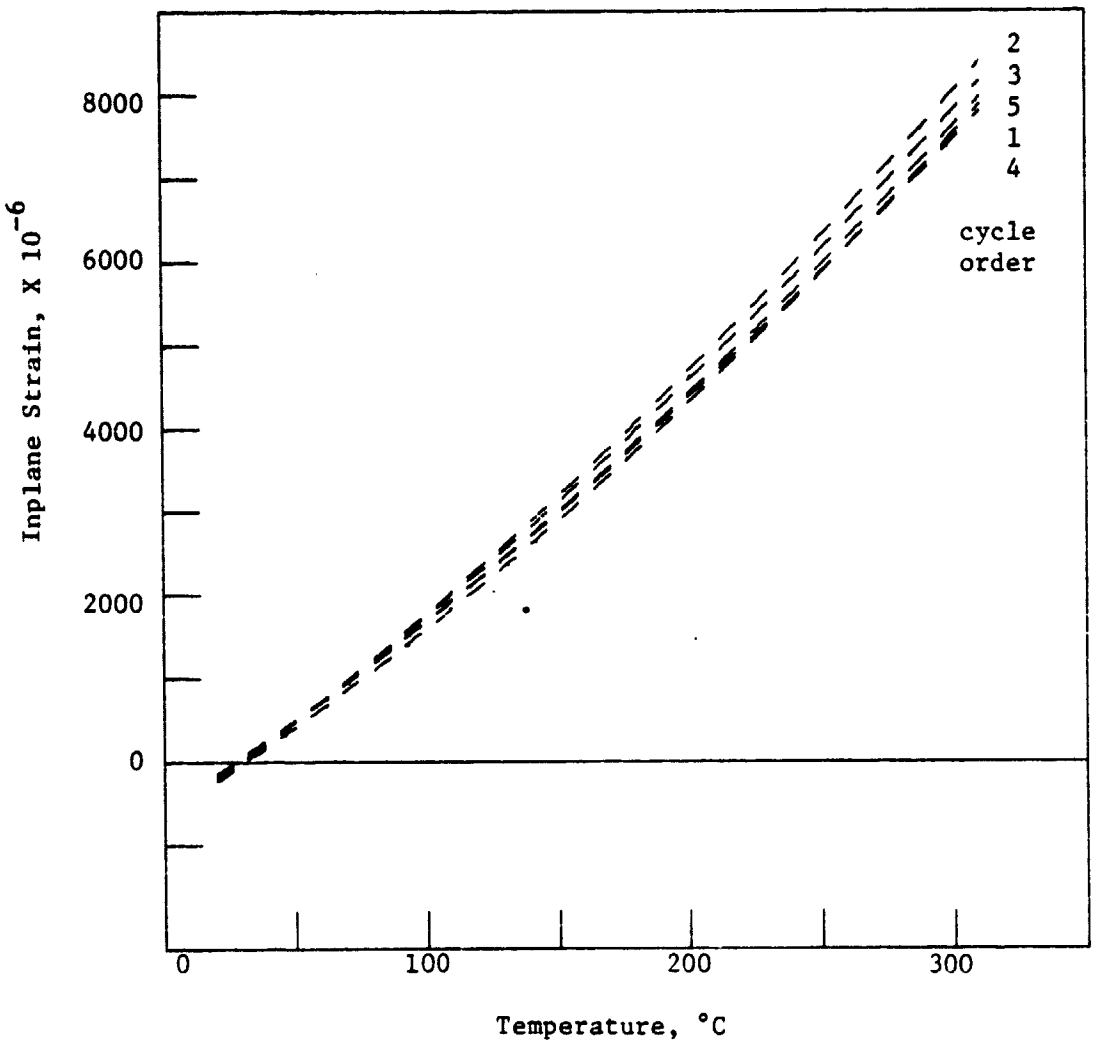

Fig. 67 Thermal Expansion of $[0^{\circ}_{8}]$ Laminate in Matrix Direction, RT-315°C, Least Squares Fit, All 5 Cycles

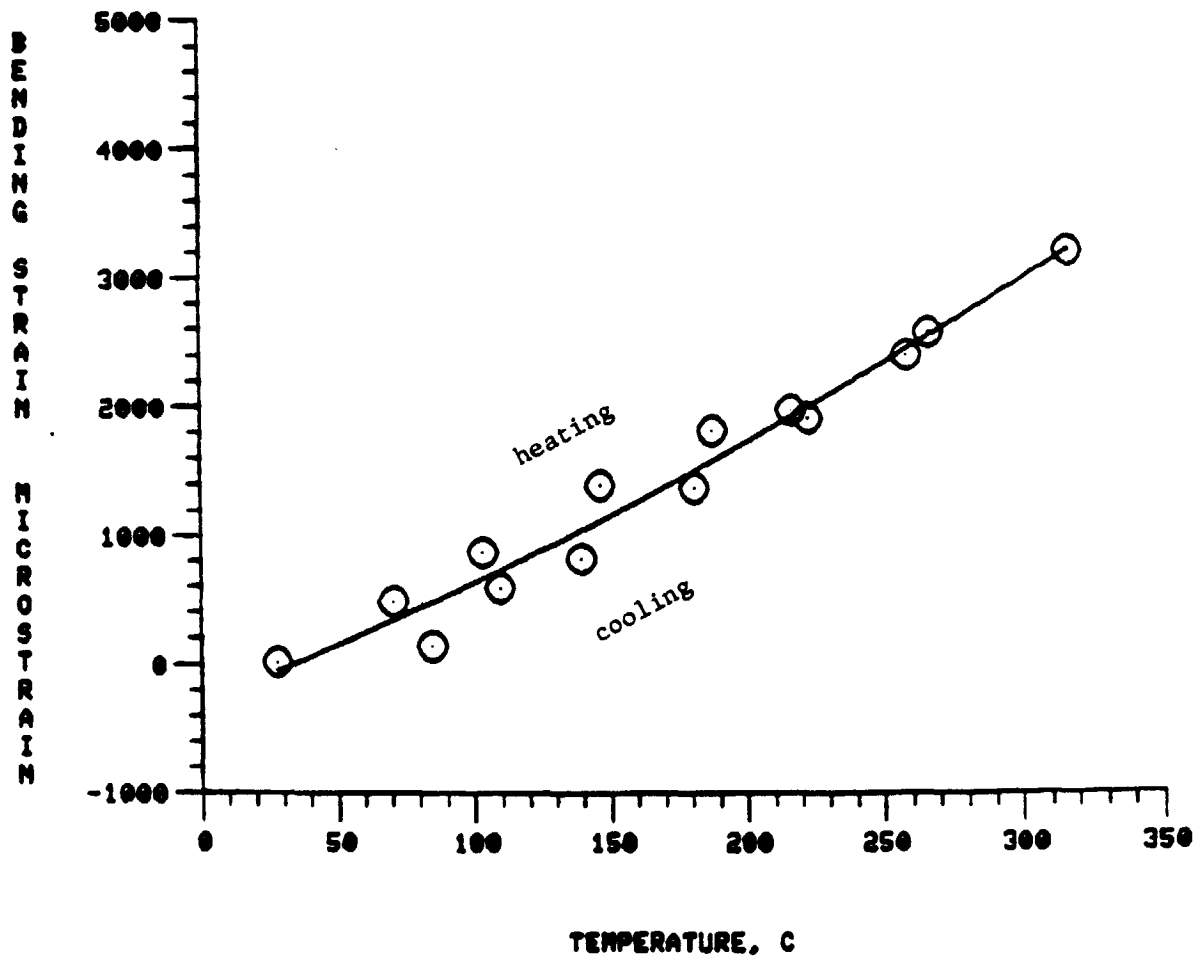

Fig. 68 Thermal Bending Strain, $[0^{\circ}_{4}/90^{\circ}_{4}]$ Laminate, RT-315°C, Cycle 1

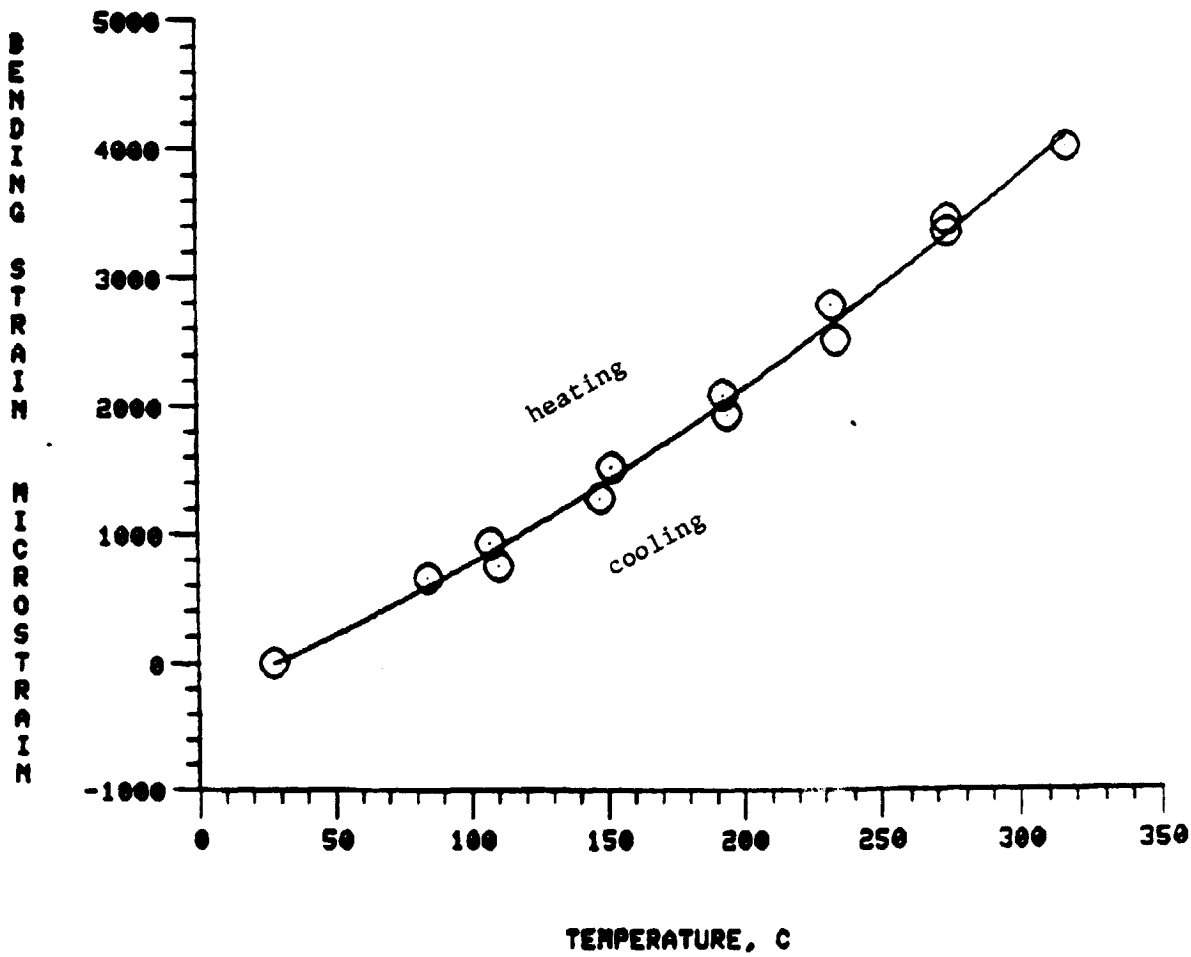

Fig. 69 Thermal Bending Strain, $[0^{\circ}_{4}/90^{\circ}_{4}]$ Laminate, RT-315°C, Cycle 2

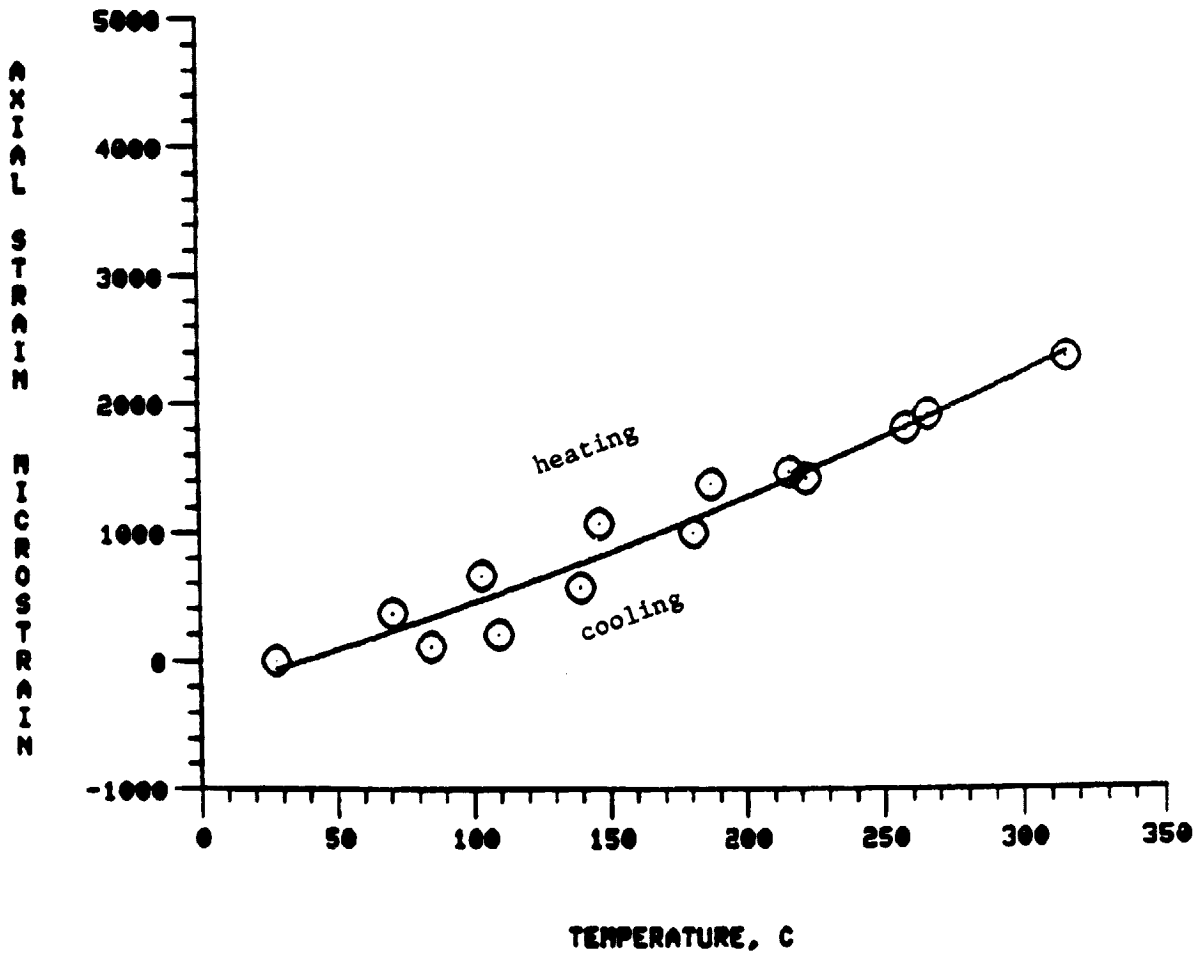

Fig. 70 Thermal Axial Strain, $[0_4^\circ/90_4^\circ]$ Laminate, RT-315°C, Cycle 1

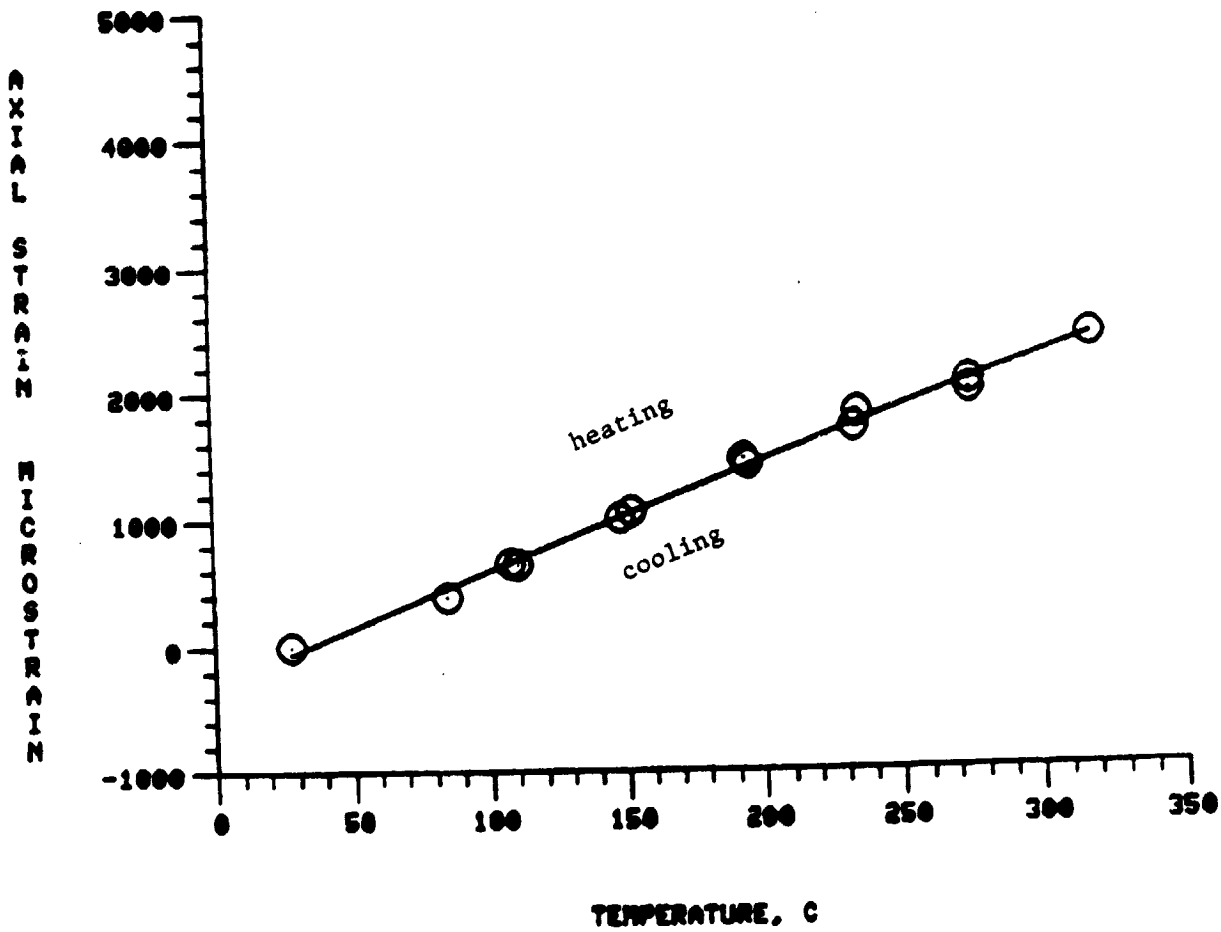

Fig. 71 Thermal Axial Strain, $[0^{\circ}_{4}/90^{\circ}_{4}]$ Laminate, RT-315°C, Cycle 2

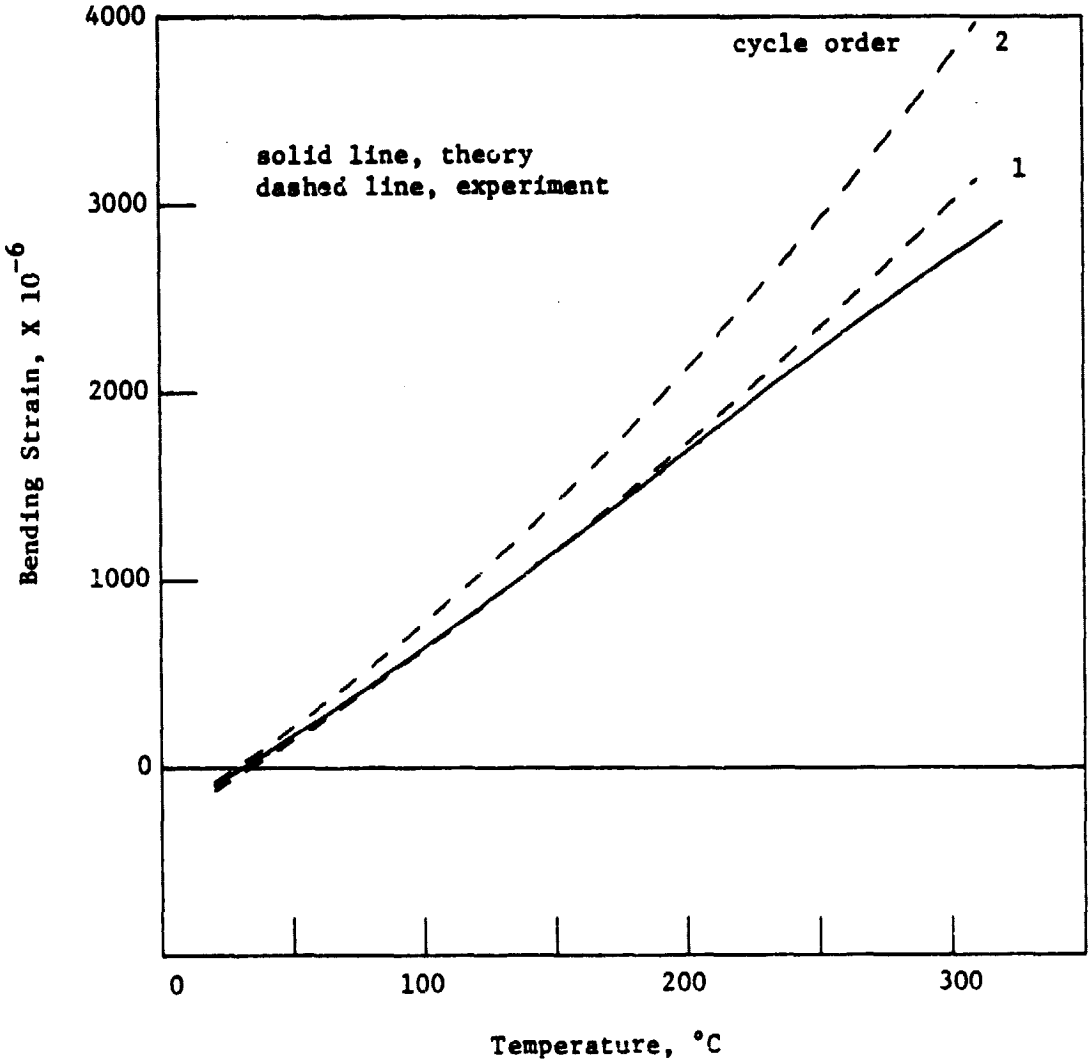

Fig. 72 Least-Squares Thermal Bending Strains and Theoretical Prediction, $[0^\circ_4/90^\circ_4]$ Laminate, RT-315°C

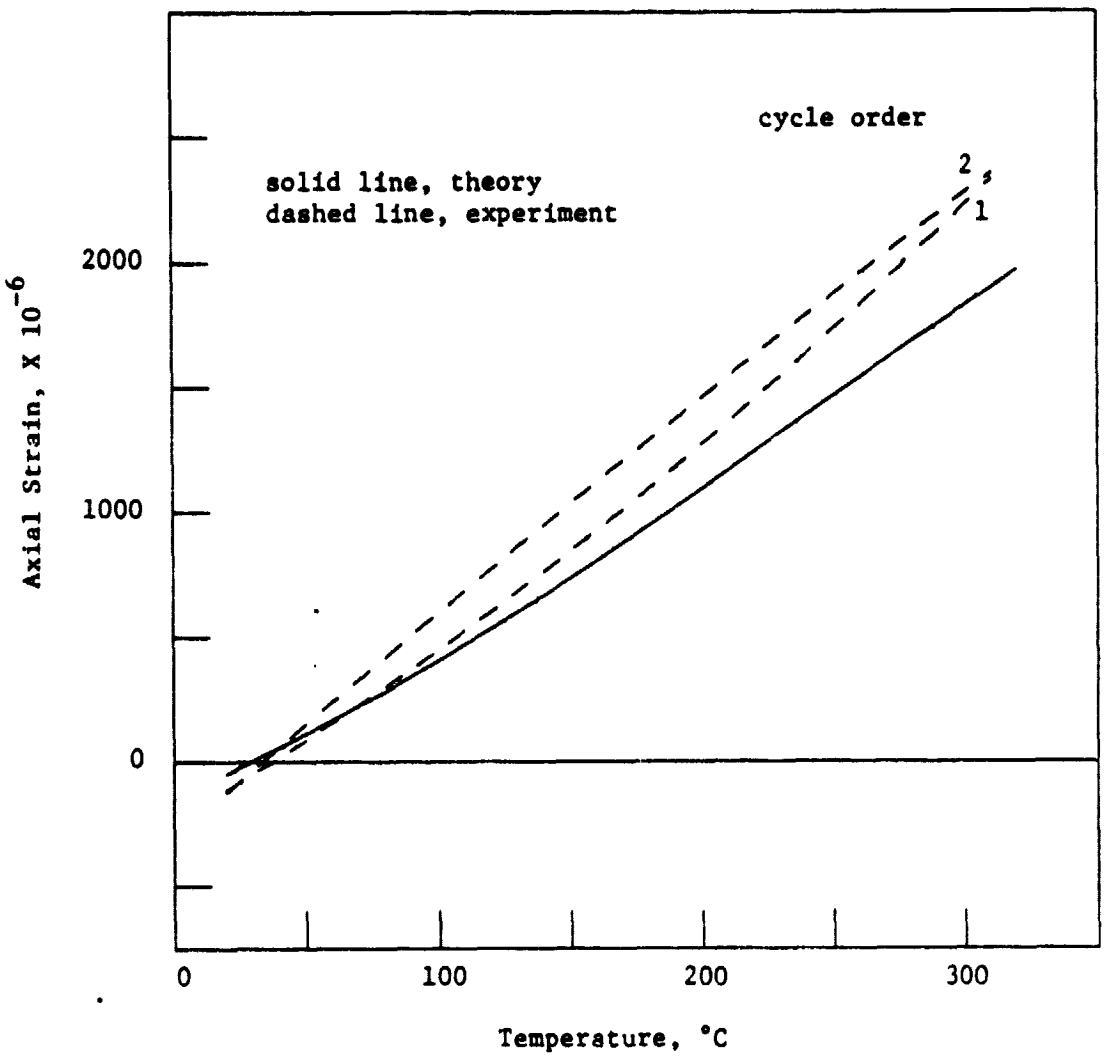

Fig. 73 Least-Squares Thermal Axial Strains and Theoretical Prediction, $[0^{\circ}_{4}/90^{\circ}_{4}]$ Laminate, RT-315°C

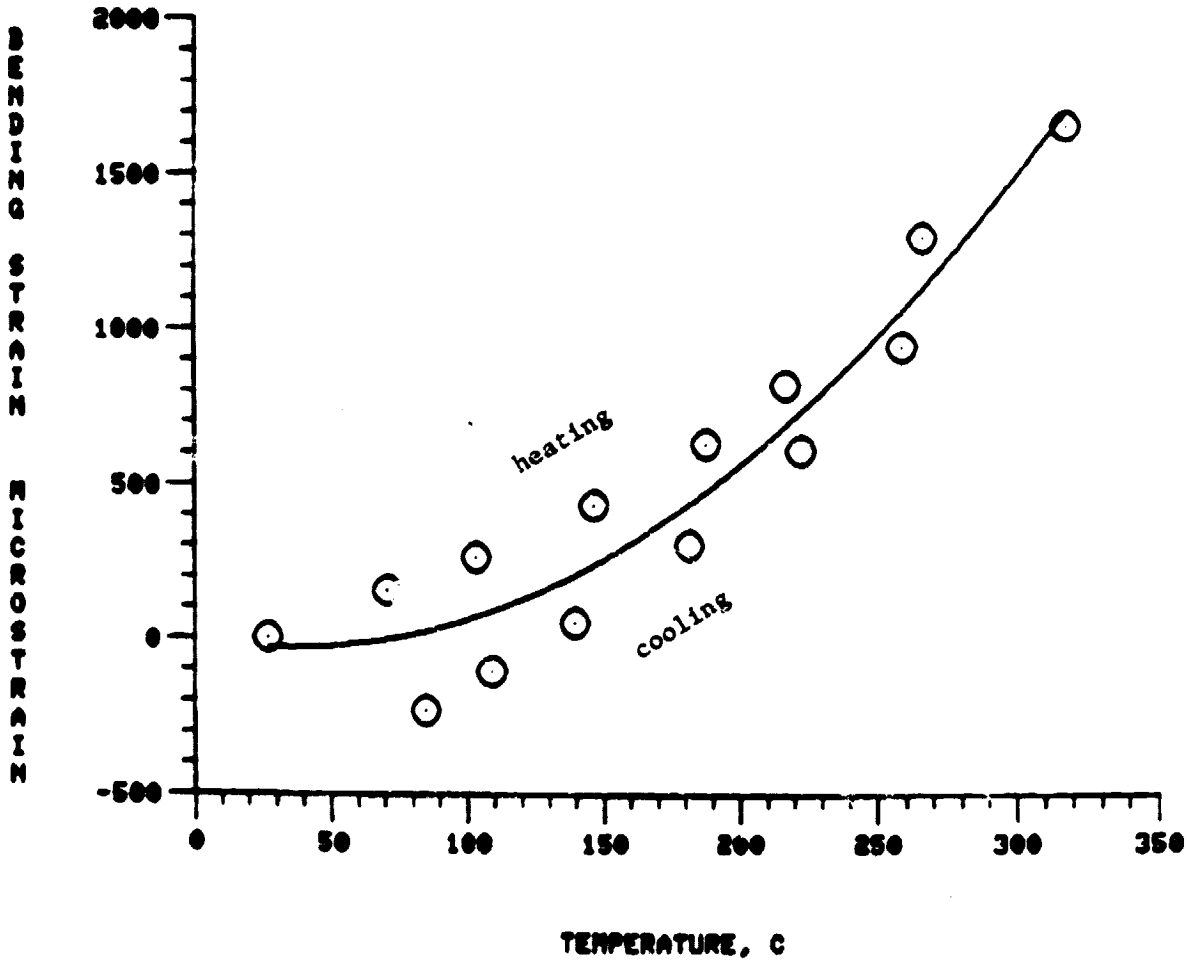

Fig. 74 Thermal Bending Strain, $[0_2^\circ/90_2^\circ]$ Laminate, RT-315°C, Cycle 1

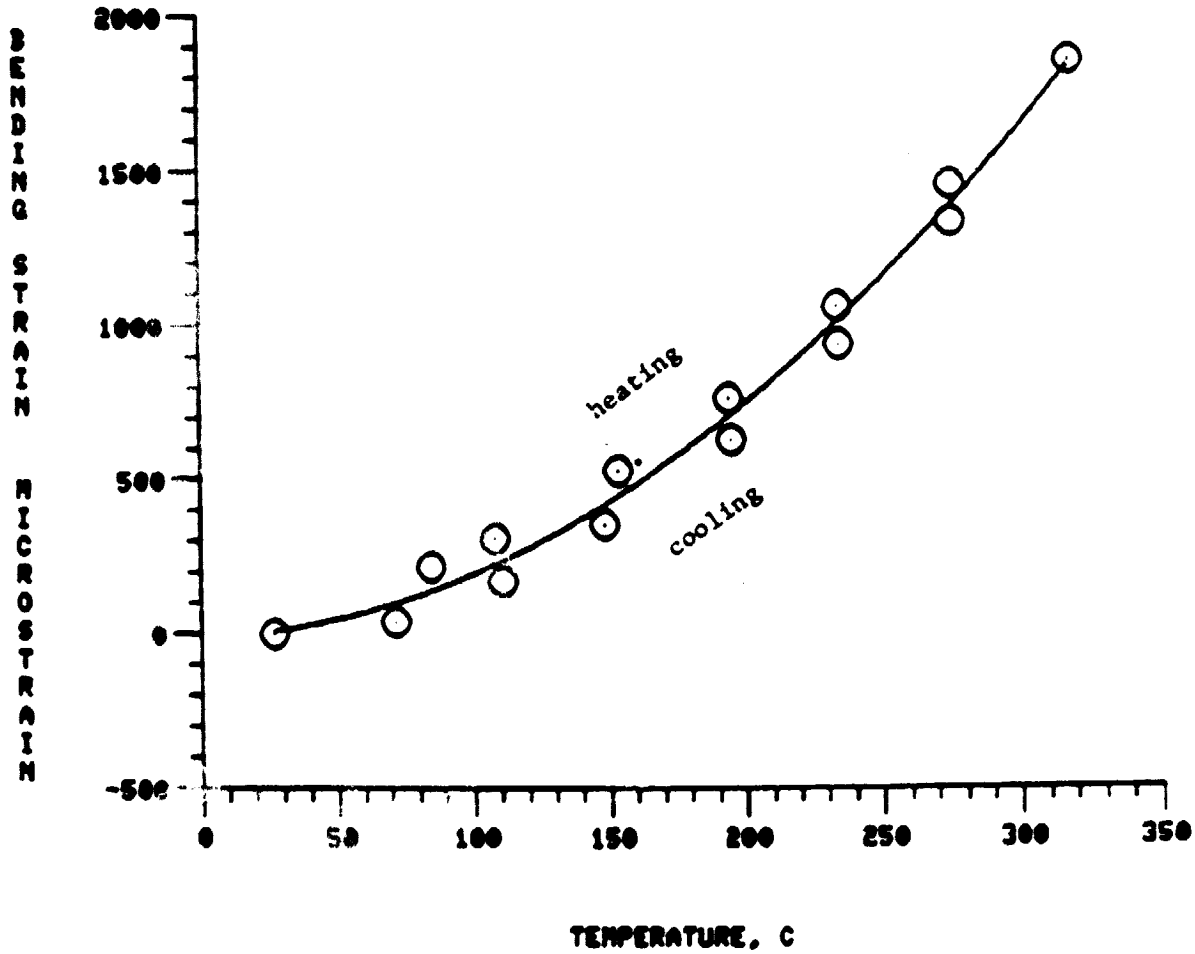

Fig. 75 Thermal Bending Strain, $[0^{\circ}_{2}/90^{\circ}_{2}]$ Laminate, RT-315°C, Cycle 2

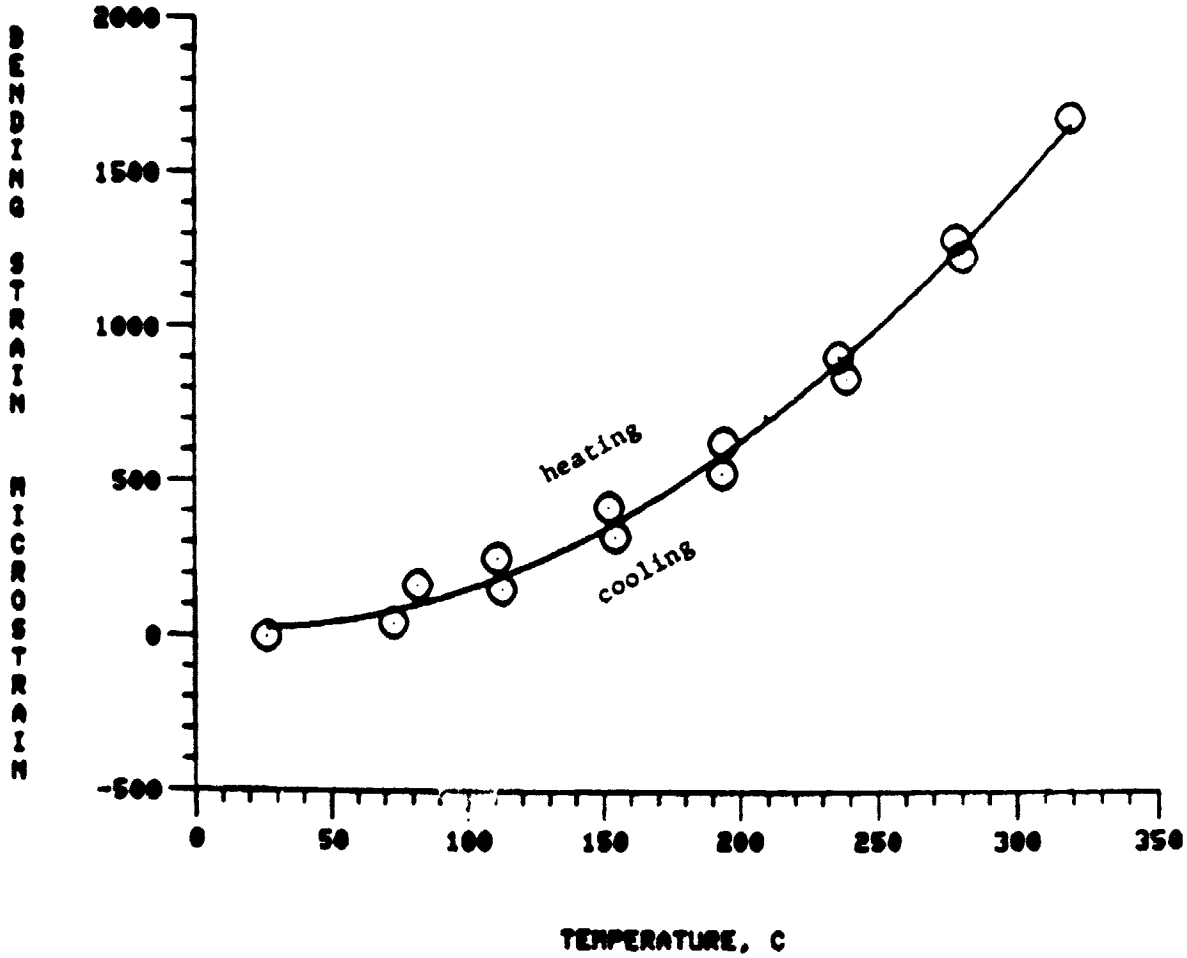

Fig. 76 Thermal Bending Strain, $[0_2^0/90_2^0]$ Laminate, RT-315°C, Cycle 3

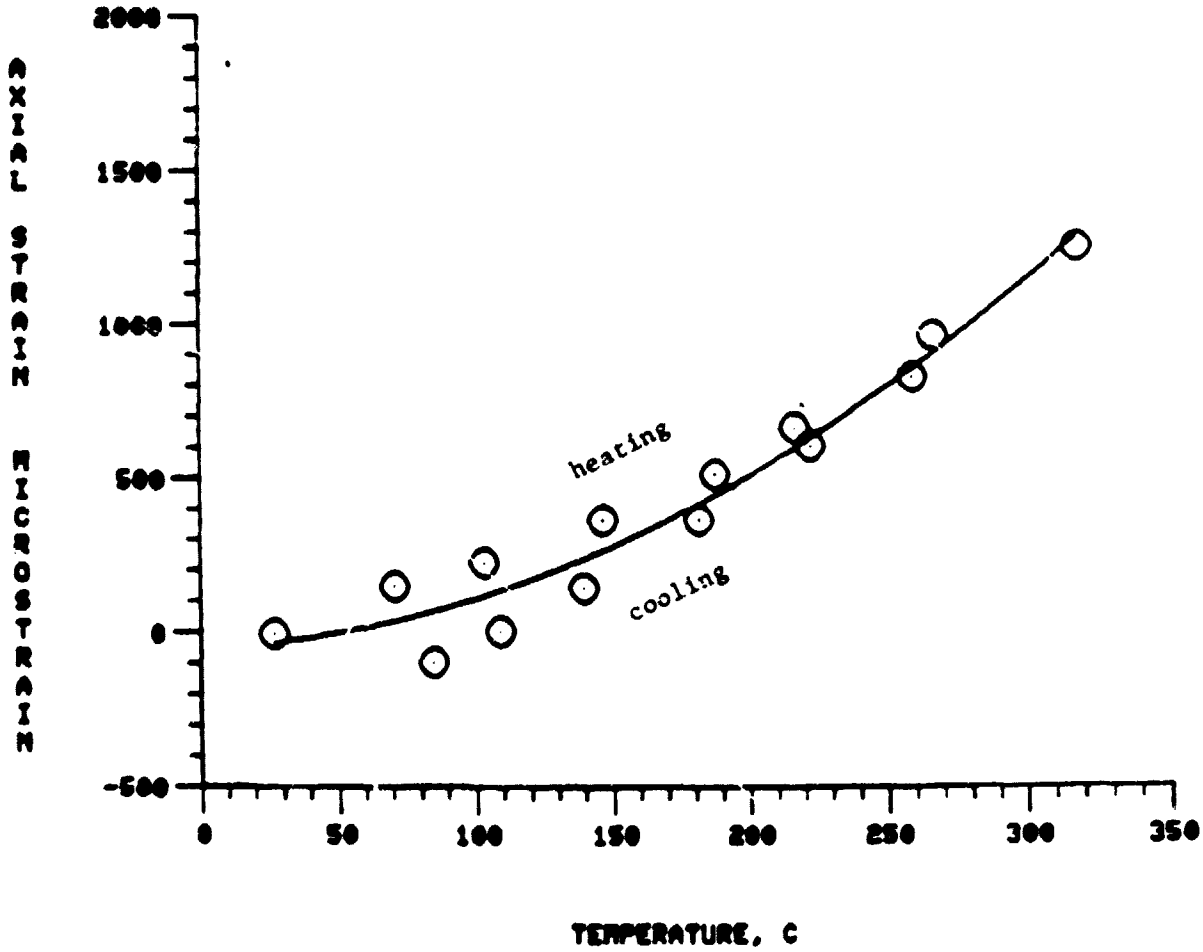

Fig. 77 Thermal Axial Strain, $[0^\circ_2/90^\circ_2]$ Laminate, RT-315°C, Cycle 1

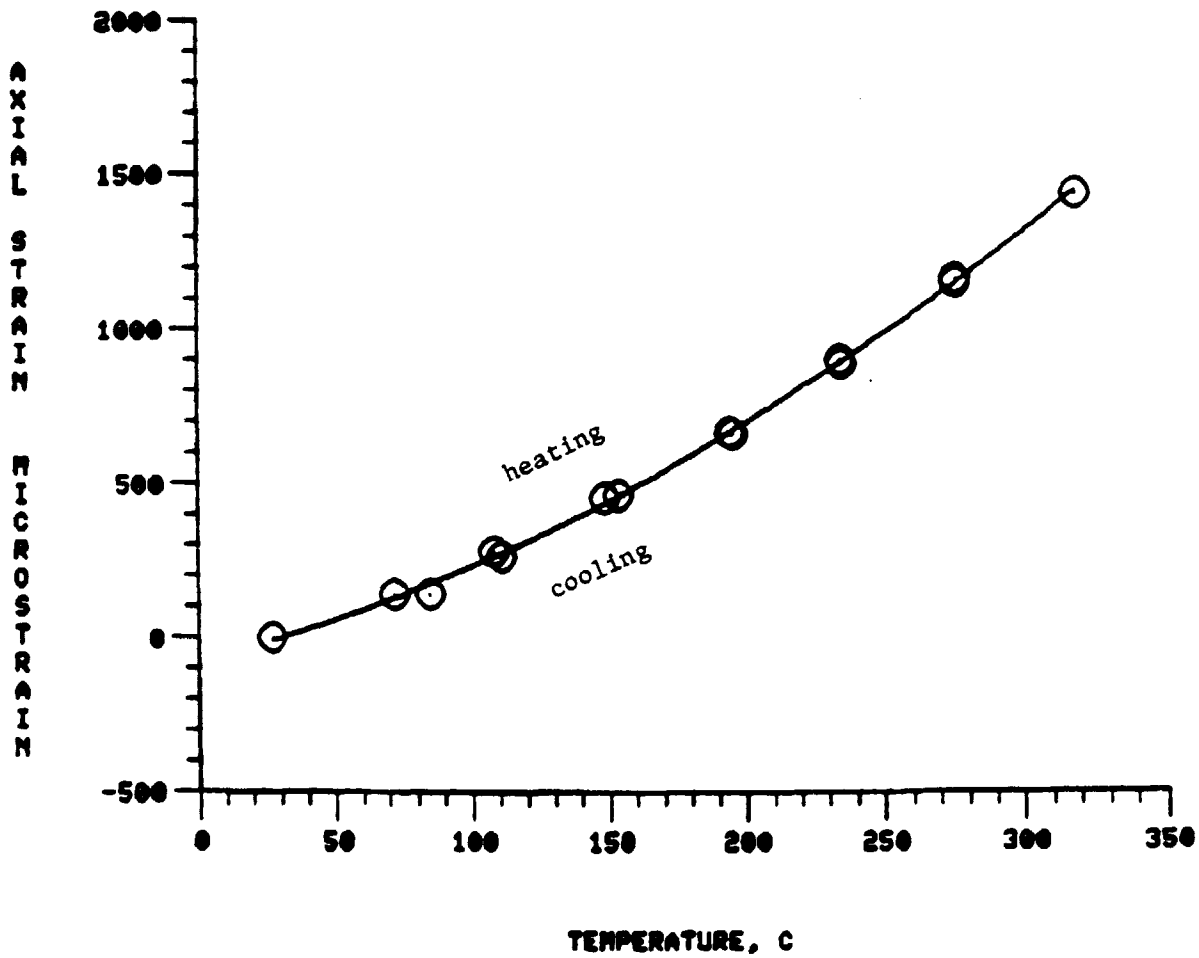

Fig. 78 Thermal Axial Strain, $[0^{\circ}_{2}/90^{\circ}_{2}]$ Laminate, RT-315°C, Cycle 2

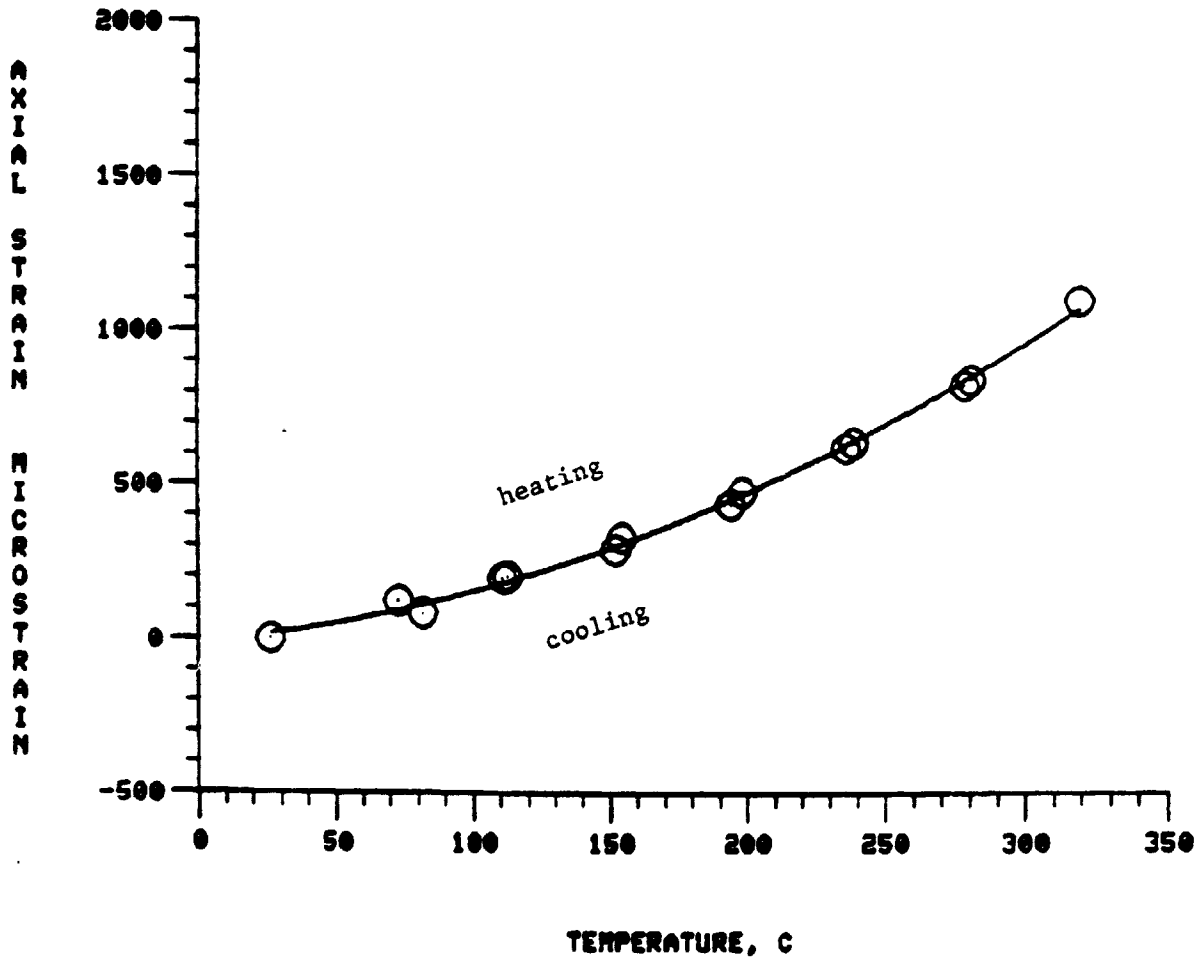

Fig. 79 Thermal Axial Strain, $[0_2^o/90_2^o]$ Laminate, RT-315°C, Cycle 3

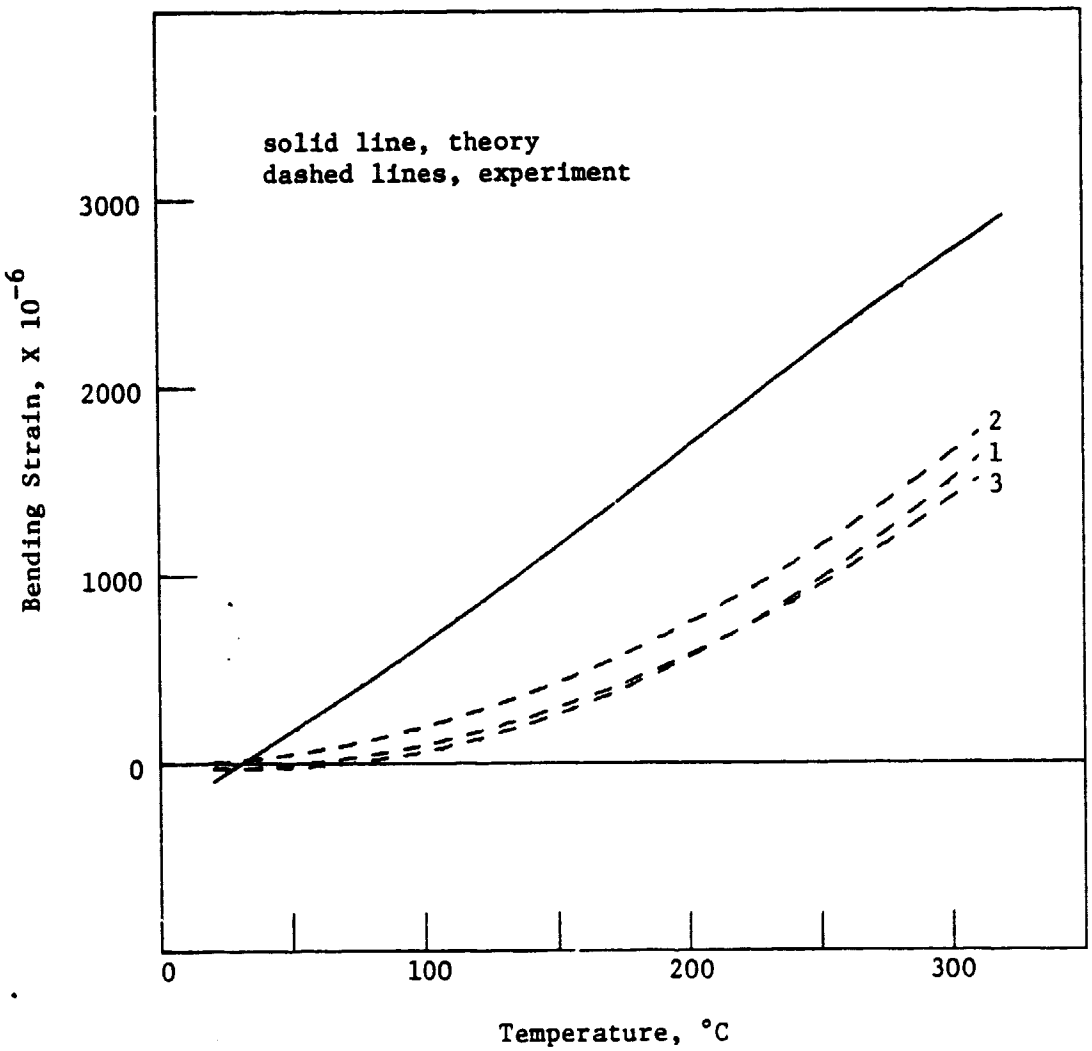

Fig. 80 Least-Squares Thermal Bending Strains and Theoretical Prediction, $[0^\circ_2/90^\circ_2]$ Laminate, RT-315°C

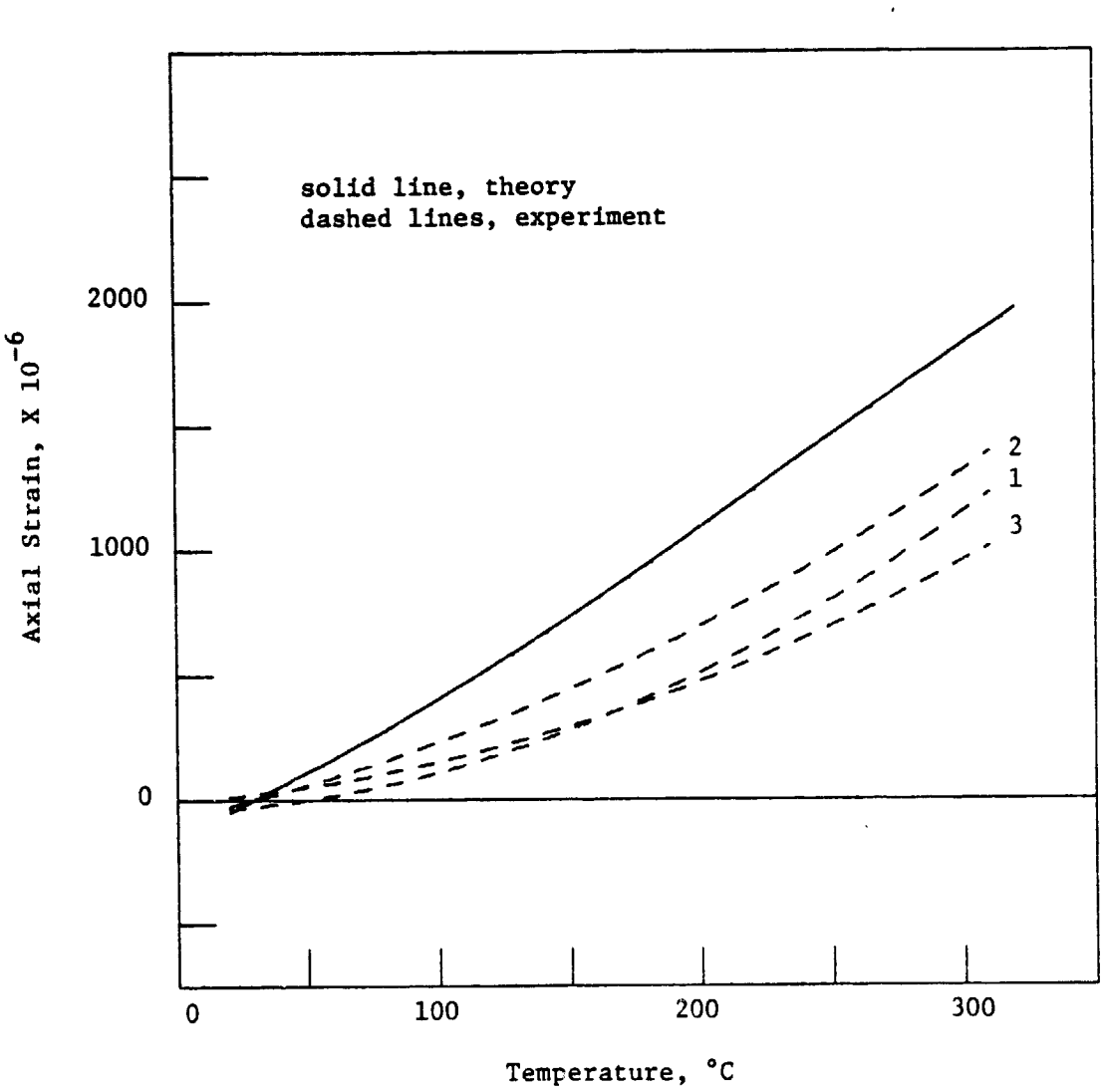

Fig. 81 Least-Squares Thermal Axial Strains and Theoretical Prediction, $[0^\circ_2/90^\circ_2]$ Laminate, RT-315°C

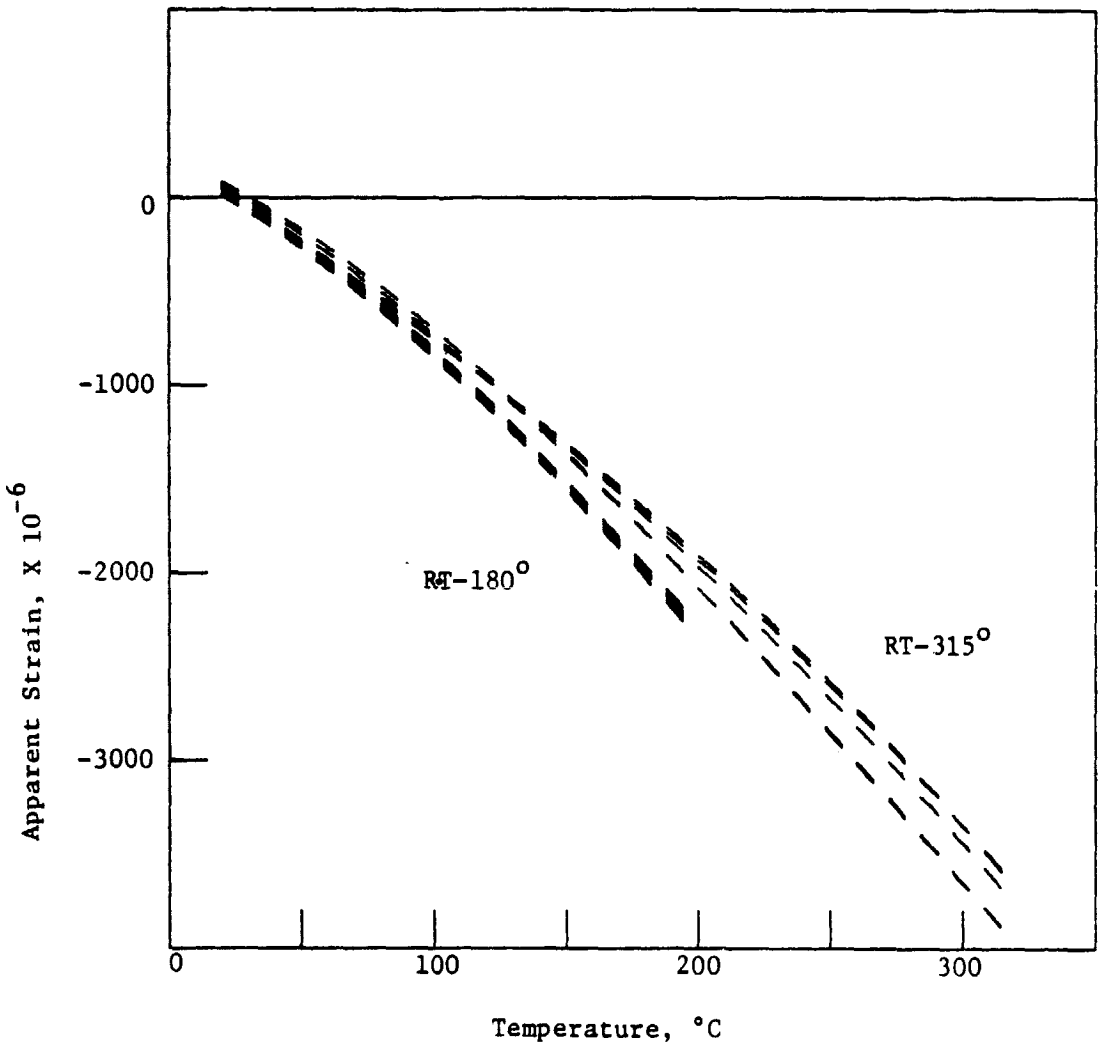

Fig. 82 Least-Squares Apparent Strain vs. Temperature, RT-180°C and RT-315°C

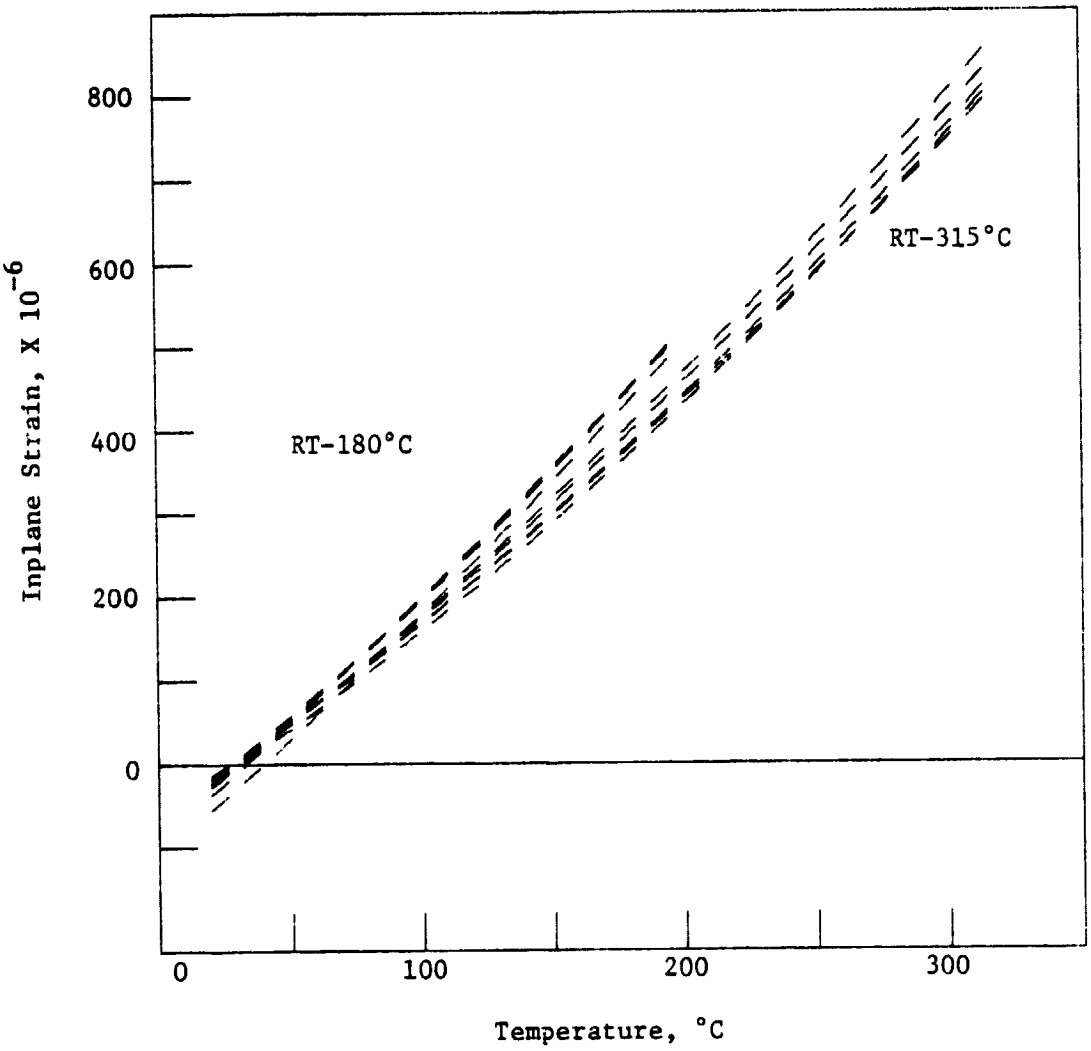

Fig. 83 Comparison of Least-Squares Matrix Direction Strains, $[0^{\circ}_{8}]$ Laminate, RT-180°C and RT-315°C

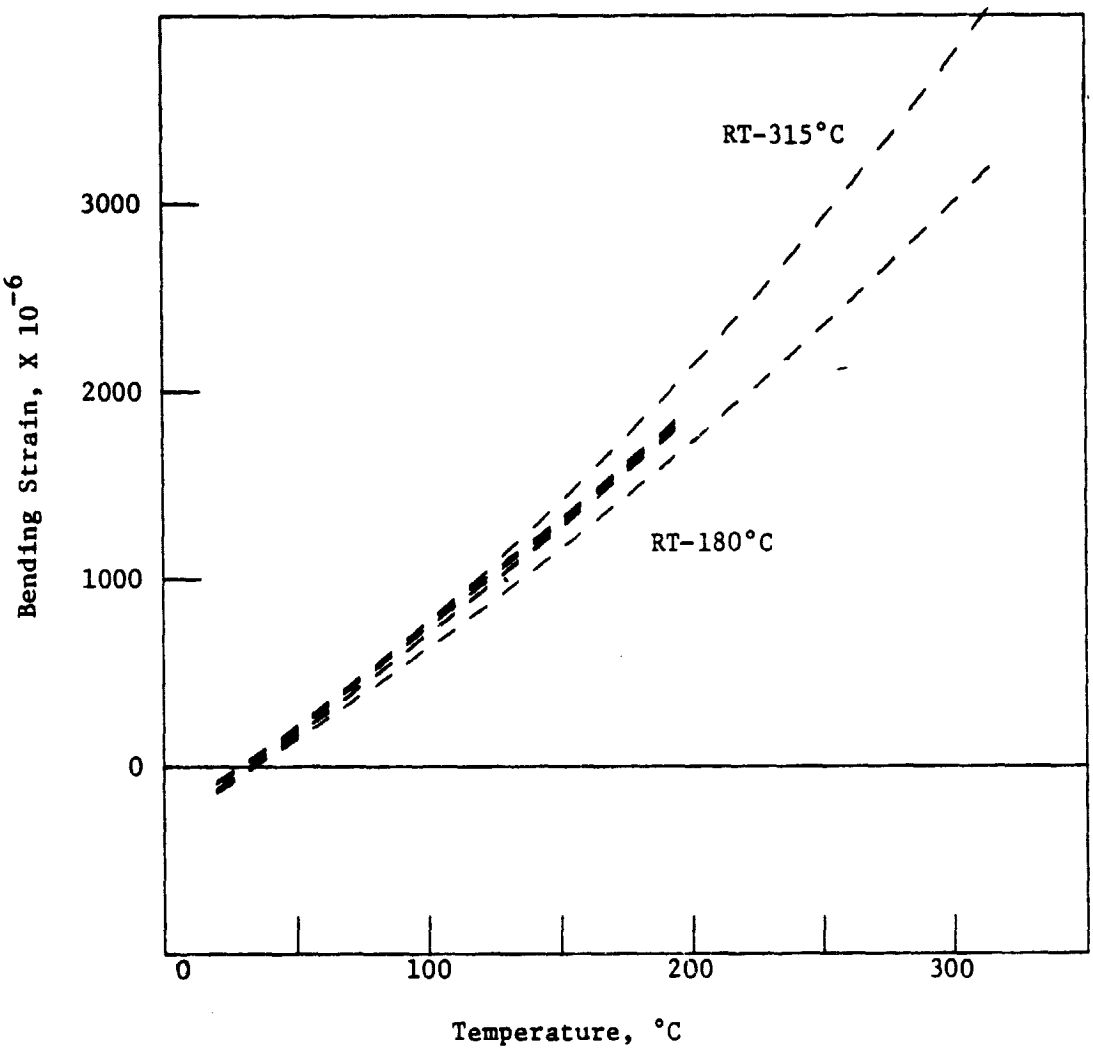

Fig. 84 Comparison of Least-Squares Bending Strains, $[0^{\circ}_{4}/90^{\circ}_{4}]$ Laminate, RT-180°C and RT-315°C

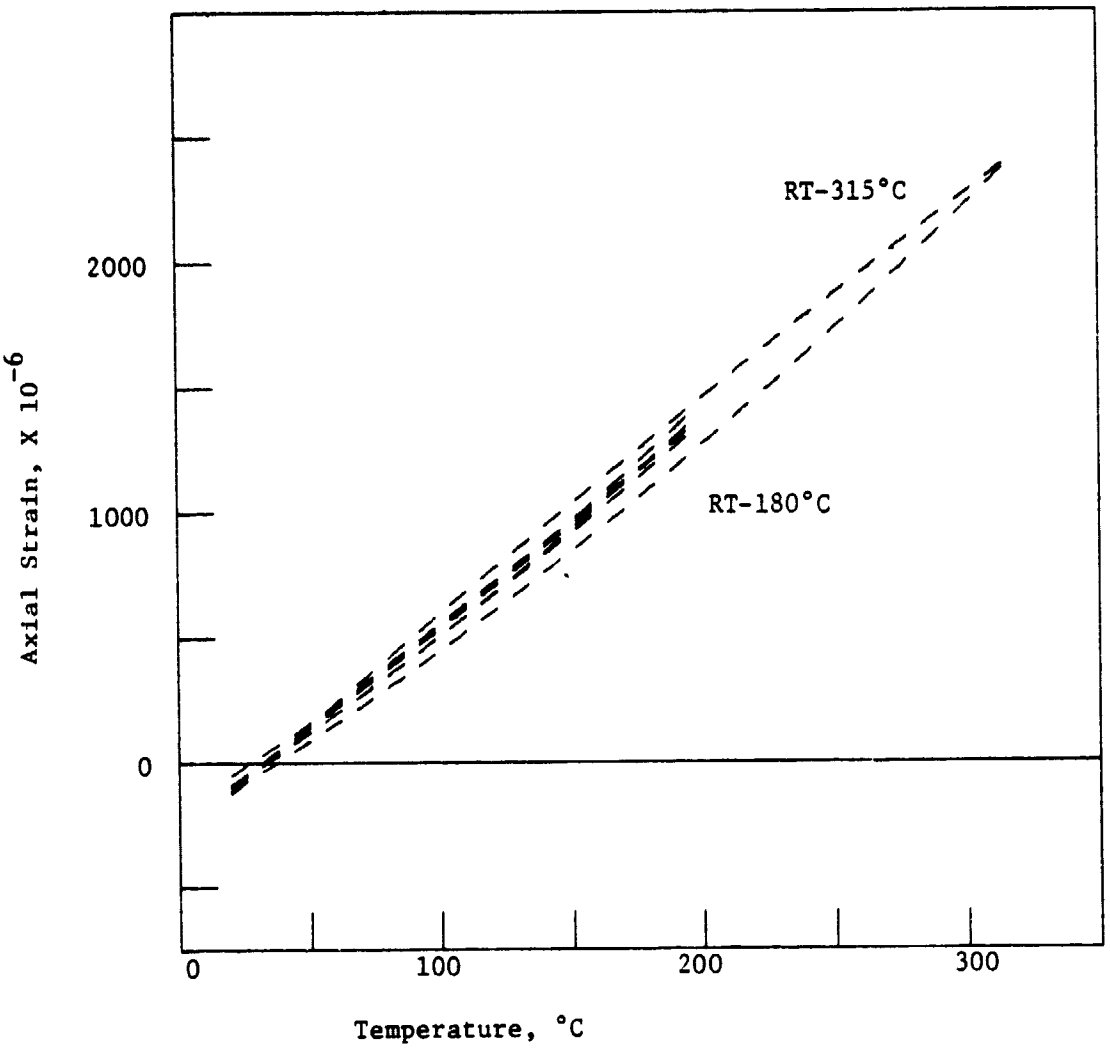

Fig. 85 Comparison of Least-Squares Axial Strains, $[0^{\circ}_{4}/90^{\circ}_{4}]$ Laminate, RT-180°C and RT-315°C

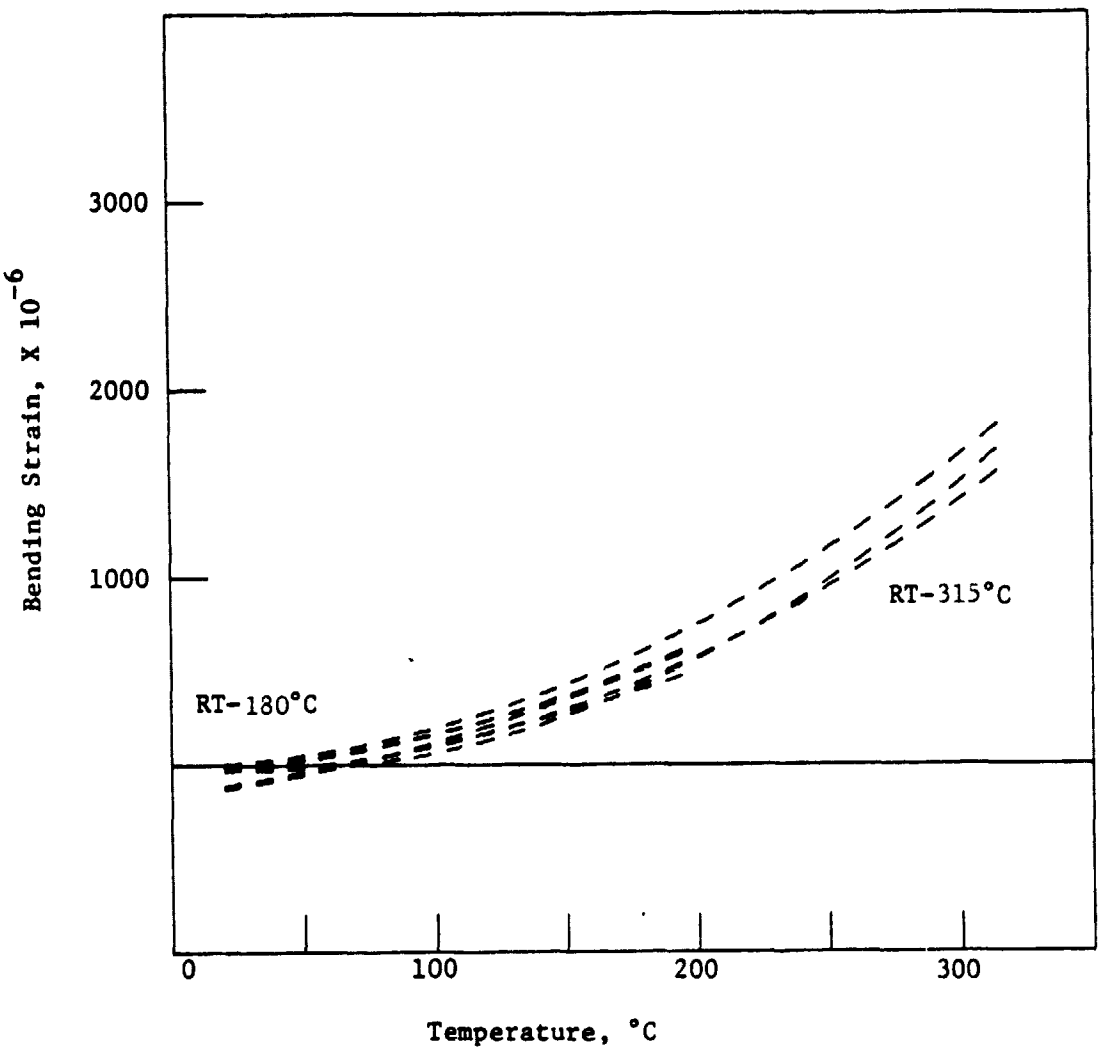

Fig. 86 Comparison of Least-Squares Bending Strains, $[0^{\circ}_{2}/90^{\circ}_{2}]$ Laminate, RT-180°C and RT-315°C

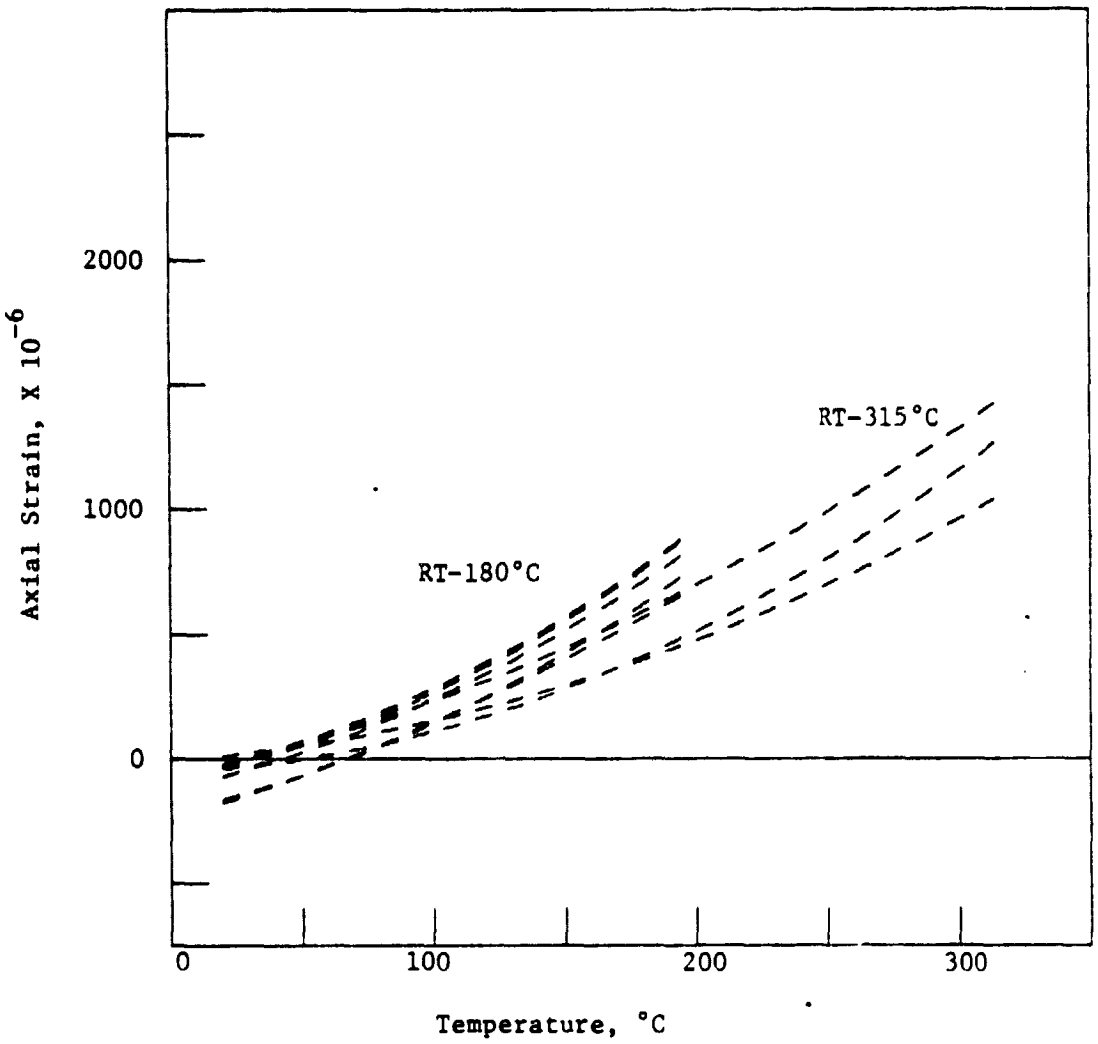

Fig. 87 Comparison of Least-Squares Axial Strains, $[0_2^o/90_2^o]$ Laminate, RT-180°C and RT-315°C